NASA TECHNICAL TRANSLATION NASA TT F-15,822

CONTRIBUTION TO THE CREATION OF BASIC DESIGN CONCEPTS FOR WIND POWER PLANTS

Ulrich Hütter

Weimar, Germany

Translation of "Beitrag zur Schaffung von Gestaltungsgrundlagen fuer Windkraftwerke," Doctoral Dissertation, Technische Hochschule Wien, Vienna, Austria, May 1942, 93 pp.

NATIONAL AERONAUTICS AND SPACE ADMINISTRATION
WASHINGTON, D.C. 20546 JULY 1974

STANDARD TITLE PAGE

1. Report No. NASA TT F-15,822	2. Government Accession No.	3. Recipient's Catalog No.
4. Title and Subtitle CONTRIBUTION TO THE CREATION OF BASIC DESIGN CONCEPTS FOR WIND POWER PLANTS		5. Report Date July 1974
		6. Performing Organization Code
7. Author(s) Ulrich Hütter		8. Performing Organization Report No.
		10. Work Unit No.
9. Performing Organization Name and Address Leo Kanner Associates Redwood City, California 94063		11. Contract or Grant No. NASw-2481
		13. Type of Report and Period Covered Translation
12. Sponsoring Agency Name and Address National Aeronautics and Space Administration, Washington, D.C. 20546		14. Sponsoring Agency Code

15. Supplementary Notes

Translation of "Beitrag zur Schaffung von Gestaltungsgrundlagen fuer Windkraftwerke," Doctoral Dissertation, Technische Hochschule Wien, Vienna, Austria, May 1942, 93 pp

16. Abstract

An estimate indicates that much more energy is available in the atmosphere than from the world's water-power resources. The most efficient dimensions of a power plant for tapping this energy are found to be a tower height of 35 meters and a rotor diameter of 40 meters, regardless of location. The concept of the rotor element, an annular part of the area covered by the rotor, is introduced for the derivation of relationships which are later applied to the entire rotor. Optimum blade planforms and section profiles are derived, and the best number of blades is found to be three.

17. Key Words (Selected by Author(s))	18. Distribution Statement
	Unclassified-Unlimited

19. Security Classif. (of this report)	20. Security Classif. (of this page)	21. No. of Pages	22. Price
Unclassified	Unclassified	89	

TABLE OF CONTENTS

CONTRIBUTION TO GAIN BASIC DESIGN CONCEPTS FOR WIND POWER PLANTS

Ulrich Hütter

1. Problem

/3

Whether wind energies can become a factor in the world energy supply is, first of all, a question of the quantities of energy present and available and, secondly, a question of the economy of the various wind power plants.

The total amount of energy is determined by the thermal budget of the atmosphere; the economy of various wind power plants is determined by the ratio of outlay for their production, installation and maintenance to the total energy yield.

For wind power plants, there is no outlay for obtaining or collecting the energy source, which constitutes the major expense in energy production based on water, coal or oil. In addition, the cost of distribution is very low, since small and very small groups of consumers can maintain plants of the required power on location. The source of energy is the wind. It is therefore also possible to make statements having a certain general validity regarding the dimensions and configuration of highly efficient wind power plants with a given basic structure.

It is clear that in order to achieve concrete results, we must commit ourselves here from the outset. Now it can be easily demonstrated, as has already been done [1], that the free turbine rotor is the most economical means of converting the wind's kinetic energy into an industrially usable form of energy.

At the present state of the art, we thus obtain the following general type of system (Fig. 1).

Tower (1), which is designed in the form of a tubular steel truss mast, carries tower head (6), which can rotate about a vertical axis a-a. Rotor (2), rotating about a horizontal axis and bearing an arbitrary number of cantilever blades carefully designed in aerodynamic terms, drives generator (5) via gearbox (4).

We are thinking of DC or three-phase power generation here; a DC power system could supply the nearby consumer directly via an energy storage unit (e.g. battery), serving as a buffer, while the three-phase system could be connected to an available grid. /5

* Numbers in the margin indicate pagination in the foreign text.

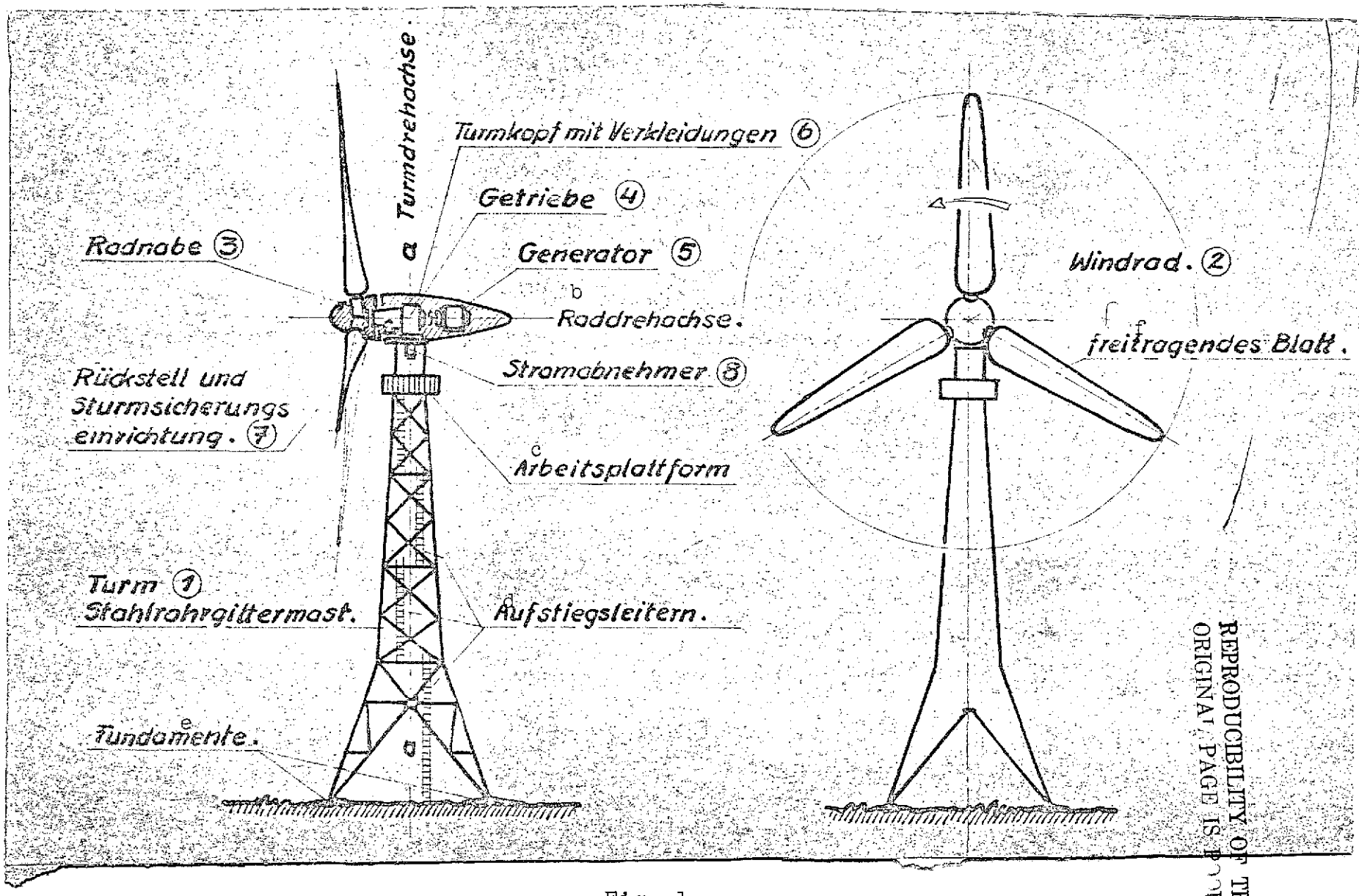

Fig. 1.

[Key on following page]

Key to Fig. 1

1. Tower: tubular steel truss mast
2. Rotor
3. Rotor hub
4. Gearbox
6. Turret head with cowlings
7. Positioning and storm-safety device
8. Sliding contact(s)

aa. Tower axis of rotation
b. Rotor axis of rotation
c. Work platform
d. Ladders
e. Foundations
f. Cantilever blade

The mechanical or electrical positioning device (7) always rotates the tower head, via a gearbox, so that the plane of the rotor remains perpendicular to the direction of prevailing wind.

To ensure against destruction of the system by storms, the plane of the rotor is rotated far enough out of the wind when a specified wind velocity is exceeded that aerodynamic forces on the rotor and the power of the rotor do not exceed specified values.

The goal of this paper is to determine the dimensions and shapes for this type of system which result in maximum economy and to establish them in the most general form possible. The task here is treated primarily as an aerodynamic and design problem. An attempt will thereby be made to delimit the area which must be covered in a careful, practical treatment of the supplying of energy primarily to regions which have not been made accessible to the energy industry.

Towers (high-tension towers, radio towers), generators and gearboxes have long since been developed to the operational stage for the various operating conditions. The task of determining the most economical dimensions therefore concentrates on the procurement of data for designing the wind rotors themselves. The amount of energy which the system can generate with a rotor of given power coefficient for a given wind frequency is a question of properly matching the rotor to the particular electrical machinery. To design the overall system it is therefore necessary to know the characteristic of the rotor, for which it is desirable to be able to make theoretical, predictive calculations without an excessive outlay, especially since the results of measurements performed on rotor models can then be better interpreted.

2. Energies in the Atmosphere

/6

Data on the level of power which could be extracted from the wind throughout the world will always remain quite hypothetical. Nevertheless, the order of magnitude of the minimum quantity of power available can be estimated from the measured radiation budget and from the measured mean velocity and mass distribution of the air as functions of altitude. Of the total energy of extraterrestrial short-wavelength radiation impinging upon the earth, according to R. Süring [15], 58% is converted in the atmosphere: a portion of the radiated energy (15%) is absorbed directly by the atmosphere, and a portion (43%) by the earth's surface, which in turn heats the air coming into contact with it by convection with 35% of the absorbed radiated energy, in addition to emitting long-wavelength thermal radiation.

The spatially uneven heating of air produces differences in density, and pressure gradients develop which cause movements of the immense masses of air. Due to the internal friction of air masses sliding by one another at different velocities (called "apparent friction" by Süring, defined in aerodynamics by shear force

---

/7

and due to friction at the earth's surface, the kinetic energy of air circulation is again converted into thermal energy and radiated back into space.

The order of magnitude of the power which must be applied in order to maintain the atmosphere's highly varying state of motion in spite of friction is estimated by Süring to be 2% of the energy absorbed. The remainder is used to increase internal energy and is lost again to space in the form of long-wavelength radiation.

The wind is thus a temporary form which the radiant energy takes.

The solar constant, i.e. the average quantity of energy received as radiation per square centimeter every minute, is

$$L_o = 1.94 \text{ grcal} \cdot \text{cm}^{-2} \cdot \text{sec}^{-1} = 1.352 \cdot 10^{-4} \text{ kW} \cdot \text{cm}^{-2}.$$

Thus the atmosphere receives a total of

/7

$$L_A = 0.58 \cdot 1.352 \cdot 10^{-4} \cdot D^2_{\text{earth}} \cdot \pi/4 = 10^{14} \text{ kW}$$

of which

$$E'_A = 2 \cdot 10^{12} \text{ KW} \qquad (1)$$

is used to maintain the state of motion. Since an energy yield is meaningful only in parts of the continents which have a certain minimum density of habitation, only a portion of the earth's surface can be used for calculation. It should be taken into consideration here that it is also possible to exploit the kinetic energy of masses of air which have taken up their energy in uninhabited areas or over the ocean. In order to cover these circumstances, total wind energy is multiplied by a factor $0 \leq K_S \leq 1$.

Only a few measurements are available of wind velocities up to high altitudes, and while their values deviate somewhat from one another, they all exhibit the same typical behavior [3, 5, 15-19].

Wind velocities at high altitudes have primarily been taken by measuring the ascent paths of meteorological balloons with theodolites. A requirement for this method is clear visibility, i.e. a certain type of weather condition. Measurements made from aircraft, taken under all weather conditions, have shown that mean wind velocity is about 7% higher at high altitudes than the means found from meteorological balloon measurements [17].

Wind velocities at altitudes between 6 and 10 km, determined by observations of cirrus clouds, indicated even higher means. Cirrus observations are possible under almost all weather conditions. It is sufficient to sight a cirrus layer through a break in the clouds (Georgii, Flugmeteorologie [Aeronautical Meteorology], p. 90 [19]) (Fig. 2).

Key to Fig. 2

a. Annual mean
b. Annual
c. Summer
d. Europe
e. Cirrus observations
f. Altitude above ground
g. Density ρ
h. Wind velocity v_H
i. Central Europe, annual
[Note: Commas in numerals are equivalent to decimal points.]

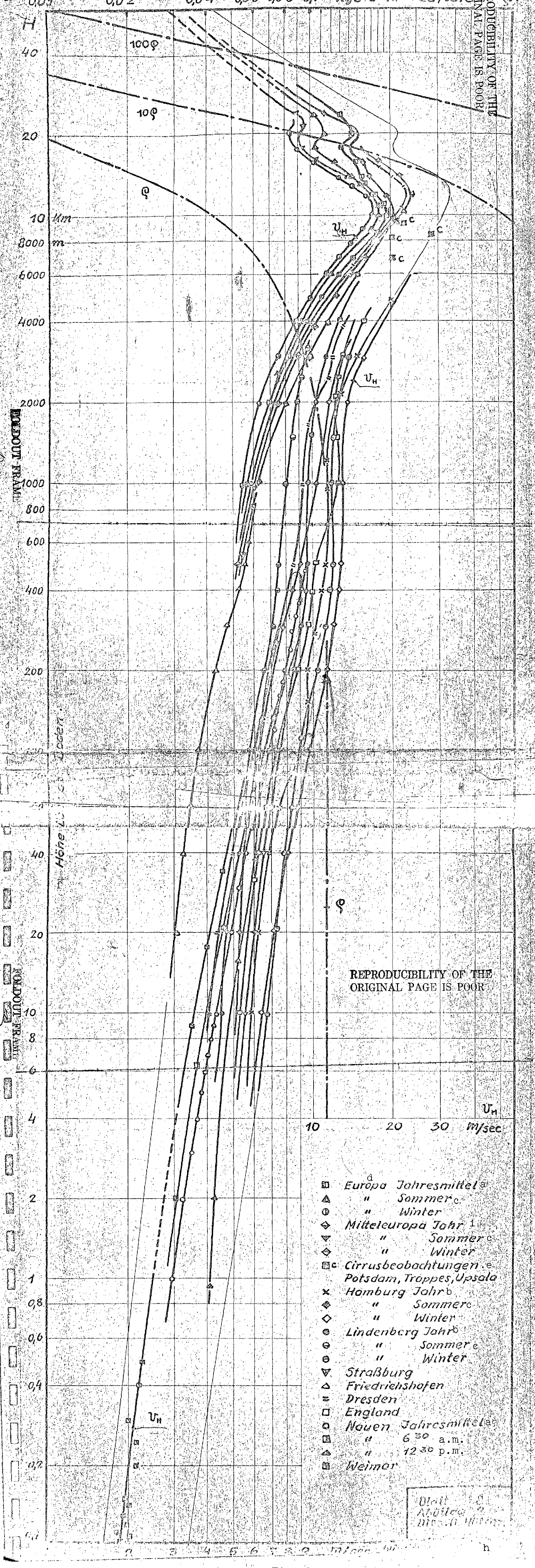

Fig. 2

The usable wind power per unit flow cross section is /9

$$\frac{dL_H}{dF} = v_H^3 \frac{\varrho_H}{2} \eta_N = l_H \qquad (2)$$

where η_N is efficiency of utilization. It is assumed to be 0.4, so only actually available quantities of energy are determined. Due to the drop in air density with altitude, power content drops off continually beyond 10 km above mean sea level, in spite of the higher wind velocities which are present there.

The quantity of energy which can be taken from the atmosphere is a function of the altitude H_n up to which energy removal extends. It must be taken into consideration here that if several series of systems are set up behind one another, removal can extend to an altitude which is higher than the maximum height of an individual system: $H_N > H_A$, since the reduction of wind velocity in a given altitude range behind the system is rapidly compensated for by the uptake of energy from faster flowing -- i.e. primarily higher-altitude, high-energy strata (Figs. 3 and 4). The setup will probably best be in several rather closely spaced rows perpendicular to the direction of prevailing winds; it may be desirable here to determine not only the polar diagram of directional frequency in the zone coming under consideration, as is common, for example, in measurements performed for laying out airfield systems, but also the polar diagram of the frequency of the wind power vector. It is conceivable that the two polar diagrams deviate from one another.

We obtain the following as total actually available power:

$$L_{i\,WIND} = \kappa_S \cdot L'_A \frac{\int_0^{H_N} l_H \, dH}{\int_0^{\infty} l_H \, dH} \quad [kW] \qquad (3)$$

(Fig. 6)

This power is a function of altitude H_n: /14

$$L_{wind} = F(H_n)$$

(Figs. 5, 6 and 7).

Even in the case of development to a level which is not at all utopian, the total output of all water power throughout the world

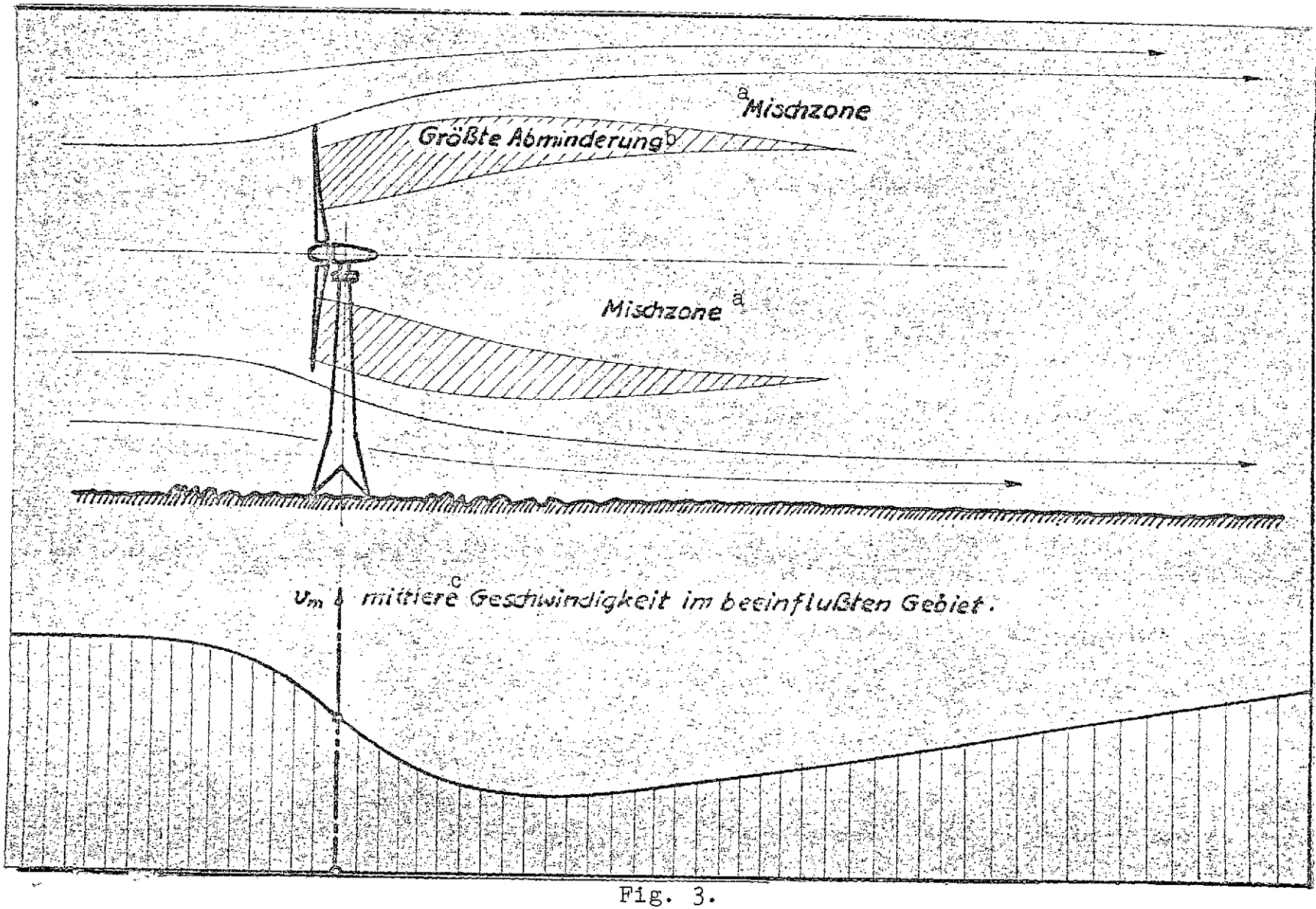

Fig. 3.

Key: a. Mixing zone; b. Maximum reduction; c. Mean velocity in affected area

Page intentionally left blank

Page intentionally left blank

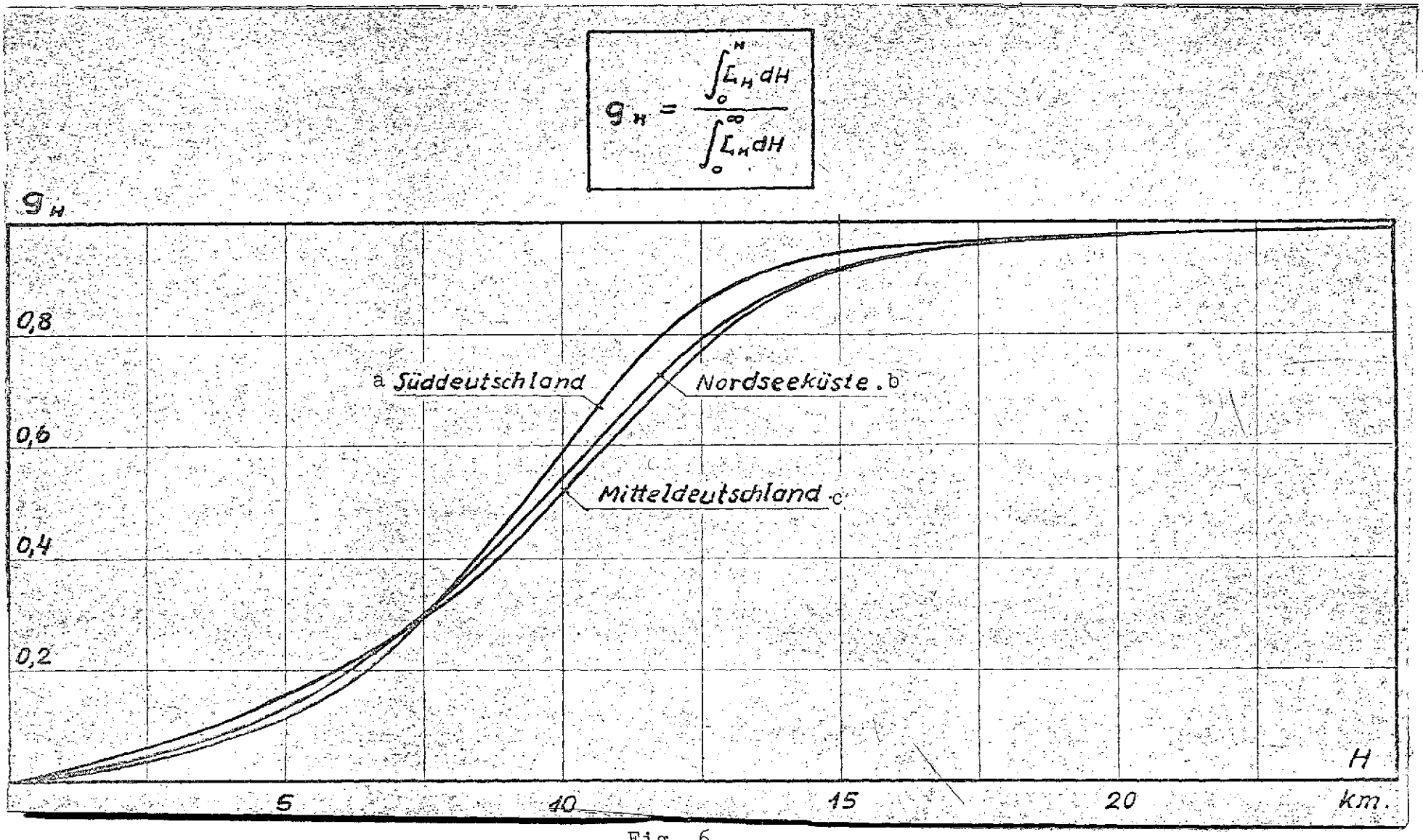

Fig. 6.

Key: a. Southern Germany
b. North Sea coast
c. Central Germany

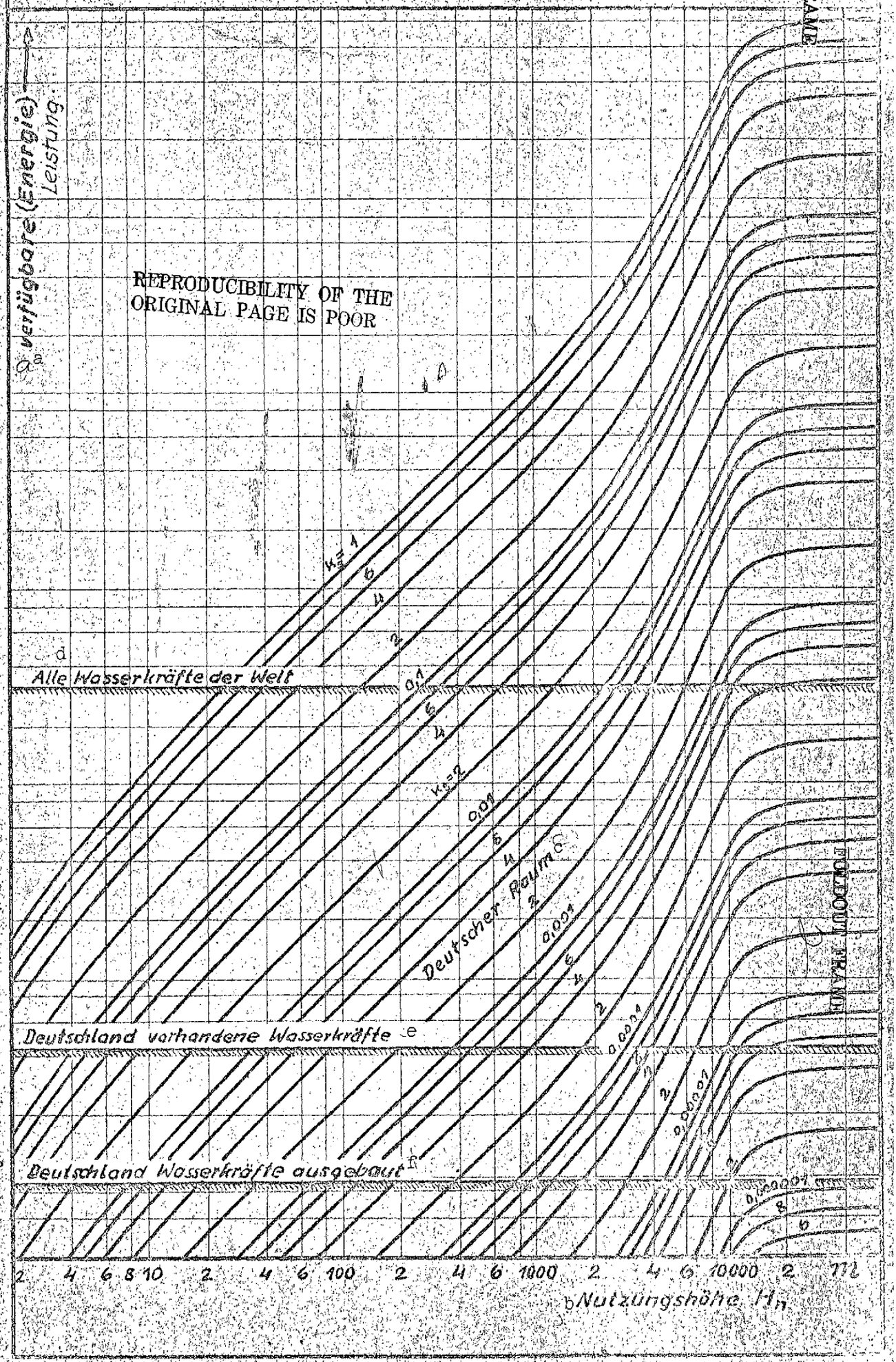

Fig. 7.

Key: a. Available (energy) power; b. Altitude of utilization H_n; c. German territory; d. Total world water power; e. Water power available in Germany; f. Water power developed in Germany

would be achieved, even that which has not been developed (according to Lütgens, $3.3 \cdot 10^8$ kW [20]).

If development is taken to even higher levels, almost unlimited quantities of energy are available, theoretically up to 2000 times all available water power.

To be sure, one circumstance has not been taken into consideration in the calculations which give us these results, namely that any significant intervention in the natural processes of atmospheric motion would also change the radiant energy budget, i.e. the conditions which were assumed at the beginning. This is insignificant for our practical results, however.

The results themselves contain only one significant uncertainty, which is due to the assumption of the percentage (2%) of the extraterrestrial radiant energy spent in the atmosphere to maintain the state of motion.

It is highly improbable, however, that less energy than that assumed here is converted into kinetic energy by the atmosphere, so the figures assumed here can be considered a lower limit on the available quantities of energy.

3. The Most Economical Principal Dimensions /16

The cost per kilowatt-hour which is obtained from amortizing capital costs for 20 years of operation is used in the following as a measure of a system's economy:

$$w = K_A/n \cdot L_m \quad \text{marks} \cdot (\text{kWh})^{-1} \text{ or pfennigs} \cdot (\text{kWh})^{-1},$$

where K_A = costs for the system, in marks or pfennigs
L_m = its mean power in kW
n = number of hours of operation in 20 years

$$n = 1.75 \cdot 10^5 \text{ hours.}$$

Since we are concerned here only with a comparison between various systems, we assume the ideal case in which all energy which occurs, i.e. is generated, is also consumed. For the same reason, outlays for maintaining and servicing the systems, as well as interest on capital, cost of the land on which the system is erected, etc. do not appear in the calculations.

The costs for the energy storage devices are likewise not covered. Aside from the fact that the size of the storage device is a function of the particular, locally determined conditions, we can also predict neither an end to the development of storage devices nor an answer to the question of whether storage devices should even be used at all and, if so, of what type these should be.

A. System Costs

System costs are broken down into four large groups:

K_R: rotor with hub
K_{GG}: generator, gearbox, positioning device, turret head cowlings
K_T: Tower with foundations
K_M: Delivery, assembly.

Experience from the construction of five rotors with diameters of 3.2 to 26 m, made of wood, was available for determining K_R (Enclosure 1). The cost of the rotors was of course available only for the prototype; values for the series production of blades were calculated on the basis of accumulated construction experience. /17

In order to obtain points of reference for the rise in rotor costs for relatively large diameters, too, the weights of two rotors with diameters of 40 and 70 m were determined using their detailed design, whereupon the costs of these rotors were calculated. Data from the literature (Hammel, Bilau [4, 10]) provided additional points of reference.

The weights and thus the costs of the rotors are a function not only of diameter but also of the velocity v_{max} at which the system is shut down to ensure against destruction.

Increased blade strengths and the associated increase in weight are of course necessary only for $v_{max} > 9\ m \cdot sec^{-1}$, since up to this velocity, the bending moments on the blade are greater in the severest storm ($v_{storm} \sim 40\ m \cdot sec^{-1}$), even with the rotor turned to the side, than those occurring in operation at maximum velocities (Fig. 8).

The specific costs for generators and gearboxes have been figured on the basis of data from the firms of Siemens-Schuckert-Werke AG and AEG, Allgemeine Elektrizitätsgesellschaft (generators), and Eisenwerk Wülfel, Hannover-Wülfel (gearboxes). It was necessary to consider here that generators and gearboxes had to be dimensioned for the system's maximum output, i.e. for the output at which $v_o = v_{max}$. High tooth pressures and thermal stresses could then be accepted, since this case is to be expected only for

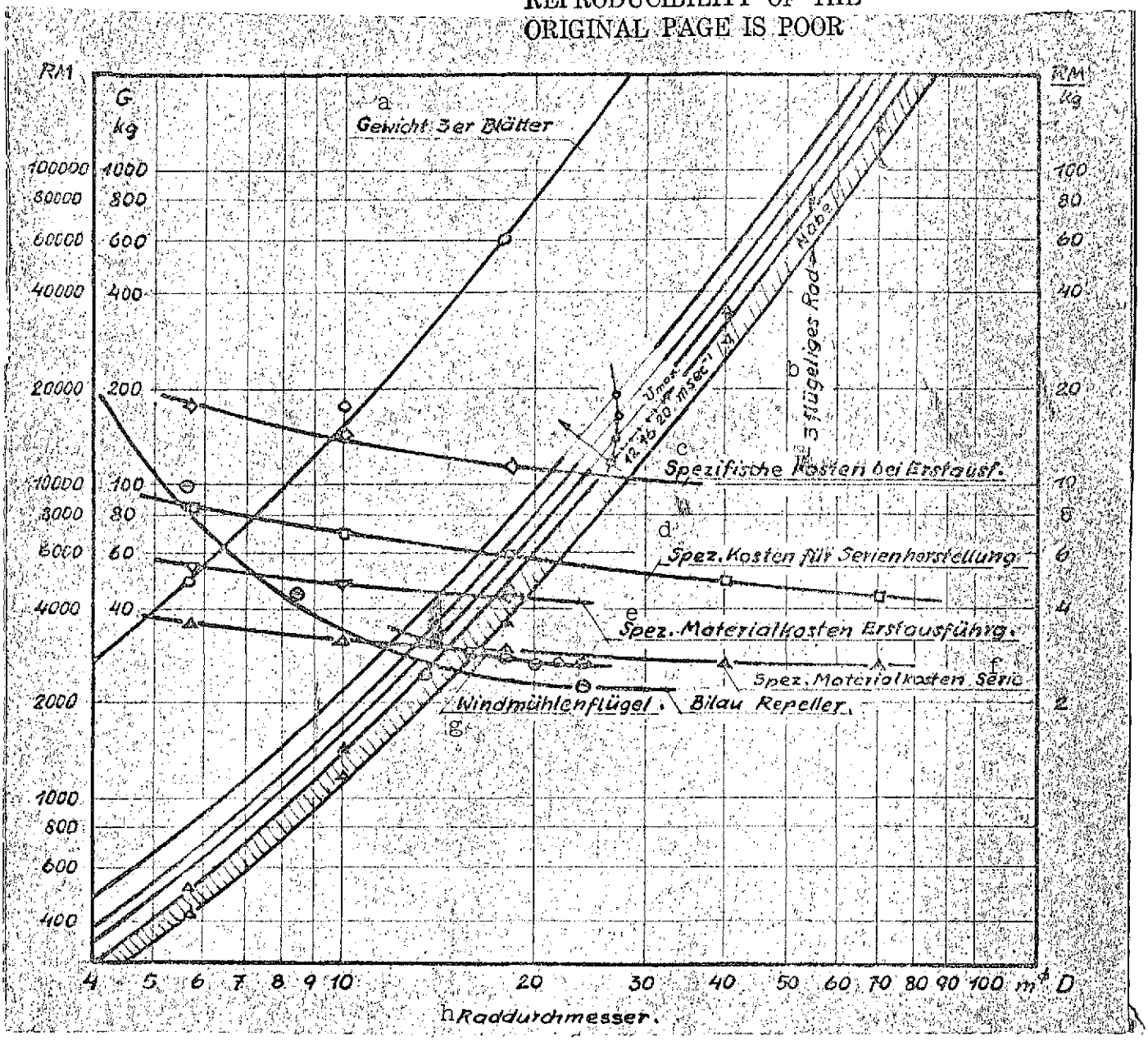

Fig. 8.

Key:
a. Weight of three blades
b. Three-blade rotor
c. Specific costs for prototype
d. Specific costs for serial production
e. Specific materials cost, prototype
f. Specific materials cost, serial production
g. Windmill blades
h. Rotor diameter
RM = marks
G = weight
Ø = D = diameter

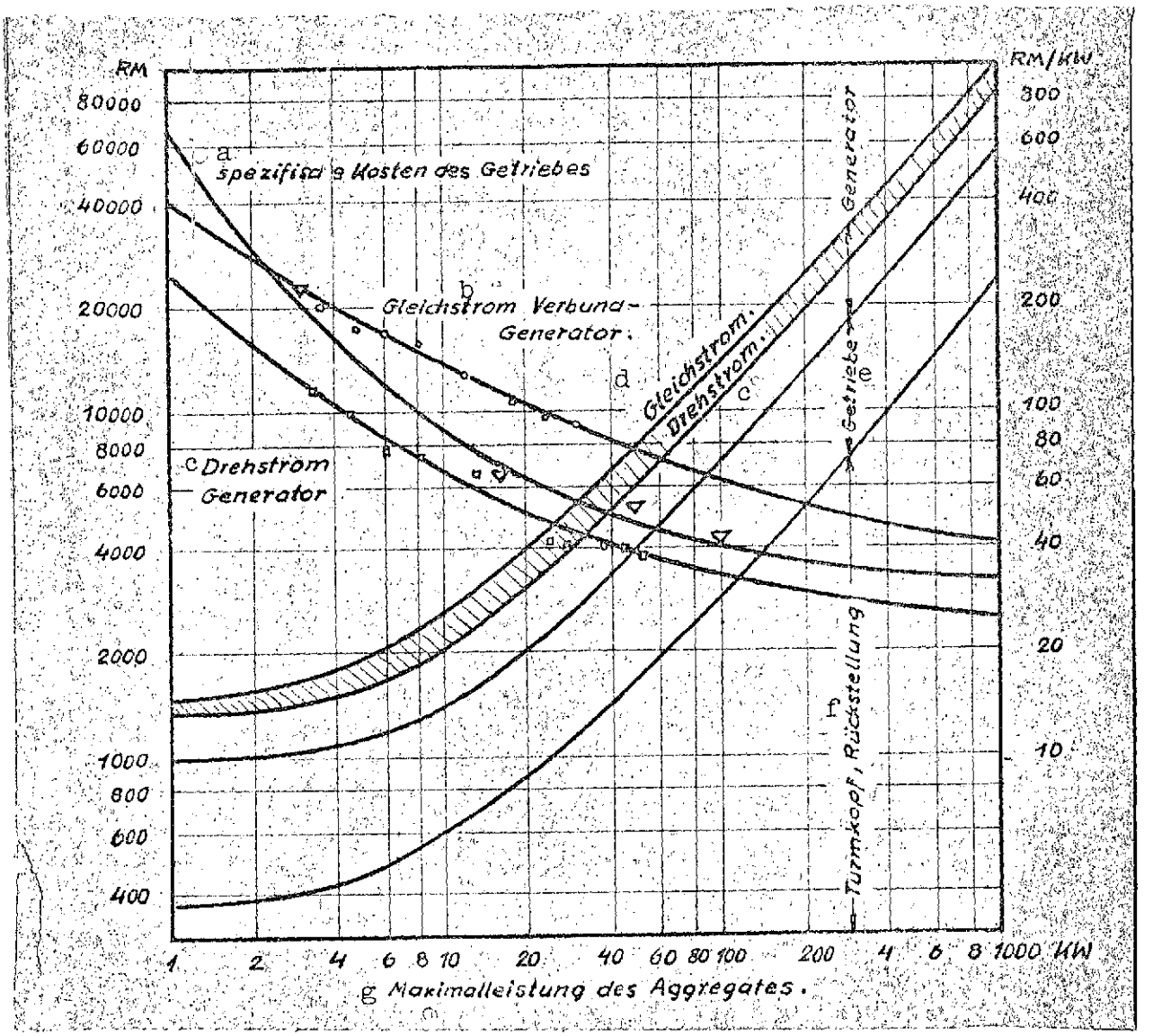

Fig. 9. Purely output-dependent costs of a system.
▽ from data provided by Wülfel, Hannover
o, □ } from data provided by Siemens-Schuckert Werke A.G. and AEG Allgemeine Elektrizitäts Gesellschaft

Key:
a. Specific costs for gearbox
b. Compound DC generator
c. Three-phase
d. DC
e. Gearbox
f. Tower head, positioning device
g. Maximum output of unit

short intervals and over a small percentage of total operating time (Fig. 9).

Costs for the positioning device, the machinery foundations, the ball bearing ring mount and the cowlings for the head were assumed to be about 28% of the generator and gearbox costs, on the basis of experience obtained in the production of four test systems (Ventimotor test system). /21

K_T could be taken from detailed designs of towers of various height for various horizontal tensile forces at the tower head, produced by the firm of Benteler-Bielefeld.

Tower costs are directly proportional to the weight of the tower. Tower weight and costs increase approximately as the $h/2$ power of horizontal tensile force at the head. This is explained by the fact that, in addition to this force, the intrinsic weight of the tower and wind pressure on the tower itself are taken into consideration in designing the tower. The magnitude of this tensile force is proportional to the square of rotor diameter and to the square of wind velocity at the altitude of the tower head (Fig. 10).

The outlay for assembly and delivery was determined from the eight test systems by Ventimotor GmbH to be about 15% of total system costs. Thus in determining total system costs, it is merely necessary to multiply the sum

$$K_R + K_{GG} + K_T$$

by 1.15:

$$K_A = (K_R + K_{GG} + K_T)1.15. \qquad (5)$$

B. Maximum Output

A large body of data can be found in the literature concerning the relative frequency of winds of various velocity v_o ([3, 5, 19] and Fig. 11). Absolute frequency can be determined from the relative frequency data by integration up to the wind velocity under consideration. We obtain wind velocity versus time as the result, with 1 selected as the time interval -- this can refer to any time unit, such as 1 year (Fig. 12).

Output frequency, i.e. the behavior of output with time, is determined from the velocity corresponding to a particular frequency figure. We can now assume, for various velocities, that rotation of the system out of the direction of the wind begins from there on, allowing output regulation in such a manner that /24

REPRODUCIBILITY OF THE
ORIGINAL PAGE IS POOR

Fig. 10

Key: a. Rotor diameter
o Data from Bentelen. Rotor diameter data applied to a shutdown velocity of 9 m sec⁻¹
RM = marks

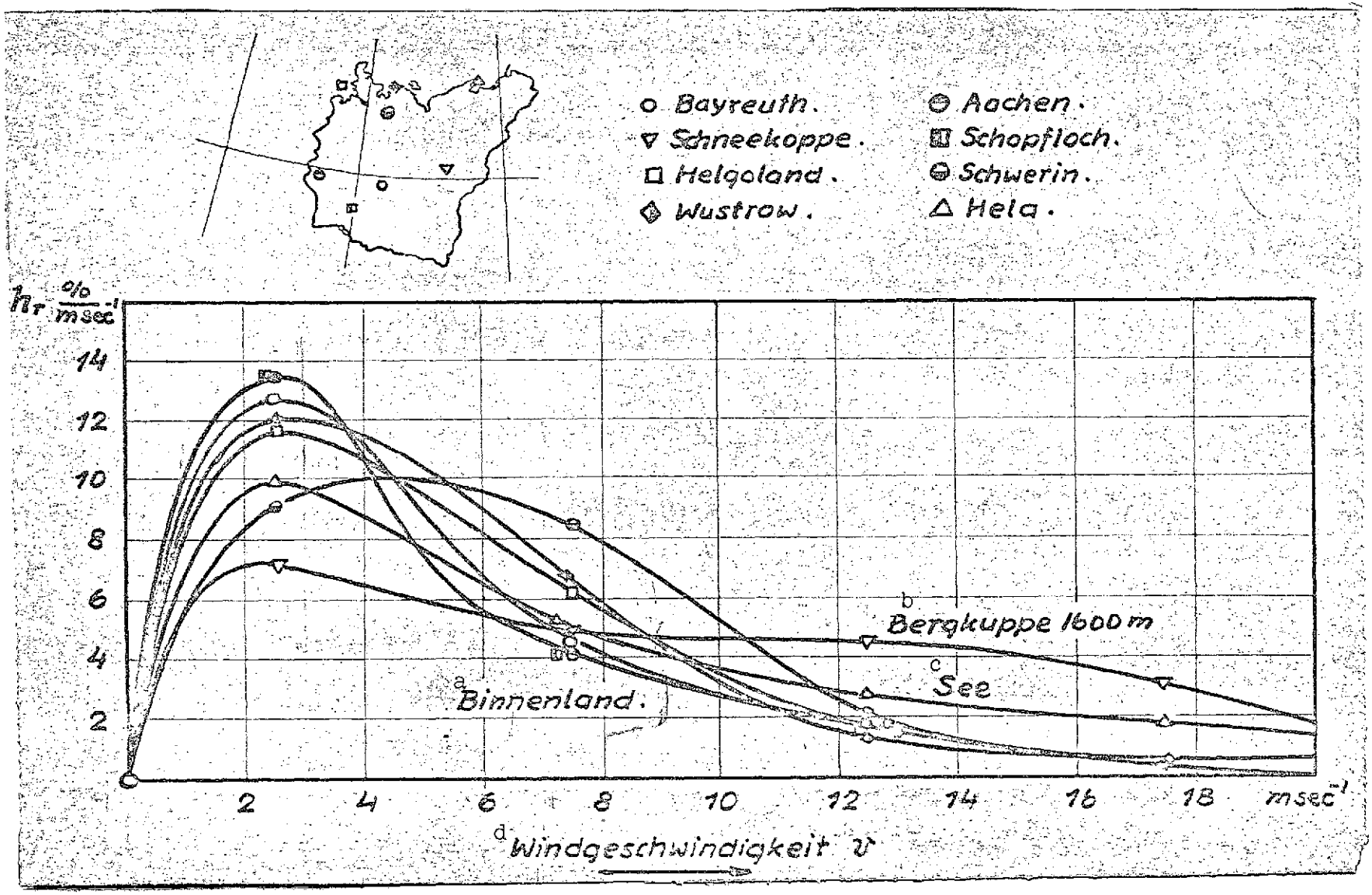

Fig. 11.

Key: a. Inland; b. Mountain peak; c. Ocean; d. Wind velocity

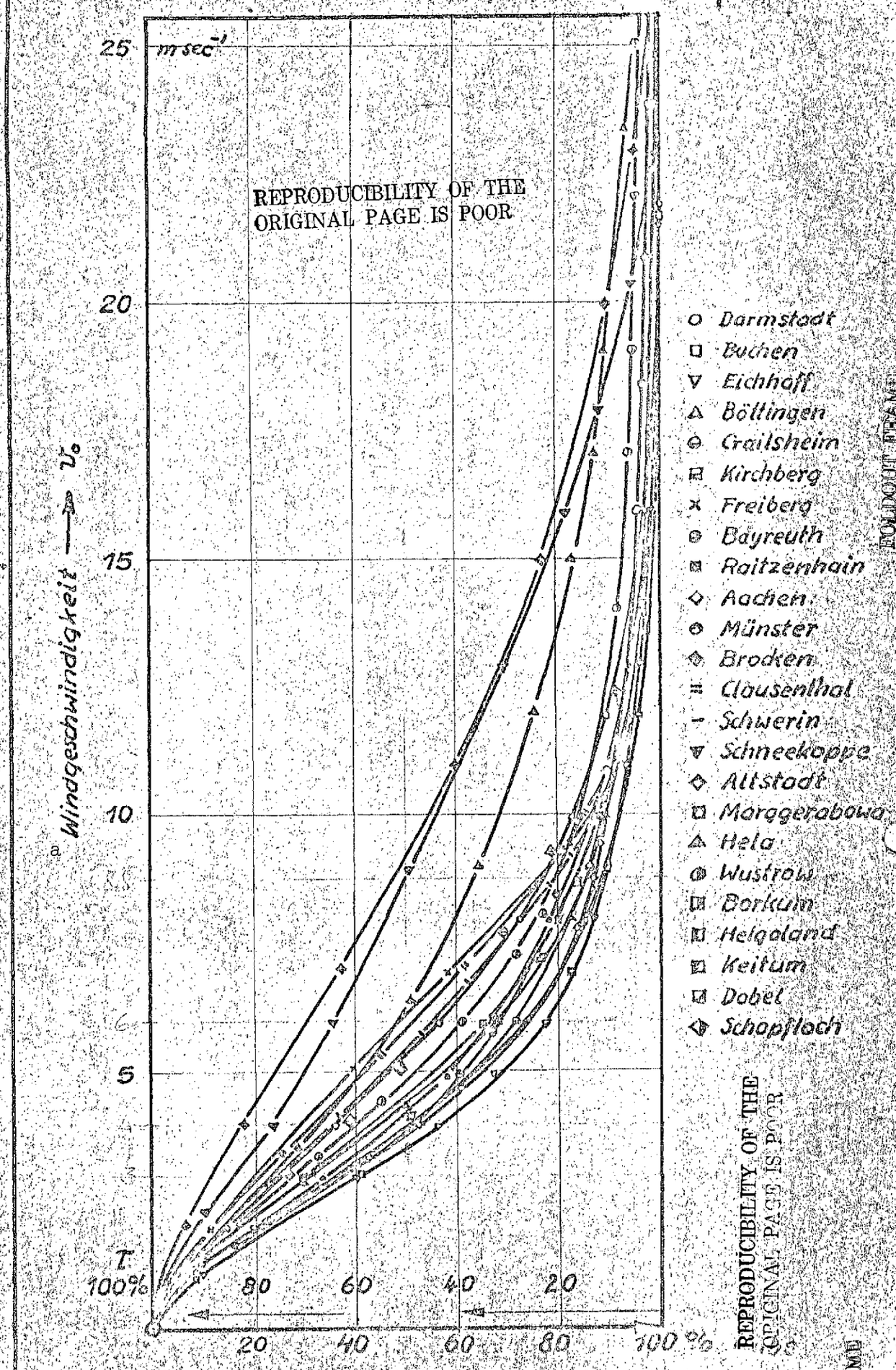

Fig. 12.

Key: a. Wind velocity
h_{abs} = absolute frequency

the output of the system is kept constant for the remaining time period without regard to velocity.

The energy taken from the wind over a period of 20 years is thus

$$E = n\int_0^{L_{v_a}} (1-h_v)\,dL = f(v_a) \quad kWh \qquad (6)$$

where L = power
h_v = frequency value
n = $1.75 \cdot 10^5$

The magnitude of this energy is a function of the velocity v_a at which the disengagement process begins and of the wind frequency curve. If maximum power increases, system costs also increase, since larger generators and gearboxes and heavier rotors and towers are necessary as power rises. The quotient of system costs and energy produced yields the economic efficiency of a given system as a function of cutoff velocity (Figs. 13 through 16).

The performance of these calculations for two extreme limiting cases (Bayreuth, with little wind, and the peak of the Brocken, with a great deal of wind) shows that the optima for cutoff velocity are extremely flat in both cases and are not far apart. The rise in specific costs as cutoff velocities decrease from the optimum is steeper than as they increase. In particular, it becomes unacceptably high at cutoff velocities below 5 m/s. To be sure, one factor has not been taken into consideration in these results, namely that the absolute frequency of high wind velocities is low. Since it is not presently possible to store large quantities of energy for a relatively long time, the possibility of utilizing peak outputs is less than the possibility of utilizing average outputs. It will therefore be desirable to give preference to the smaller values on the flat optimum curve over larger values. This yields a maximum cutoff velocity of about 8 or 9 m/s for low-wind areas and 9 to 11 m/s for high-wind locations.

C. The Output of the System

/27

The mean usable power which can be extracted from the wind is

$$L_m = \int_{H_r - \frac{D}{2}}^{H_r + \frac{D}{2}} l_H\,dF \qquad (7)$$

System with a tower height H_T of 35 m and a rotor diameter D of 25 m.

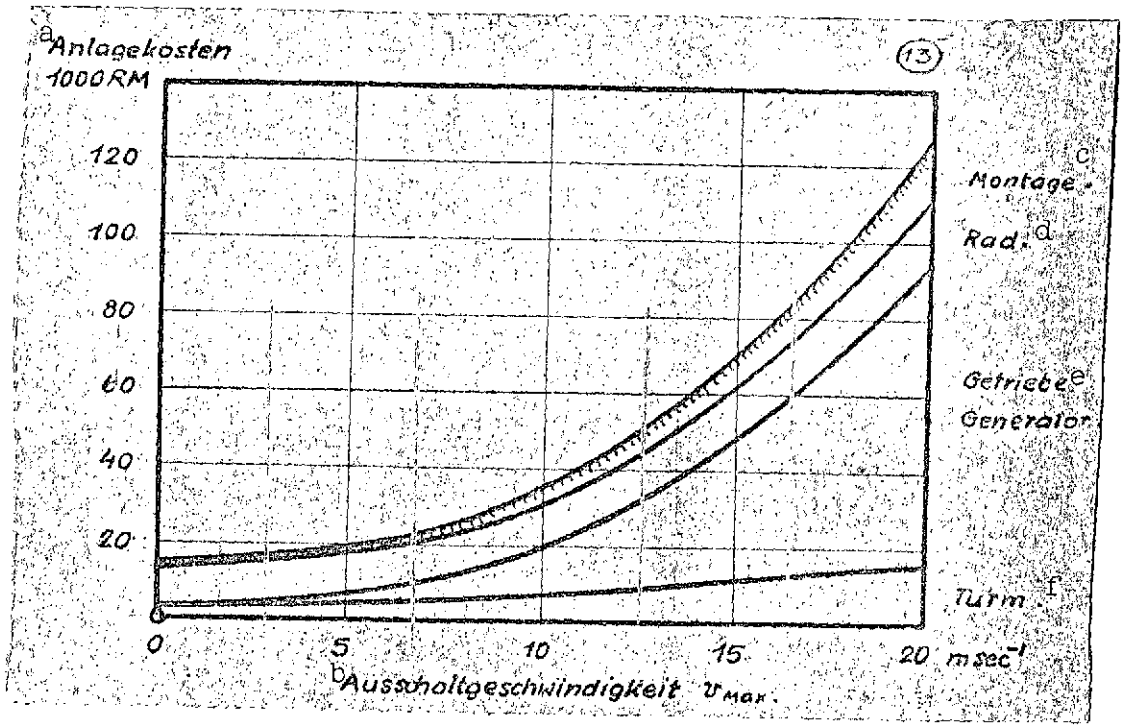

Fig. 13.

Key:
a. System costs
b. Cutoff velocity
c. Assembly
d. Rotor
e. Gearbox
f. Tower
RM = marks

where

$$l_H = v_H^3 \cdot \frac{\varrho_H}{2} \cdot \eta_N \quad \text{ist.} \quad (2) \tag{2}$$

The magnitude of wind velocity versus altitude varies appreciably as a function of the location at which measurements are made, as already mentioned, but is of very similar character for all locations.

The function

$$v_H = v_{H_1} \cdot H^{\frac{k}{3}} \quad (8) \tag{8}$$

System with a tower height H_T of 35 m and a rotor diameter D of 25 m.

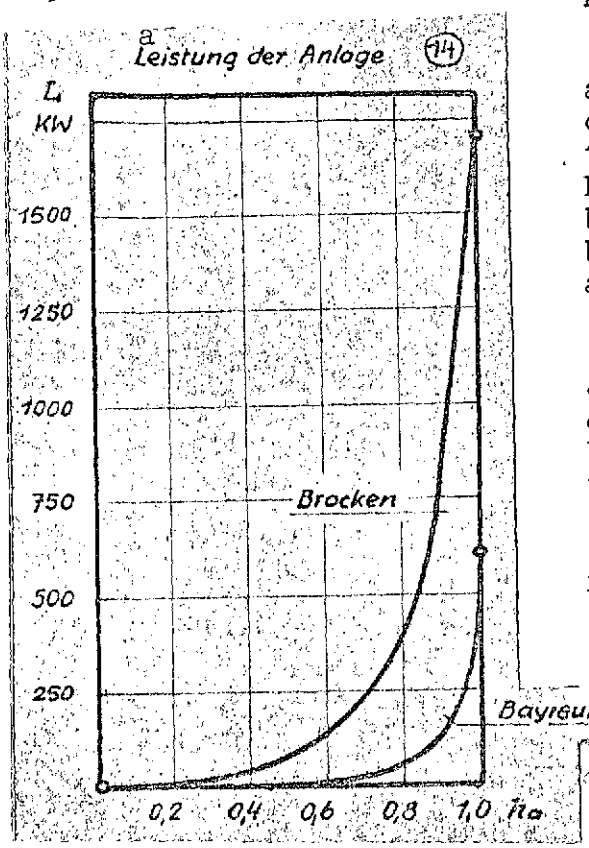

Fig. 14.

Key: a. System power
L = power
h = frequency

provides a good approximation for the behavior of wind velocity versus altitude in the area of the plane of rotor rotation.

In order to increase the accuracy of calculation, K and v_{H1} can be obtained as functions of tower height, i.e. of the mean height of the circular area swept by the rotor, from the measured behavior of wind velocity versus altitude (Fig. 18).

The variation in air density over rotor height is insignificant over the rotor sizes to be expected. We therefore assume $\rho_H = \rho_{H_T}$ over the entire circular area.

If we now substitute into formula (7)

$$dF = r\,dr\cdot d\varphi$$

$$H = H_r + r\cos\varphi$$

$$l_H = \eta_N \frac{\rho_H}{2}\cdot v_{H1}^3 H^K$$

$$a_{H_T} = \eta_N \frac{\rho_{H_T}}{2}\cdot v_{H1}^3$$

(Fig. 17)

and expand l_H in a Taylor series, we obtain

$$\frac{d^{(n)} l_H}{dH^{(n)}} = a_{H_T}\cdot K(K-1)(K-2)\ldots(K-n+1)\,H^{K-n}$$

$$l_H = a_{H_T}\left(H_r^K + \sum_2^\infty \frac{K(K-1)(K-2)\ldots(K-n+1)}{n!}\,H_r^{K-n}\cdot r^n\cdot\cos^n\varphi\right)$$

We integrate separately over the regions $H \geq H_T$ and $H \leq H_T$. When the sums are taken, the individual integrals with odd powers of $+r\cos\phi$ and $-r\cos\phi$ cancel out, and only the integrals with even powers appear in the result:

$$L_m = a_{Hr}\left(4\int_0^{\pi/2}\int_0^{D/2} H_T^k\, r\, d\varphi\, dr + 2\int_0^{\pi/2}\int_0^{D/2}\sum_2^{\infty n}\frac{k(k-1)(k-2)\ldots(k-n+1)}{n!}\, H_T^{k-n}(\pm r)^n \cos^n\varphi\, r\, dr\, d\varphi\right)$$

The integrals over $\cos^{2p}\phi\, d\phi$ all have the following solution:

$$\int_0^{\pi/2}\cos^{2p}\varphi\, d\varphi = \frac{\pi}{2}\,\frac{1(1+2)\ldots.[1+2(p-1)]}{2(2+2)\ldots.[2+2(p-1)]}$$

Thus after transformation we obtain

$$L_m = a_{Hr}\frac{\pi}{4}D^2 H_T^k\left(1+\sum_1^{\infty p}\left(\frac{D}{2H_T}\right)^{2p}\frac{k(k-1)\ldots(k-2p-1).1.(1+2)\ldots[1+2(p-1)]}{2p!(p+1).2(2+2)\ldots[2+2(p-1)]}\right) \quad (9)$$

However, $\eta_N \frac{\varrho_{Hr}}{2} v_{H1}^3 H_T^k \frac{\pi}{4} D^2 = l_{Hr}\cdot F_{\text{rotor}}$ (circular area)

If we substitute this expression into equation (9), it simplifies to

$$L_m = l_{Hr} F_{\text{rot.}}\cdot\mu_L \quad (10)$$

$$\mu_L = 1+\sum_1^{\infty p}\left(\frac{D}{2H_T}\right)^{2p}\frac{k(k-1)\ldots(k-2p-1).1.(1+2)\ldots[1+2(p-1)]}{2p!\,(p+1)\,2(2+2)\ldots[2+2(p-1)]} \quad (11)$$

This series converges very rapidly. For all cases occurring in practice, it is sufficient to consider a small number of terms.

The factor μ_L is thus a function of K and D/H_T (Fig. 19). /30

In any case, it is necessary that $D/H_T \leq 2$, since the rotors would otherwise reach the ground.

For this limiting case, with k = 3/5, for example,

$$\mu_L = 1 - 0.0300 - 0.004205 - \ldots = 0.9658.$$

The level of output of each system can thus now easily be calculated as a function of D and H_T (Figs. 20, 21). But it is determined from yearly mean wind velocity, rather than from actual mean power, since this is proportional to the third power of wind velocity. It would therefore be necessary to determine mean power from the mean of cubed wind velocities, i.e. from the power frequency curve. Depending upon the shape of the frequency curve, mean power is from 1.4 to 2 times the power which results from mean wind velocity[1]. A simple estimate shows this immediately. If we assume linear behavior for power frequencies, we obtain the following for the ratio of mean power values to power derived from mean velocity:

h = frequency value (see Fig. 12)

For $h = 0$, $v = 0$.
$h = 1$, $v = v_{max}$.
$v_h = h \cdot v_{max}$.

$$L_{v\,mean} = \frac{\varrho}{2} F \cdot \eta_N \left(\frac{v_{max}}{2}\right)^3 = \frac{\varrho}{2} F \cdot \eta_N \cdot v_{max}^3 \cdot \frac{1}{8}$$

$$L_{mean} = \frac{\frac{\varrho}{2} F \cdot \eta_N \cdot \int_0^1 v_h^3 \, dh}{1} = \frac{\varrho}{2} F \cdot \eta_N \, v_{max}^3 \int_0^1 h^3 \, dh = \frac{\varrho}{2} F \eta_N \cdot v_{max}^3 \cdot \frac{1}{4}$$

The system's maximum output must be fixed in order to determine power-dependent costs, i.e. to determine the costs of the generator, gearbox, etc. This maximum output is of course higher than mean system output. The following means are obtained for Bayreuth and for the peak of the Brocken:

/34

	Bayreuth	Brocken	
Mean velocity	5.355	10.4	m/sec
Power from mean velocity	14.8	108	kW
Ideal mean power	43.6	248	kW
Mean power for peak cutoff	25.3	111	kW
Peak power	91	254	kW
Peak power ÷ mean power	3.6	2.29	

[1] A factor of 1.6 has been assumed for the curves in Figs. 20 and 21.

System with a tower height H_T of 35 m and a rotor diameter D of 25 m.

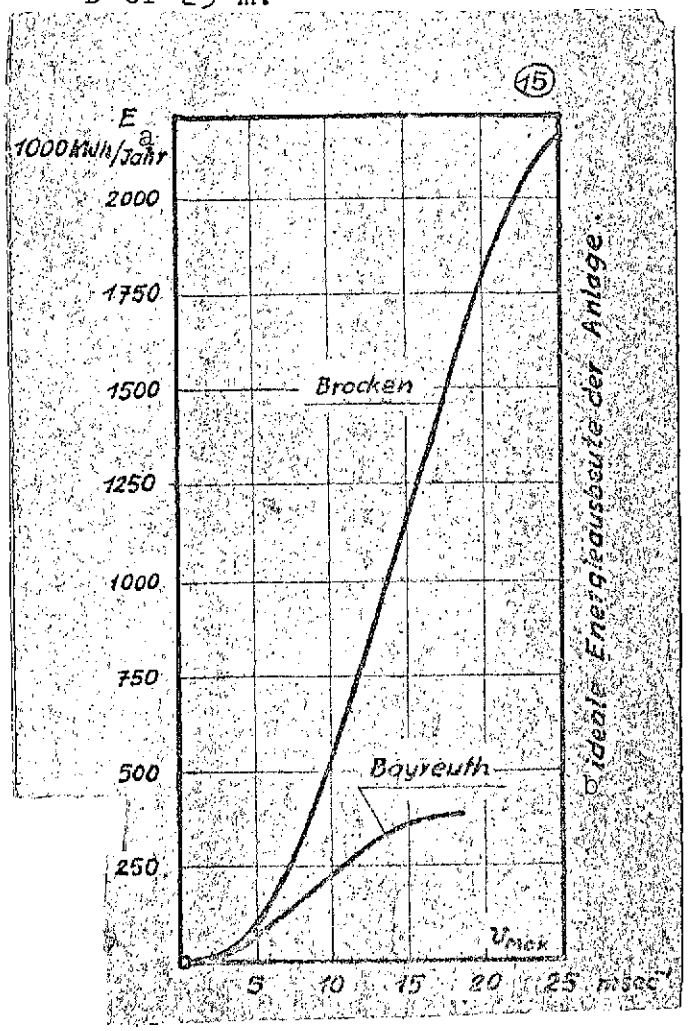

Fig. 15.

Key: a. Year
b. Ideal energy yield of system

A peak power to mean power ratio of 3.2 was assumed for determining power-dependent costs.

D. Economic Efficiency /35

It now merely remains to determine the quotients w for a number of systems of different tower height and different rotor diameter. Curves of constant economic efficiency are plotted in Fig. 22 in D, H_T coordinates. In the two limiting cases studied, that of an inland system (Bayreuth) and of a system for the coastal region (Hamburg), it is found that the most economic dimensions are approximately the same and that the optimum is extremely flat.

In making these calculations, though, it was necessary to extrapolate markedly for relatively large tower heights and rotor diameters. Thus the values applicable to large rotor diameters and high towers are less reliable than those for rotor diameters and tower heights of 0 to 100 m.

In both cases, however, the optimum lies within this range. It is found in any case that quite small systems are definitely much less economical than medium-size systems. A certain amount of "freedom" exists above this level. It is probably more desirable, however, to construct a relatively large number of medium-size systems than a smaller number of large systems of approximately the same economic efficiency.

The following factors are primarily determinant in this regard:

1. In the case of a larger number of smaller power plants the distance from the power plants to the consumers is very

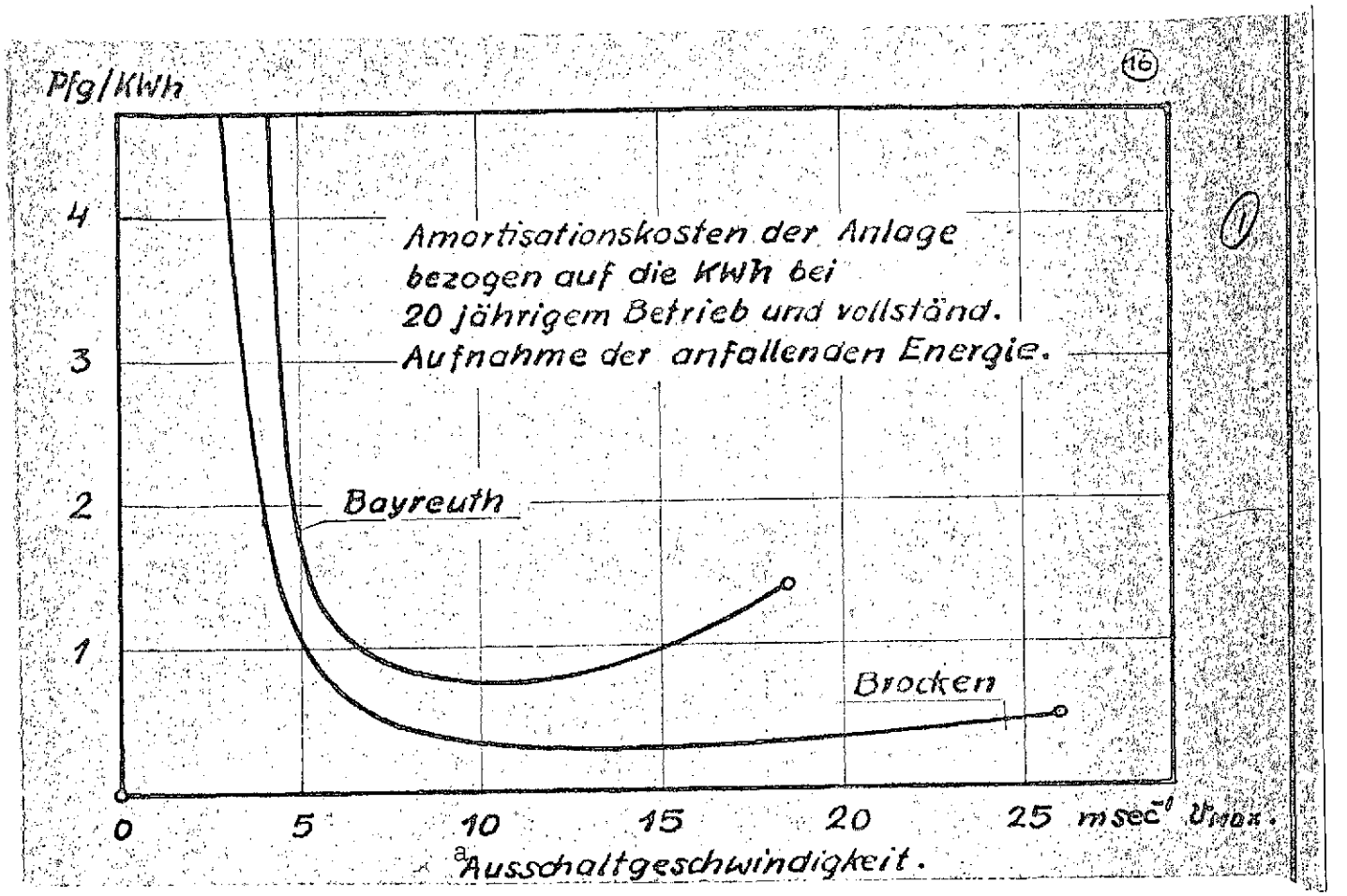

Fig. 16. Amortization costs of system per kWh in 20 years of operation and complete extraction of available energy.

Key: a. Cutoff velocity
Pfg = pfennigs

probably smaller, i.e. the inherently low distribution cost is kept at a minimum.

2. A larger number of smaller power plants -- if connected with one another, say, via a ring main system -- will yield a more uniform supply of power than a small number or just a single larger power plant. All air movements are cyclic, particularly close to the ground. The curve of wind velocity versus time is thus subject to large-scale local fluctuations. If several power plants are located at a certain distance from one another over the countryside, the probability that minima or maxima in wind velocity will occur simultaneously at all of them is extremely low. The resultant equalization is made more complete as the number of interconnected systems is increased. When power is /36

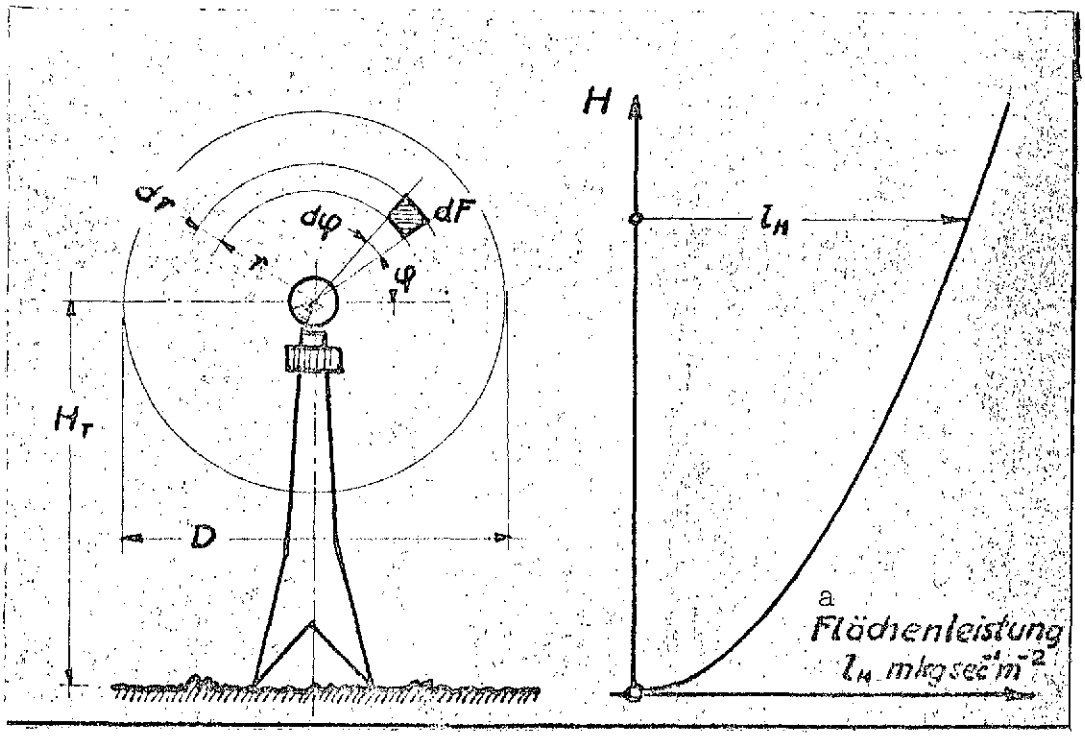

Fig. 17.

Key: a. Power per unit area

supplied on a large scale by wind power plants, the most remote of which are several hundred kilometers apart, the probability that days of zero energy generation will occur at all is so low that we can rule it out completely.

3. When an energy supply system involving a relatively large number of smaller wind power plants is set up, power can start being supplied once the first plant is constructed. The total available power thus increases continually as the number of plants put into operation increases. In the case of a large power plant whose erection requires the same length of time as several smaller power plants, energy can only be supplied once this single plant has been completely finished. This set of circumstances also represents a certain advantage of wind power over water power plants.

4. Relatively large numbers of equivalent power plants of medium size are more desirable in terms of installation. Fewer extensive facilities are required for their construction and for the delivery of all materials.

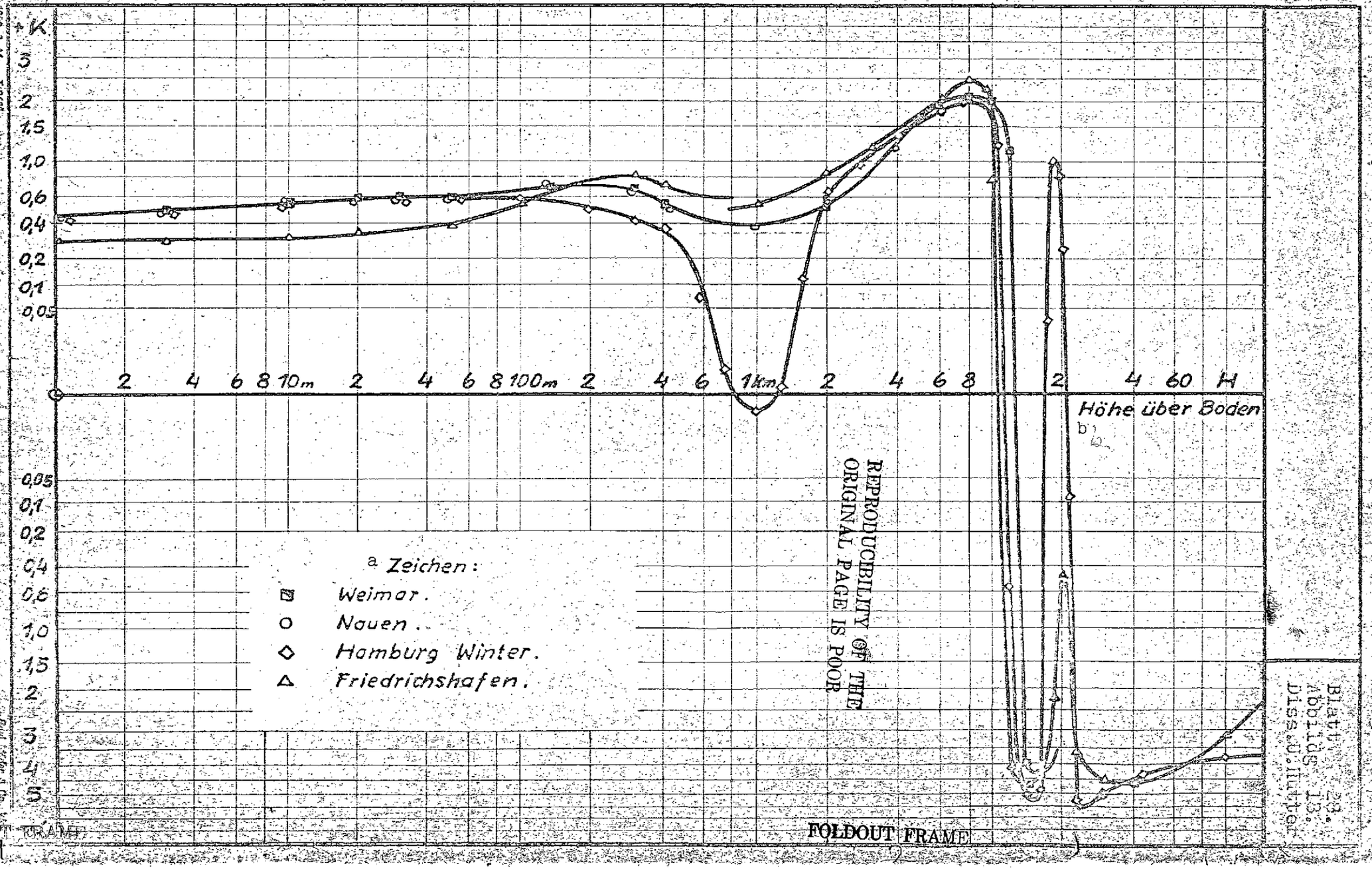

Fig. 18.

Key: a. Symbols; b. Altitude above ground

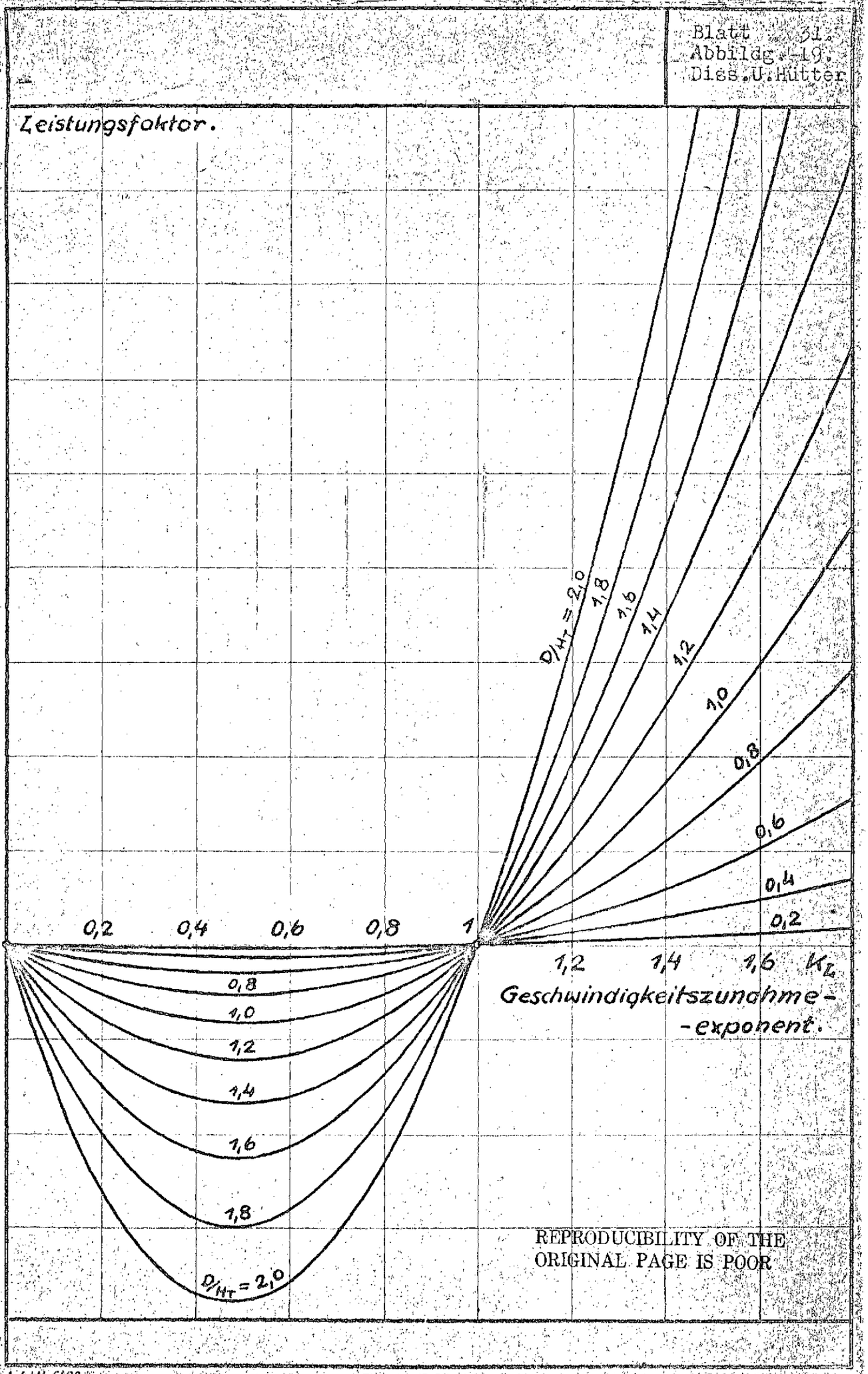

A 4 | N. 6900 Carl Schleicher & Schüll, D-5...

Fig. 19.

Key: a. Power factor; b. Velocity increase exponent

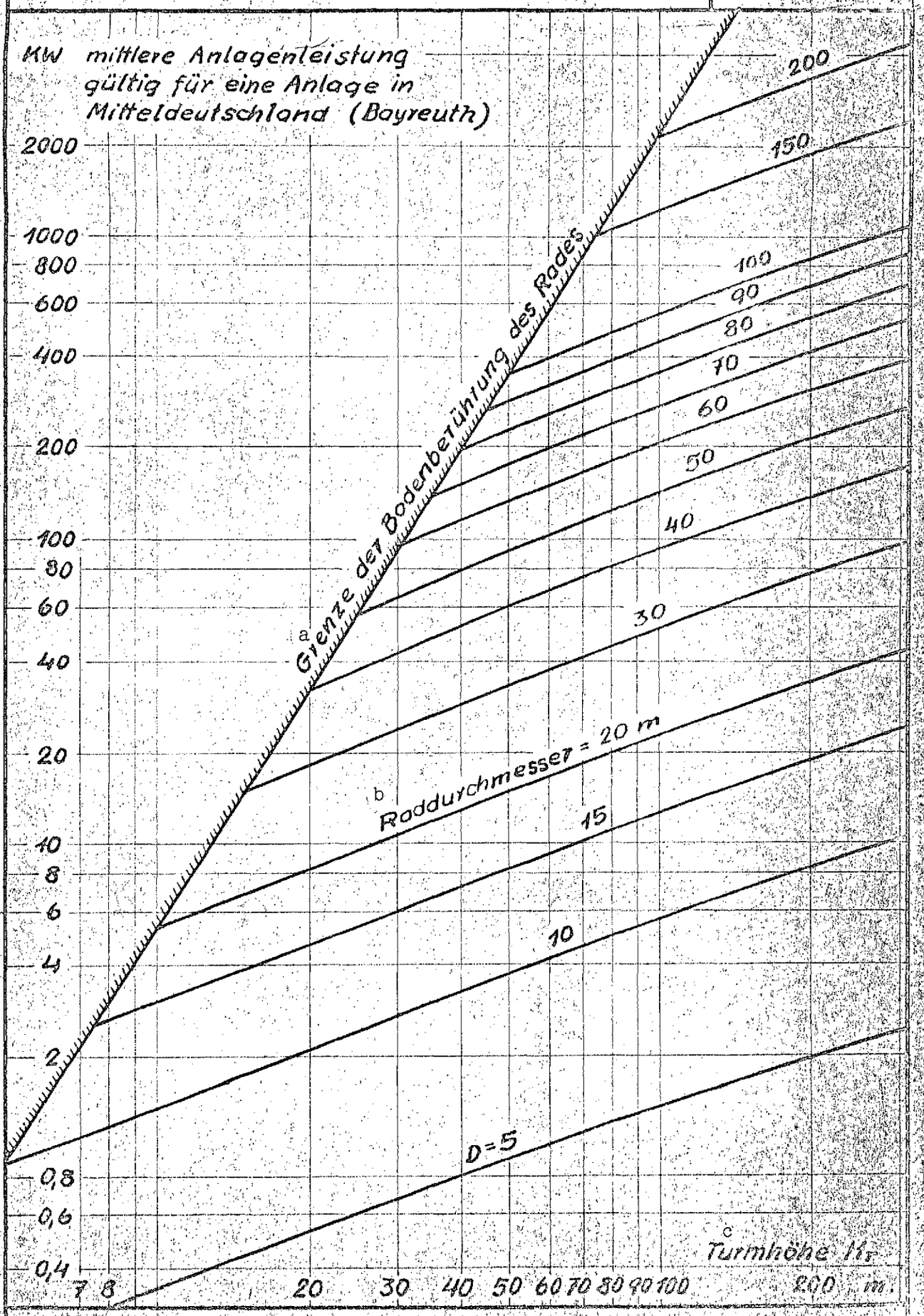

Fig. 20. Mean system power applicable to a system in central Germany (Bayreuth).

Key: a. Limit set by rotor contact with the ground; b. Rotor diameter; c. Tower height

Blatt 32.
Abbild. 21.
Dias.U.Hutter

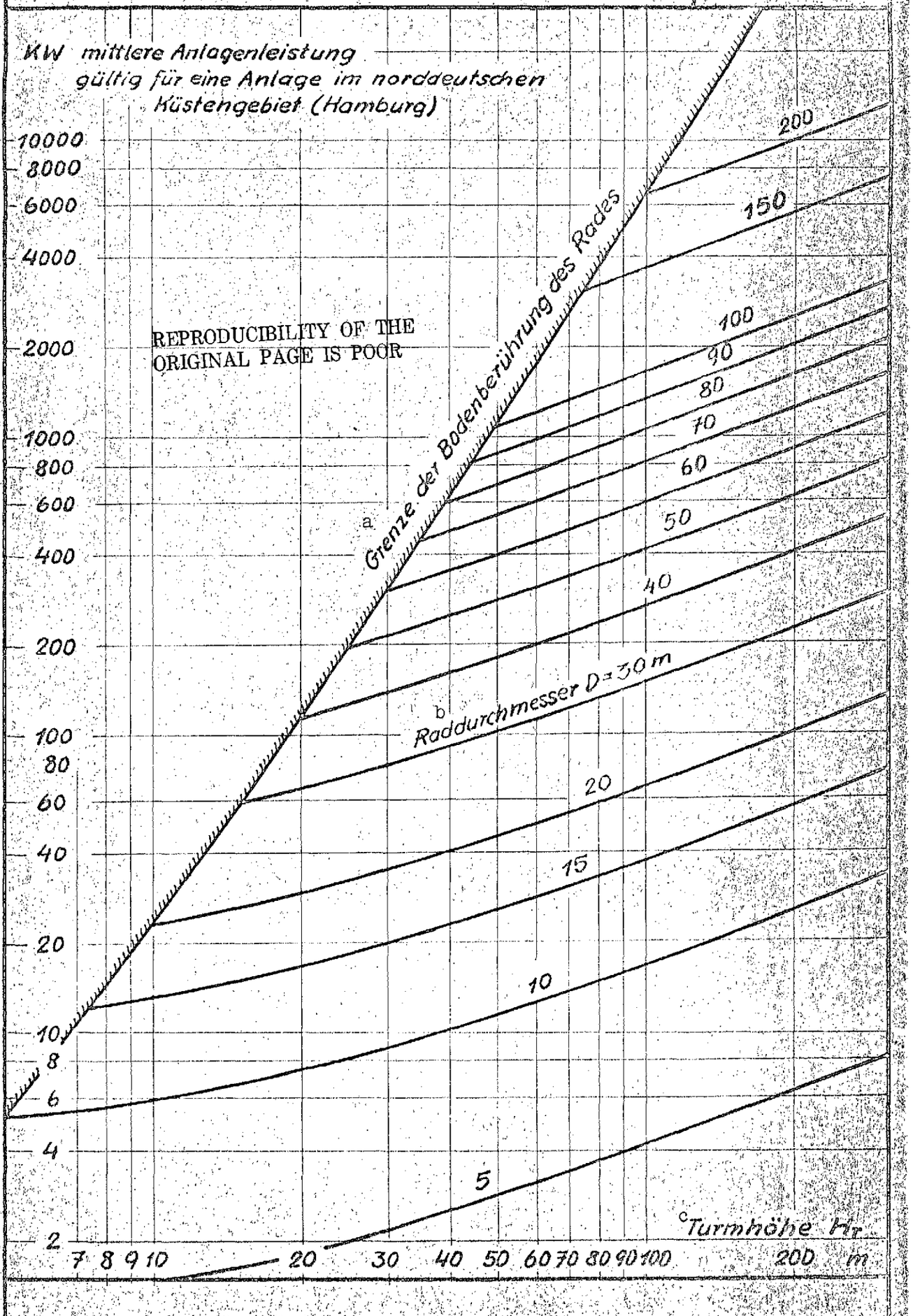

1000. 3. 41. - 1/0186 Paul Müller & Co.

Fig. 21. Mean system power applicable to a system in the Northern German coastal region (Hamburg)

Key: a. Limit set by rotor contact with the ground; b. Rotor diameter; c. Tower height

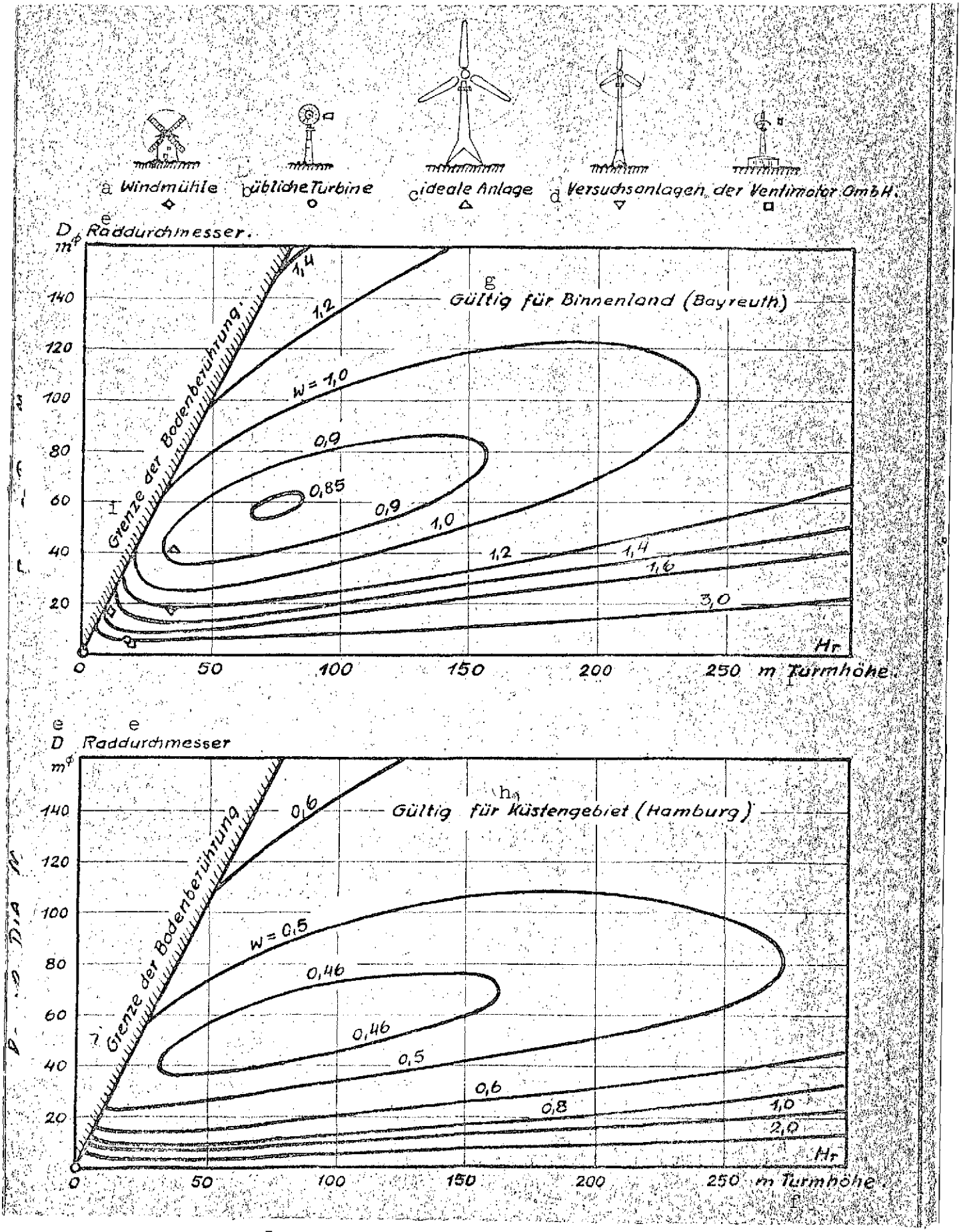

Fig. 22 [key on following page]

	5,355	10,4	m/sec
	14,8	108	kW
	43,6	248	kW
	25,3	111	kW
	91	254	kW
	3,6	2,29	

Key to Fig. 22.

a. Windmill
b. Conventional turbine
c. Ideal system
d. Experimental systems by Ventimotor GmbH
e. Rotor diameter
f. Turbine height
g. Applicable to inland areas (Bayreuth)
h. Applicable to coastal area (Hamburg)
i. Limit due to ground contact

5. Large power plants are dangerous obstacles to aviation. The hazard to aviation increases with power plant height. Since we must expect greater density in military and particularly in private air travel, especially after the War, this is an aspect which may by no means be underestimated. It should also be mentioned here that it is possible to also equip wind power plants with small shortwave transmitters and use them as beacon stations.

6. A rather obvious and important military advantage is the decentralization of the power supply system. In addition, smaller power plants are easier to camoflage and are also smaller targets.

Power plants with very small rotors are quite uneconomical. In particular, the effect of tower height is smaller for such systems than generally assumed. It is interesting that the old windmills are considerably more efficient than the "American" /37
wind turbines, in spite of the relatively low power coefficients of their rotors. In addition to this, the towers of windmills simultaneously serve as the mill buildings, and thus tower costs are practically nonexistent.

If the large-scale development of wind energy is planned for supplying power, it should also not be forgotten that the picture presented by the landscape will be given a unique character by the large number of power plants. These would therefore have to possess a timeless beauty, in a rather profound sense, so that they do not represent a burden to a later generation, three or four decades hence, as enduring skeletons of a hasty experiment indifferent to imponderable values of our lebensraum. (Fig. 23)

4. Behavior of a Rotor Element /39

The concept of the rotor element is introduced for the following discussion. Let this element consist of an annular

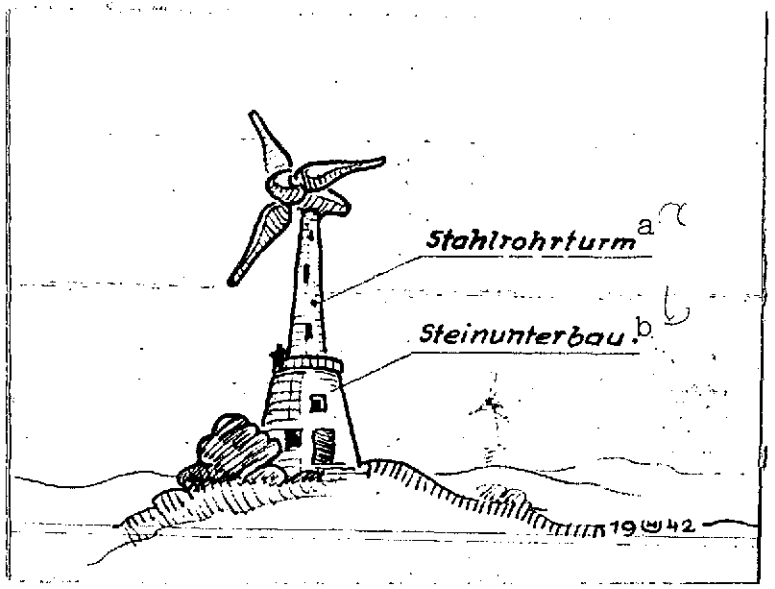

Fig. 23.

Key: a. Tubular steel tower; b. Substructure of rock

deflection mechanism of height dr at a distance r from the center. It is assumed for the time being that the effects of the remaining parts of the rotor do not influence this element [3, 9] (Fig. 24).

A. Velocities

In accordance with the notation which is conventional in turbine and propeller theory, let velocity far upstream from the element be v_0, velocity during passage through the element be v_∞, and velocity far downstream from it be v_3. Let the element rotate about the axis at angular velocity ω; thus its tangential velocity is $u_0 = r \cdot \omega$.

In the absence of a twist effect, the power taken up by the element is

$$dL = S \cdot v_\infty . \tag{12}$$

The kinetic energy of the wind is converted into the element's energy of rotation $dL = dM \cdot \omega$. This is possible only if an angular momentum is imparted to the air, i.e. a tangential velocity $\Delta u = r \cdot \Delta\omega$ imparted to the mass passing through the annulus per second. Reactive moment dM is then [9, 14]

$$dM = r \cdot \dot{m} \cdot \Delta u = \dot{J} \Delta\omega \tag{13}$$

and the power loss due to twist is

$$dL_D = \dot{J} \frac{\Delta\omega^2}{2} = dM \cdot \frac{\Delta\omega}{2}$$

Power equilibrium can thus be formulated:

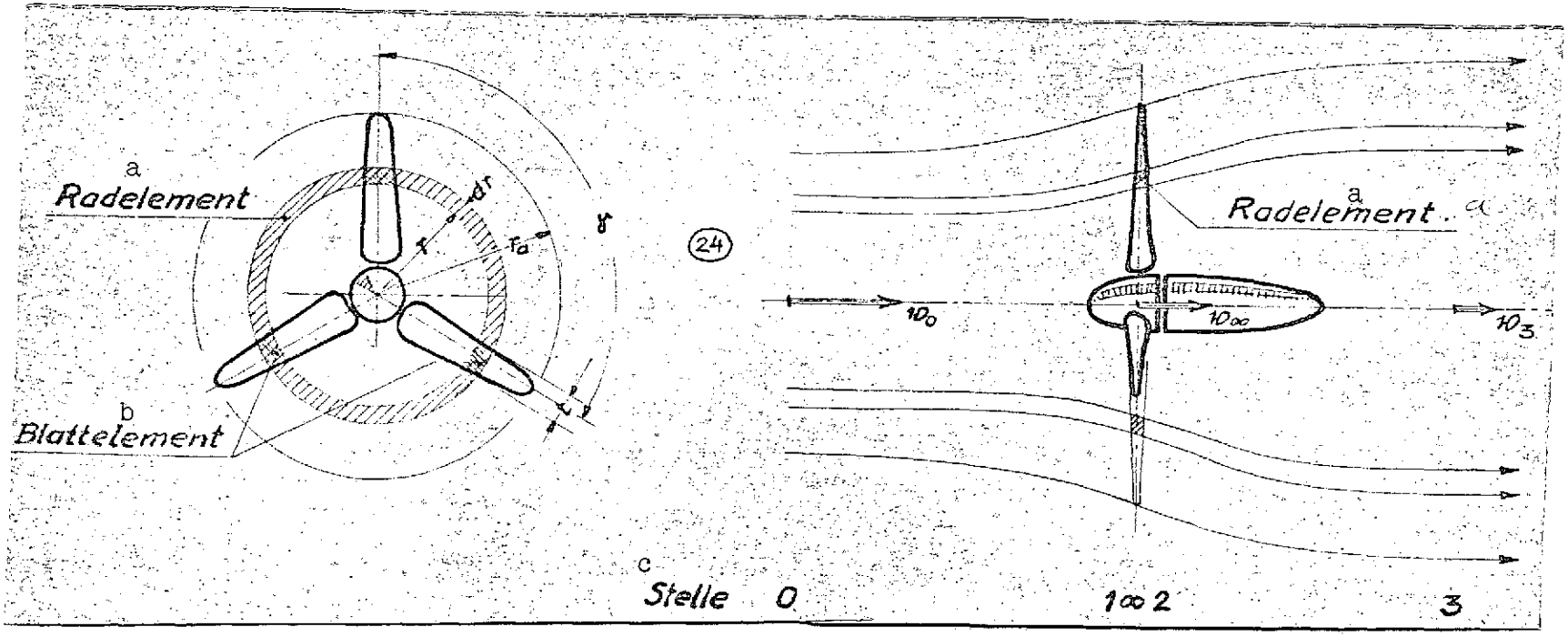

Fig. 24.

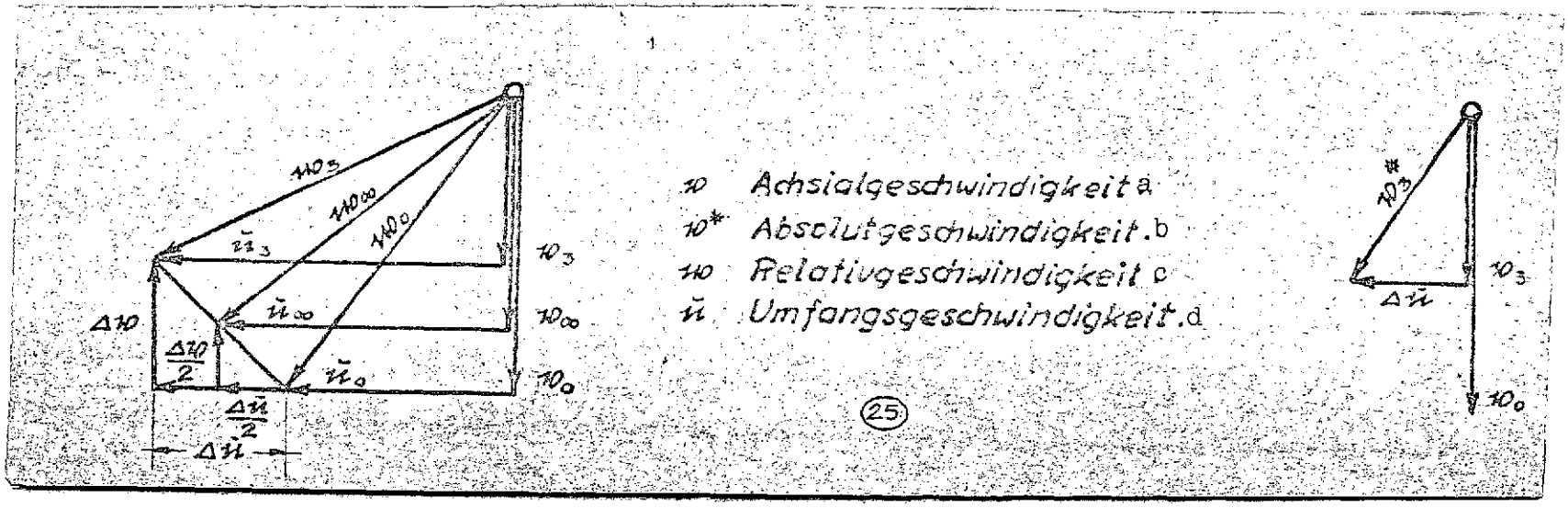

Fig. 25.
[Keys on following page].

Key to Fig. 24

a. Rotor element
b. Blade element
c. Position

Key to Fig. 25

a. Axial velocity
b. Absolute velocity
c. Relative velocity
d. Tangential velocity

$$dM \cdot \omega = dS \cdot v_\infty - dM \frac{dw}{2} \tag{14}$$

where /41

$$v_\infty = v_0 - \frac{\Delta v}{2}$$

$$v_\infty = \frac{v_0 + v_3}{2} \tag{15}$$

We obtain these results from a consideration of momentum and power [3].

Momentum: $dS = v_\infty \cdot \rho \cdot dF \cdot \Delta v$

Power: $dS \cdot v_\infty = v_\infty \frac{\rho}{2} dF \cdot (v_0^2 - v_3^2)$

$$\frac{\rho}{2} dF (v_0 - v_3)(v_0 + v_3) = \rho \cdot dF \cdot (v_0 - v_3) \cdot v_\infty$$

If we call the tangential force on the element dT, we obtain the following from (14):

$$dT = \frac{dM}{r}$$

$$dT\left(u_0 + \frac{\Delta u}{2}\right) = dS\left(v_0 - \frac{\Delta v}{2}\right)$$

$$dT \cdot u_\infty = dS \cdot v_\infty$$

$$u_\infty = u_0 + \frac{\Delta u}{2} \qquad (16)$$

The power actually taken up by the rotor can now be determined by comparing the energy content of flow far upstream and far downstream from the rotor. Velocity far downstream from the rotor is

$$w_3^* = w_3 + \Delta\tilde{u} \qquad \text{(Fig. 25)}$$

$$dM\,\omega = \frac{\dot{m}}{2}\left(v_0^2 - v_3^{*2}\right)$$

$$v_3^{*2} = v_3^2 + \Delta\tilde{u}^2$$

$$\dot{m}\, r\, \Delta\tilde{u}\, \frac{\tilde{u}}{r} = \frac{\dot{m}}{2}\left(v_0^2 - v_3^2 - \Delta u^2\right) \qquad (17)$$

If we introduce the concept of the velocity-reduction ratio $\xi = v_3/v_0$ and make use of the following abbreviations, /42

$$\xi = \frac{v_3}{v_0}$$
$$\mu = 1 + \xi$$
$$\kappa = 1 - \xi^2 \qquad (18)$$

we then obtain the following from (17)

$$2u\,\Delta u = v_0^2 \cdot \kappa - \Delta u$$

$$(u + \Delta u)^2 = v_0^2 \kappa + u$$

$$\Delta u = \sqrt{v_0^2 \kappa + u^2} - u \qquad (19)$$

$$u_\infty = u + \frac{\Delta u}{2} = \frac{1}{2}\left(u_0 + \sqrt{v_0^2 \kappa + u^2}\right) \tag{20}$$

$$v_\infty = v_0 \frac{\mu}{2} \tag{15a}$$

$$v_3 = v_0 \xi \tag{21}$$

$$v_3^* = \sqrt{v_0^2 \xi^2 + \Delta u^2} \tag{22}$$

B. Power Coefficient Without Friction

If we now define the ratio of the power actually extracted from the wind to the power content of the wind flowing undisturbed through the plane of the rotor as the power coefficient

$$c_L = \frac{L}{L_m} \tag{23}$$

where $L_m = F_{RAD} \cdot q \cdot v_0 = v_0^3 \cdot \frac{\varrho}{2} \cdot F_{RAD}$ (24) (see 2),

we obtain the following power coefficient for the element without friction, taking twist into effect: /43

$$c_{La} = \frac{F \frac{\varrho}{2} v_\infty \left(v_0^2 \kappa - \Delta u^2\right)}{F \frac{\varrho}{2} v_0^3} = \frac{\mu}{2 v_0^2}\left(v_0^2 \kappa - \Delta u^2\right)$$

$$c_{La} = \frac{\mu}{2}\left(\kappa - \frac{\Delta u^2}{v_0^2}\right) \tag{25}$$

If we apply the following general notation:

(26)

$\lambda = \frac{u}{v}$ specific speed,

$\lambda_0 = \frac{u_0}{v_0}$ ratio of undisturbed velocities,

$\lambda_\infty = \frac{u_\infty}{v_\infty}$ ratio of velocities in plane of rotor,

we obtain the following from (19):

$$\Delta u^2 = v_0^2 k + u_0^2 - 2u_0\sqrt{v_0^2 k + u_0^2} + u_0^2$$

$$\frac{\Delta u^2}{v_0^2} = k + 2\lambda_0^2 - 2\lambda_0\sqrt{k+\lambda_0^2}$$

$$c_{La} = \lambda_0 \mu \left(\sqrt{k+\lambda_0^2} - \lambda_0\right) \qquad (27)$$

If we introduce the symbol

$$\sigma = \sqrt{k+\lambda_0^2} \qquad (28)$$

for the root, the expression simplifies to

$$c_{La} = \lambda_0 \mu (\sigma - \lambda_0) \qquad (29)$$

The actual power coefficient is accordingly a function of specific speed and velocity ratio, only (Figs. 26 and 27).

For a given specific speed, it is possible to determine the best value for the velocity ratio by means of a simple maximum calculation. From (29) we obtain the following with (18):

$$\frac{dc_{La}}{d\xi} = \frac{\lambda_0}{\sqrt{1+\lambda_0^2-\xi^2}}\left(1+\lambda_0^2-2\xi^2-\xi-\lambda_0\sqrt{1+\lambda_0^2-\xi^2}\right) = 0 \qquad /45$$

$$4\xi^4 + 4\xi^3 - 3a\xi^2 - 2a\xi + a = 0 \quad ; \quad a = 1+\lambda_0^2 \qquad (30)$$

In solving this equation we obtain a relationship between $\xi_{optimum}$ and λ_0. All ξ_{opt} lie between 1/2 and 1/3. Even just beyond $\lambda_0 \sim 3$, ξ_{opt} very rapidly approaches the limiting value 1/3, corresponding to the optimum condition formulated by Professor Betz for a twist-free jet [3]. (Table, p. 44)

It should just be noted here, too, that the optimum is quite flat. The permissible deviation from the best value of ξ_{opt} is ± 0.020 if we permit a power loss of 1 %.

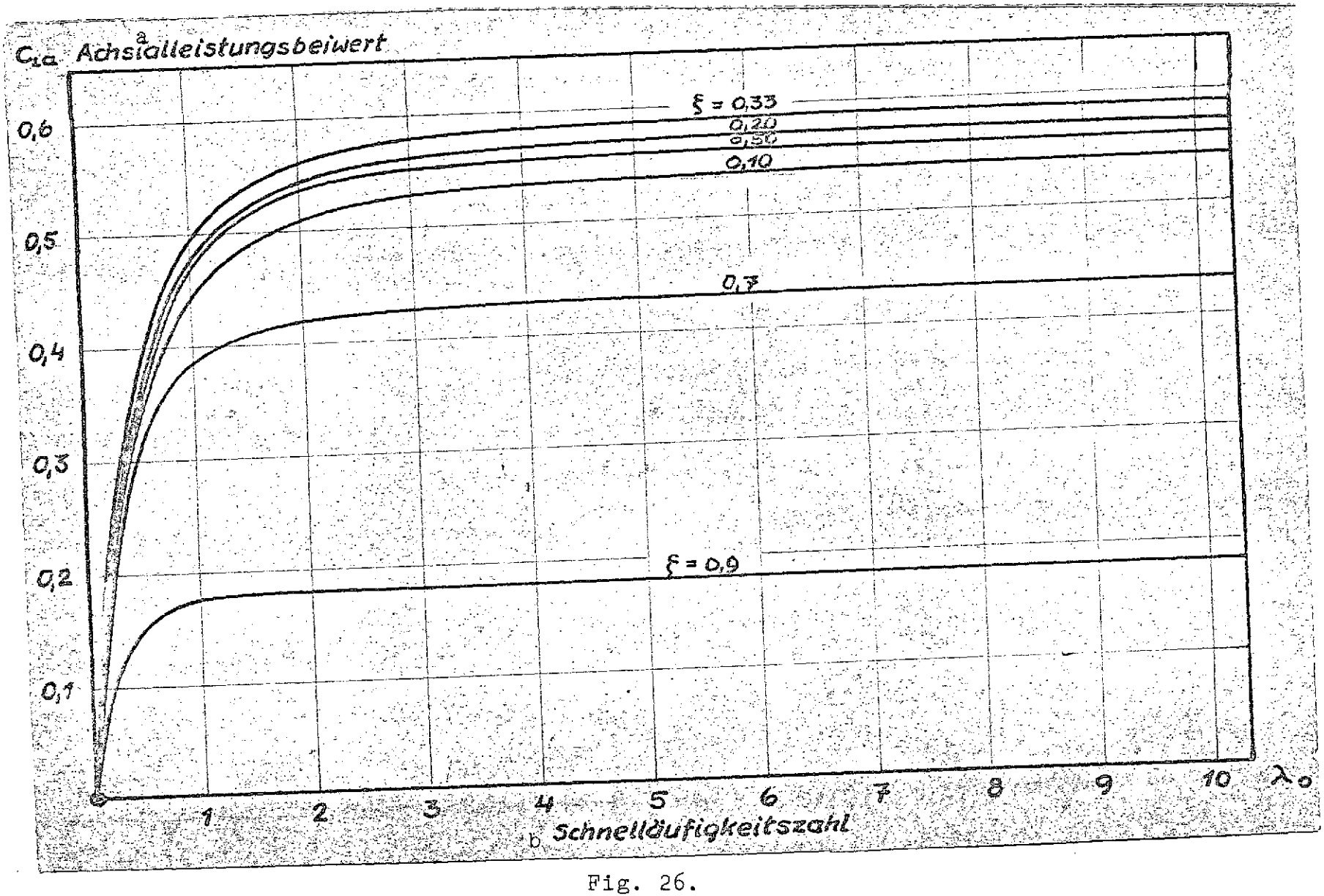

Fig. 26.

Key: a. Axial power coefficient
b. Specific speed

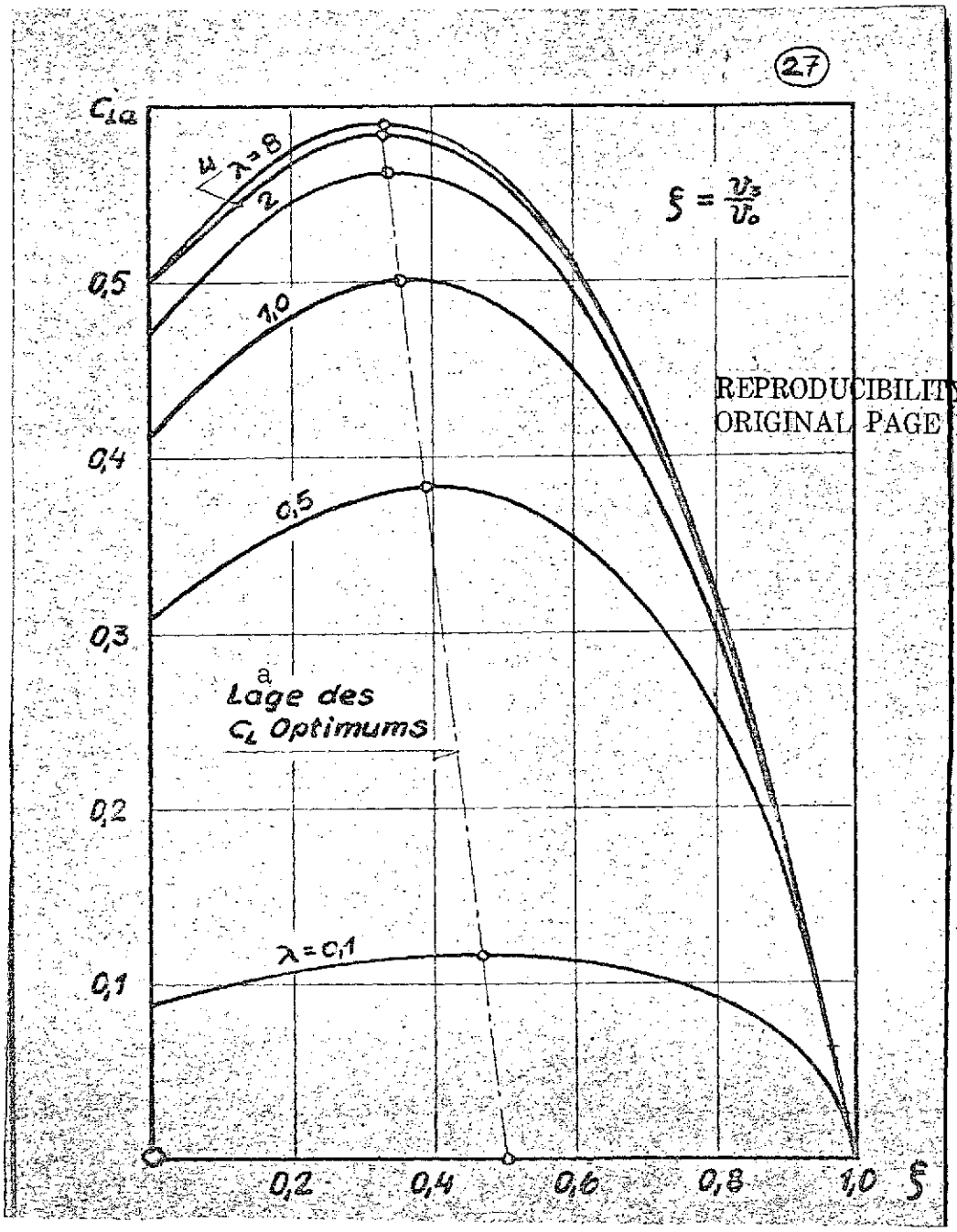

Fig. 27.

Key: a. Location of optimum in c_L

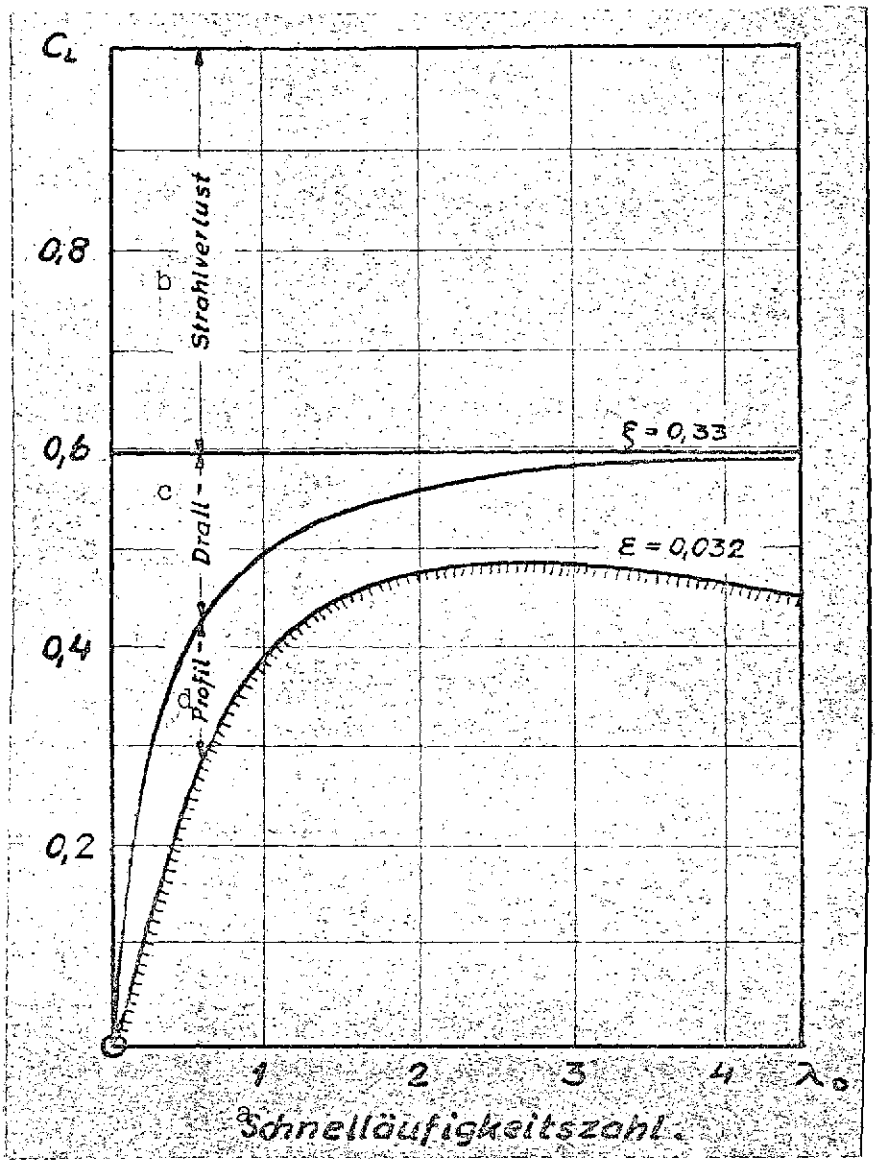

Fig. 28. Losses at rotor element.

Key: a. Specific speed
b. Jet loss
c. Twist
d. Profile

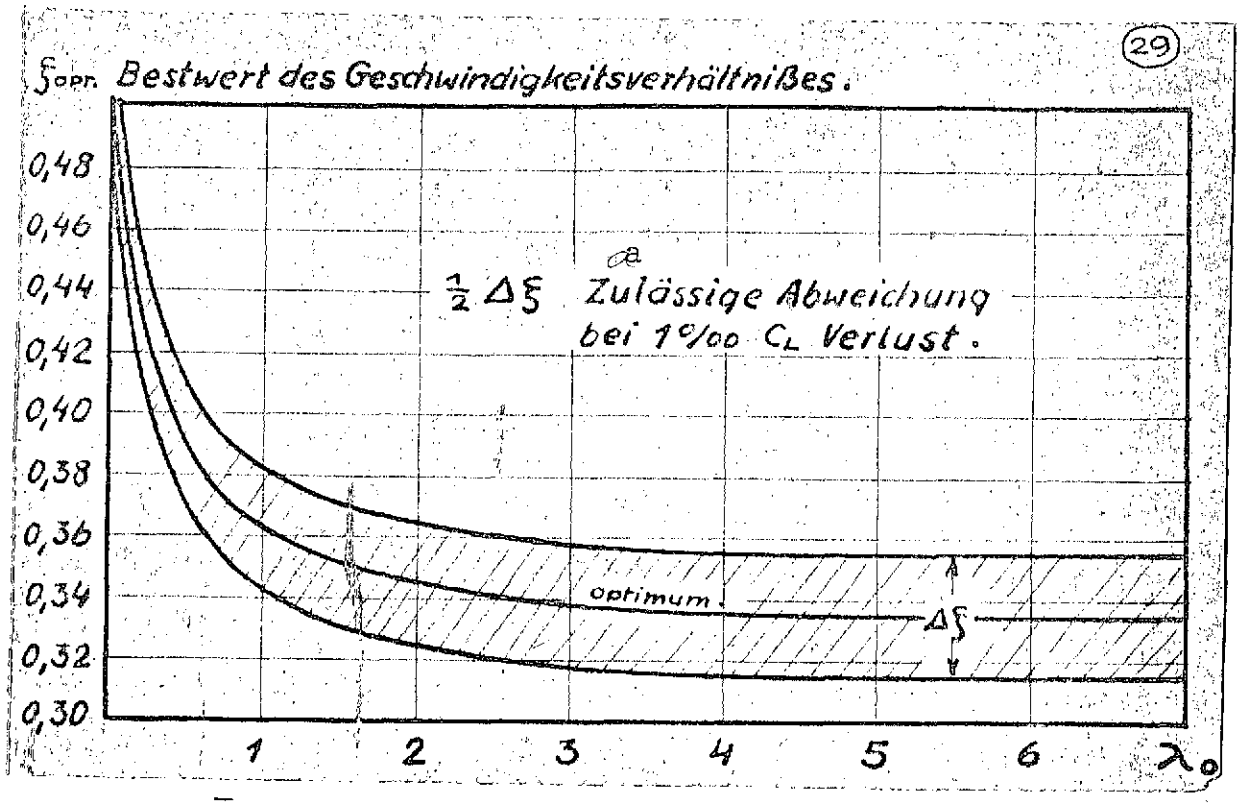

Fig. 29. Best value for velocity ratio.

Key: a. Permissible deviation for 1 °/oo c_L loss.

C. The Moment Coefficient. /48

If we define the moment coefficient to be

$$c_d = \frac{M_d}{q \cdot r_a \cdot F_{rotor}} \qquad (31)$$

λ_o	ξ optimum
0	0,500
0,2	0,436
0,4	0,420
0,6	0,371
1,2	0,357
2,0	0,345
2,6	0,339
3,6	0,336
6,0	0,335
∞	0,333

we obtain the following for the element:

$$dM_d = c_d \cdot v_0^2 \frac{\rho}{2} \cdot r_a \, dF$$

$$dL = dM \, \omega = dM \cdot \frac{u}{r_a}$$

$$c_L = \frac{dL}{dL_m} = \frac{c_d \, v_0^2 \frac{\rho}{2} \cdot r_a \cdot dF \frac{u}{r_a}}{v_0^3 \frac{\rho}{2} dF} = c_d \cdot \frac{u}{v_0}$$

Thus $c_L = c_d \cdot \lambda_0$ and $\boxed{c_d = \frac{c_L}{\lambda_0}}$ (32)

This relationship has quite general validity (Fig. 33).

The moment coefficient can thus be determined from the power coefficient, with the exception of the point $\lambda_0 = 0$. (It is also possible to determine c_d there from $dc_L/d\lambda$.)

D. Inclusion of Friction

In the case of no friction, the direction of resultant aerodynamic force from dS and dT,

$$\boxed{dR = dT + dS} \qquad (33)$$

is given by the perpendicular to the direction of the vector of the velocity of flow through the plane of the blade (Fig. 30). This and the axial direction enclose the angle ϕ_∞. The deflection process actually does not take place without friction. The resultant aerodynamic force is therefore inclined at angle of glide $\varepsilon = \arctan dW/dA$ relative to R_{ideal}; dA and dW are the components of dR perpendicular to W_∞ and in w_∞.

We can now specify the energy taken up by the rotor and that removed from the wind as the products of tangential velocity or velocity of flow through the rotor and the axial and tangential forces, in terms of their components (derived in a somewhat different form by Betz and Weinig):

power taken up by rotor: $L_R = dT \cdot u_0$

energy removed from wind: $L_W = dS \cdot v_\infty$ (34)

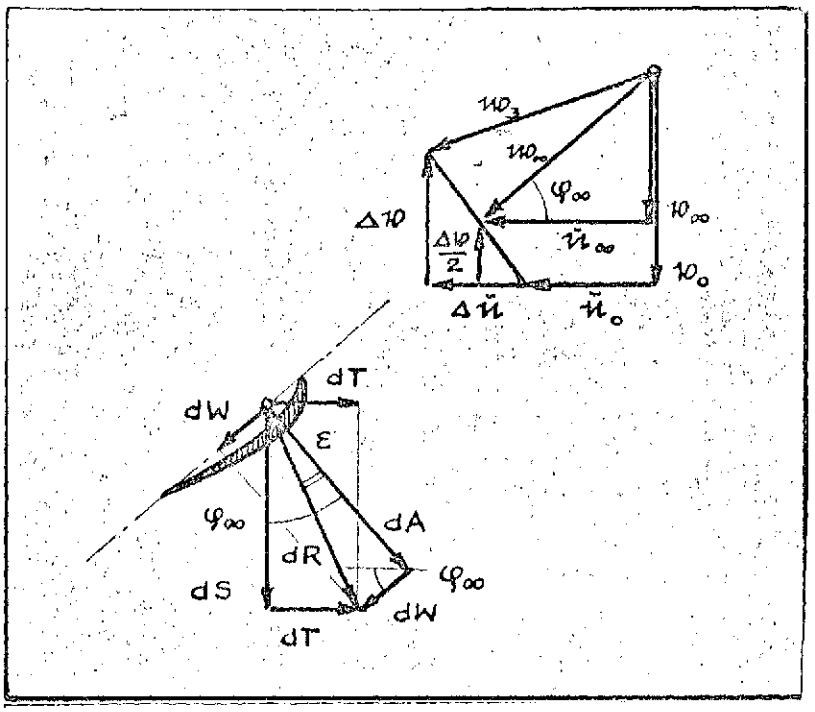

Fig. 30.

The ratio between these powers is the profile efficiency of the rotor: /49

$$\eta_p = \frac{L_R}{L_W} \tag{35}$$

where

$$dT = dA \cdot \sin\varphi_\infty - dW \cos\varphi_\infty$$

$$dS = dA \cos\varphi_\infty + dW \sin\varphi_\infty$$

$$\eta_p = \frac{u_0 (dA \sin\varphi_\infty - dW \cos\varphi_\infty)}{v_\infty (dA \cos\varphi_\infty + dW \sin\varphi_\infty)} \tag{36}$$

and, after transformation

$$\eta_p = \frac{2\lambda_0}{\mu} \operatorname{tg}\varphi_\infty \frac{1 - \frac{\operatorname{tg}\varepsilon}{\operatorname{tg}\varphi_\infty}}{1 + \operatorname{tg}\varepsilon \operatorname{tg}\varphi_\infty}$$

i.e.

$$\eta_p = \frac{2\lambda_0}{\mu\lambda_\infty} \cdot \frac{1 - \operatorname{tg}\varepsilon\,\lambda_\infty}{1 + \frac{\operatorname{tg}\varepsilon}{\lambda_\infty}} \tag{37}$$

$$v_\infty = v_0 \frac{\mu}{2} \qquad \operatorname{tg}\varepsilon = \frac{dW}{dA}$$

$$\frac{u_0}{v_0} = \lambda_0 \qquad \operatorname{cotg}\varphi_\infty = \frac{u_\infty}{v_\infty} = \lambda_\infty$$

If, as is conventional in the mechanics of flight, we designate ctn ε as fineness ratio E and calculate λ_∞ from (14), (19), (20) and (29),

$$\lambda_\infty = \frac{\lambda_0 + \sigma}{\mu} \tag{38}$$

then, after transformation, we obtain

$$\eta_p = \frac{2\lambda_0}{\mu} \cdot \frac{E - \lambda_\infty}{E\lambda_\infty + 1} \tag{39}$$

(Fig. 31).

Now if $\lambda >> k$, then $\lambda_\infty \sim 2\lambda_0/\mu$, and if E is large, as will almost always be the case, i.e. ε is a small angle, then $1 + 1/E\lambda_\infty \sim 1$ in ( ) [sic], and profile efficiency assumes the following particularly simple form: /50

$$\eta_p = 1 - \frac{\lambda_\infty}{E} \tag{40}$$

If we take friction into consideration, the power and moment coefficients of the rotor element thus become

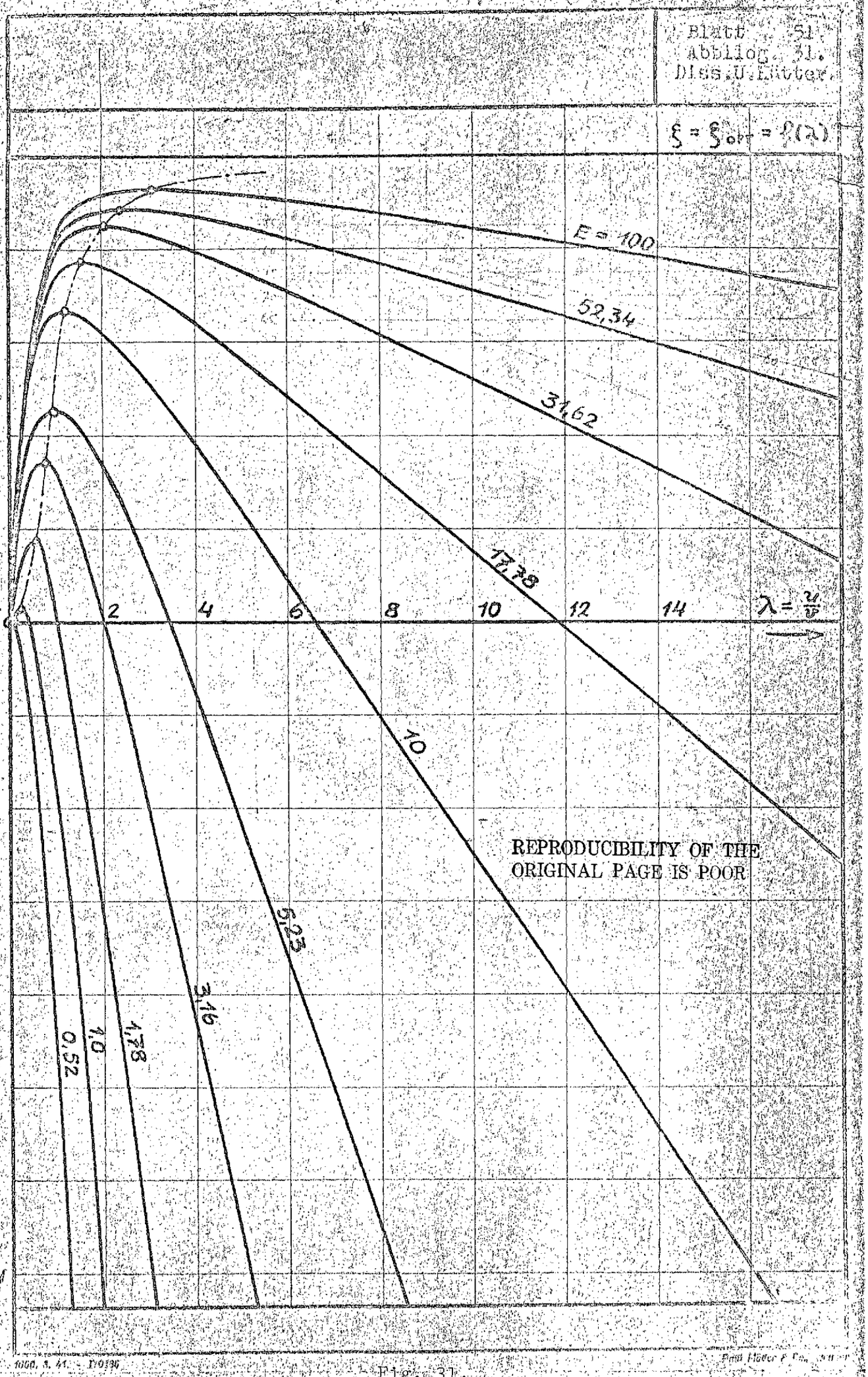

Fig. 31.

$$q = c_{La} \cdot \eta_P \qquad (32)$$

$$c_d = \frac{c_L}{\lambda_o}$$

$$c_L = 2\lambda_o^2 (\sigma - \lambda_o) \frac{\mu E - (\sigma + \lambda_o)}{\mu + E(\sigma + \lambda_o)} \qquad (41)$$

(Fig. 28).

E. Drag Coefficient Referred to the Circular Area

It is necessary to know the magnitude of a rotor's drag coefficient, referred to the circular area swept by the rotor, for the purpose of tower dimensioning.

We have

$$c_W = \frac{dS}{v_o^2 \frac{\varrho}{2} dF} \qquad (42)$$

For zero friction, with (14), (15) and (18) we have

$$c_W = 2 \frac{v_\infty \varrho \, dF (v_o - v_3)}{v_o^2 \varrho \cdot dF} = (1+\xi)(1-\xi)$$

i.e.

$$c_W = 1 - \xi^2 = K \qquad (43)$$

/52

An obvious result: c_W increases with increasing velocity reduction, i.e. with decreasing ξ; $c_W = 1.0$ can be reached as the limiting value.

Taking friction into consideration, we obtain the following with (15) and (40):

$$c_W = 2 \frac{dA \cos\varphi_\infty + dW \sin\varphi_\infty}{v_o^2 \varrho \cdot dF} = 2 \frac{dS}{v_o^2 \varrho \, dF} (1 + tg\varepsilon tg\varphi_\infty)$$

$$c_w = k\left(1 + \frac{\lambda_\infty}{E}\right) \qquad (44)$$

(Fig. 32)

This means that the highest drag coefficients are obtained when the profile exhibits poor fineness ratios at a high specific speed.

5. Rotor Characteristic

/54

It is necessary to know the relationship between the power coefficient and specific speed in order to evaluate the power which can actually be removed from the wind with a rotor and to match a rotor to a given piece of, say, electrical machinery. This relationship will first be determined for the rotor element.

A. Determination of the Relationship Between λ, ξ, c_a and E

For the following discussion it is necessary to imagine the deflection mechanism which forms the rotor element to actually be made up of a lattice[2] of profiles. We are given the angle enclosed by the O∞freestream direction of the lattice profile and the rotor's plane of rotation. Freestream velocity v_o is assumed to be fixed.

The specific speed of the element varies as rotor speed varies. It is also possible to consider rotor speed to be fixed and freestream velocity to be variable. The direction in which flow approaches the profile varies in both cases. The magnitude of lift on the element is obtained, on the one hand, from the momentum of the mass of air which passes through the annular area $2r\pi dr$ per unit time (Fig. 24) and, on the other hand, from the effective angle of attack of the individual lattice profile and the increase in lift coefficient with effective angle of attack for the given lattice. We thus obtain two relationships for the lift coefficient; in both cases, the lift coefficient is a function of velocity ratio ξ and specific speed λ_o. The slope of the lift coefficient versus effective angle of attack α_∞ has been calculated by F. Weinig [8, 9] for various lattice spacings.

---

[2] [Translator's note: Literal translation; sometimes refers to a cascade of vanes.]

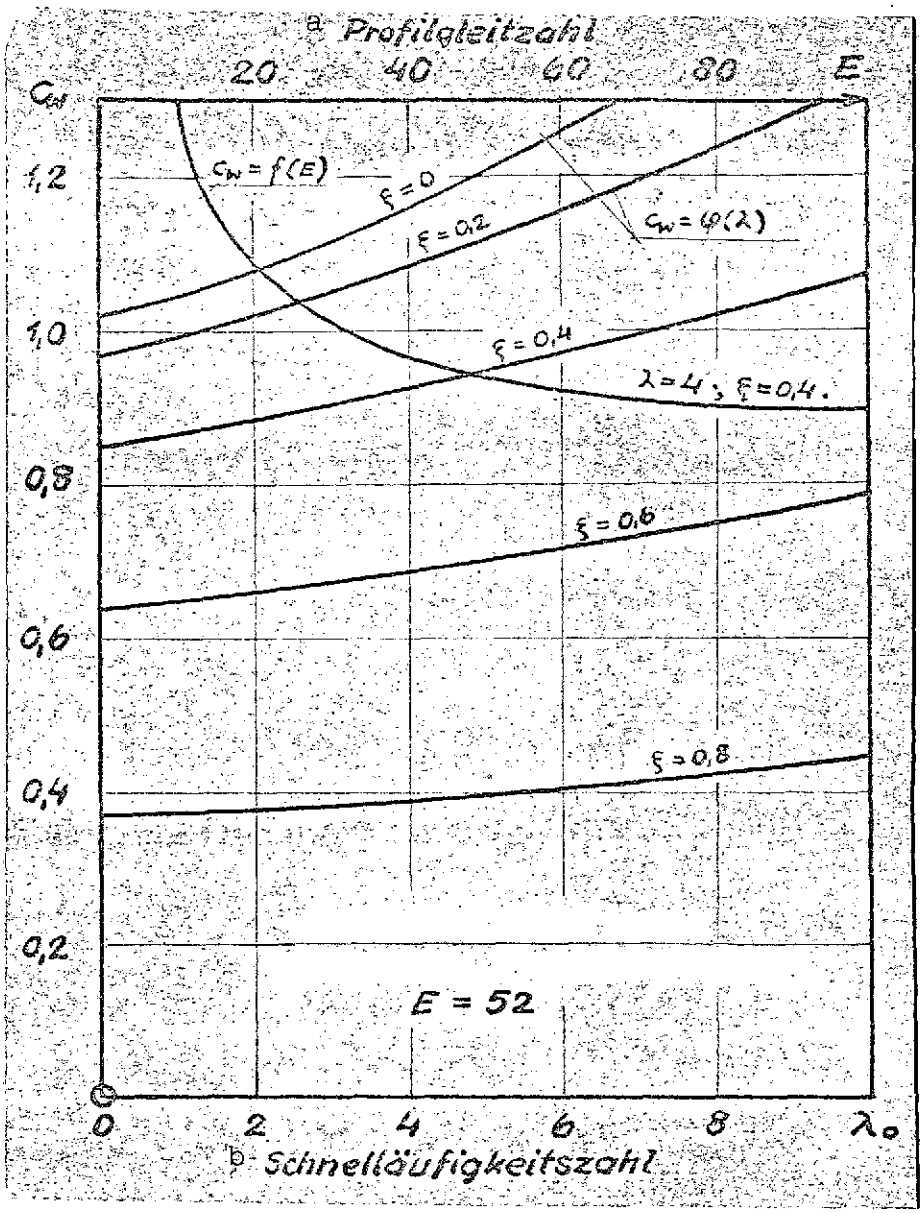

Fig. 32. Drag coefficient c_w, referred to the rotor's circular area.

Key: a. Profile fineness ratio
b. Specific speed

Momentum:

$$dA = \dot{m} \cdot \Delta w_1$$
$$\dot{m} = \varrho \cdot v_\infty \cdot 2r\pi\, dr \qquad (45)$$

General equation of aerodynamic forces:

$$dA = \frac{1}{2} c_a \cdot w_\infty^2 \cdot \varrho \cdot z \cdot t \cdot dr \qquad (46)$$ /55

where

z = number of blades
t = blade depth.

If we define lattice spacing as the ratio

$$\tau = \frac{2\pi}{z \cdot t} \tag{47}$$

then

$$c_a \cdot w_\infty^2 = 2\tau v_\infty \Delta w_\perp$$

$$c_a = 2\tau \frac{v_\infty \Delta w_\perp}{w_\infty^2} \tag{48}$$

where

$$\Delta w_\perp = \Delta w + \Delta \tilde{u} \tag{49}$$

(Fig. 29)

$$w_\infty = w_\infty + \tilde{u}_\infty \tag{50}$$

$$\Delta w_\perp = v_0 \sqrt{(1-\xi)^2 + (\sigma - \lambda_0)^2} \tag{49a}$$

$$w_\infty = \frac{v_0}{2} \sqrt{\mu^2 + (\sigma + \lambda_0)^2} \tag{50a}$$

$$v_\infty = v_0 \frac{\mu}{2} \tag{15a}$$

$$c_a = 4\tau\mu \frac{\sqrt{(1-\xi)^2 + (\sigma - \lambda_0)^2}}{\mu^2 + (\sigma + \lambda_0)^2} \tag{51}$$

(Fig. 34)

According to Weinig [8, 9], the lift coefficient for the profiles of the lattice is

$$c_a = 2\pi k_G \eta_d \sin \alpha_\infty \tag{52}$$

where α_∞ is the angle enclosed by w_∞ and the zero-lift direction of the profile; k_G indicates the effect of the lattice on the slope of the lift coefficient; η_d is the reduction in the slope of c_a due to different boundary layer thickness on the suction and compression sides.

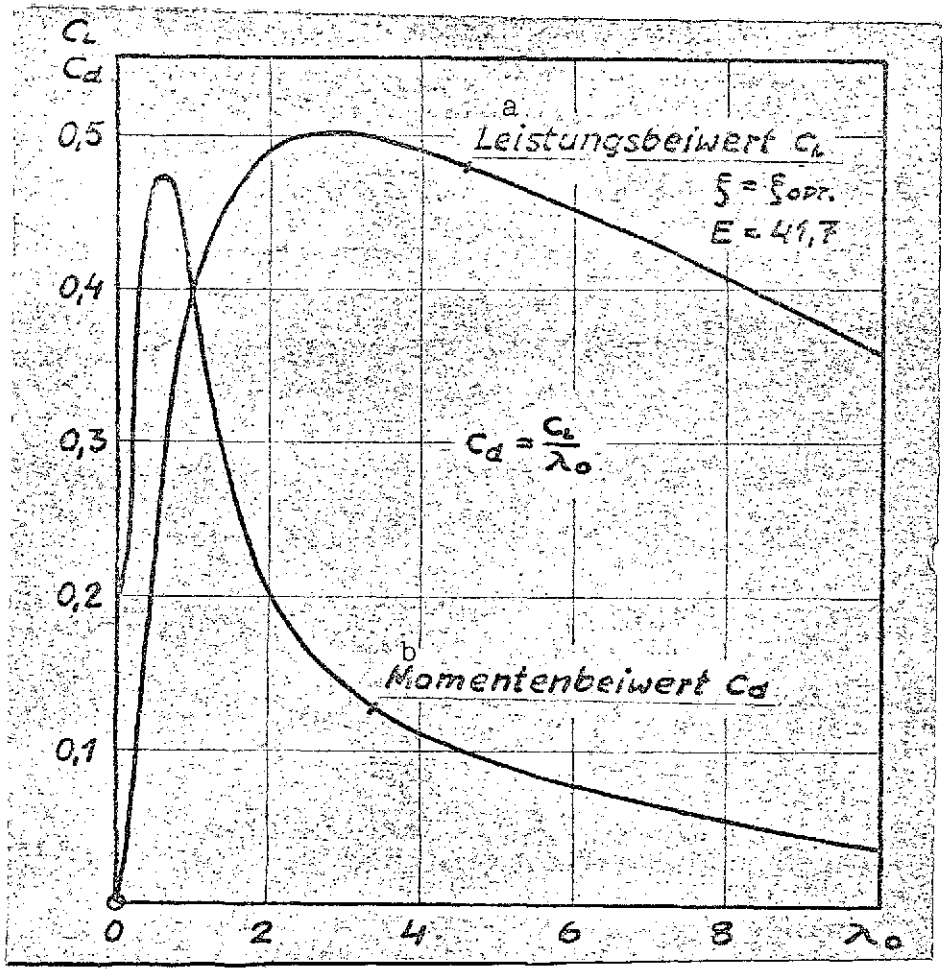

Fig. 33. Moment coefficient of the rotor element.

Key: a. Power coefficient
b. Moment coefficient

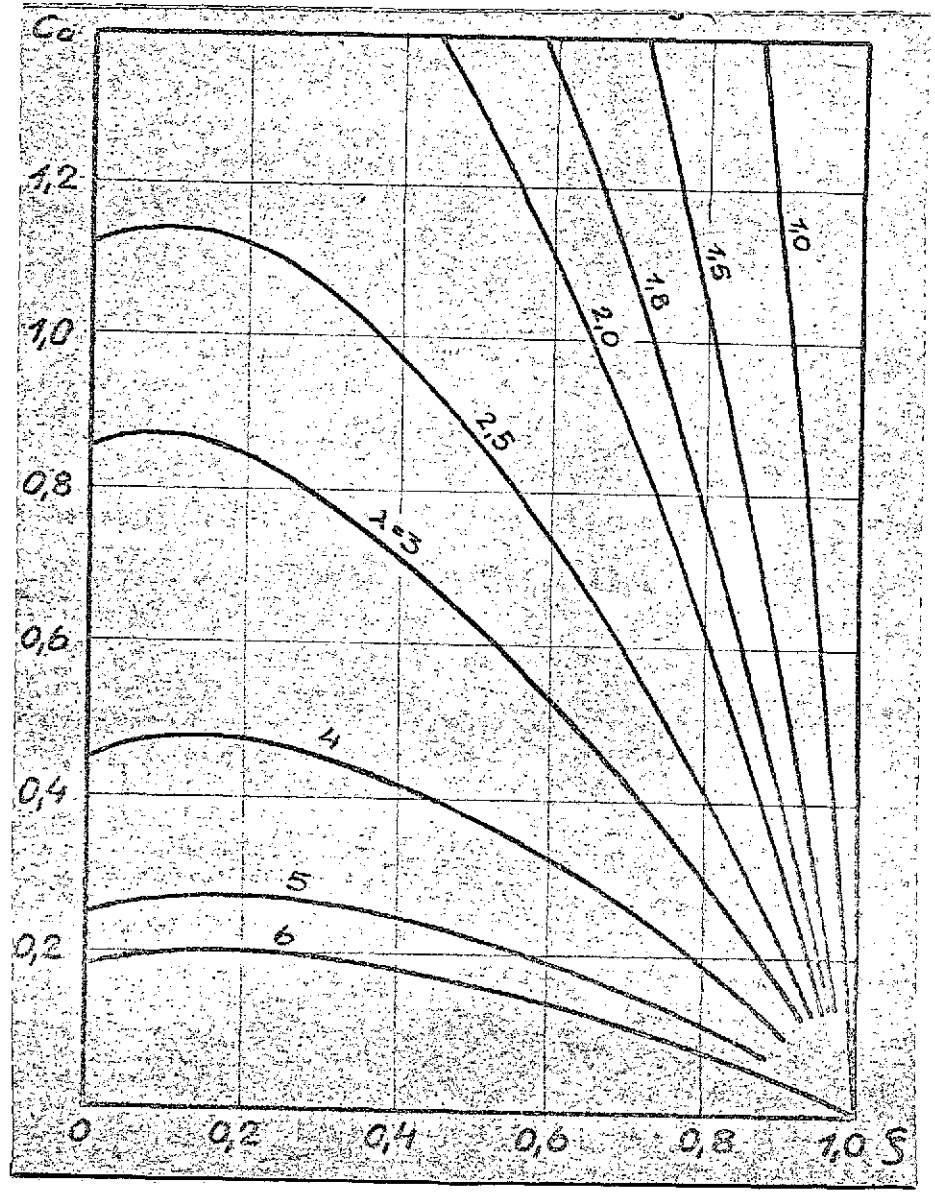

Fig. 34. Lift coefficient c_a from a consideration of momentum.

$$\eta_d = f(\text{profile thickness})$$

If the angle between the plane of the rotor and the zero-lift direction is β_o, then

$$\alpha_\infty = \varphi_\infty - \beta_o \tag{53}$$

and

$$c_a = 2\pi k_G \eta_d \cdot \sin\varphi_\infty \left(\cos\beta_o - \lambda_\infty \sin\beta_o\right)$$

where

$$\sin\varphi_\infty = \frac{v_\infty}{w_\infty}$$

and

$$\lambda_\infty = \operatorname{cotg}\varphi_\infty = \frac{u_\infty}{v_\infty} \tag{26}$$

Thus

$$c_a = \frac{2\pi k_G \eta_d}{w_\infty}\left(v_\infty \cos\beta_o - u_\infty \sin\beta_o\right)$$

With (19), (20) and (49a), we obtain

(Fig. 35)

$$c_a = \frac{2\pi k_G \eta_d}{\sqrt{\mu^2 + (\sigma+\lambda_o)^2}}\left(\mu\cos\beta_o - (\sigma+\lambda_o)\sin\beta_o\right) \tag{54}$$

The two relationships (51) and (54) are functions only of λ_o and ξ for given β_o, τ, k_G and η_d.

The magnitude of ξ can be determined for given λ_o by equating (51) and (54), yielding the axial power coefficients.

A graphic calculation brings us to our goal fastest here. The curves which represent c_a as a function of ξ are determined for the 4 to 7 λ_o values required, both from (51) and from (54).

The two families of curves plotted with the same c_a/ξ coordinates exhibit intersections for equal λ_o values which indicate c_a and ξ for the corresponding λ_o.

The relationship between lift coefficient c_a and fineness ratio E and thus profile efficiency is obtained from the measured polar curves for the profile used (Fig. 38).

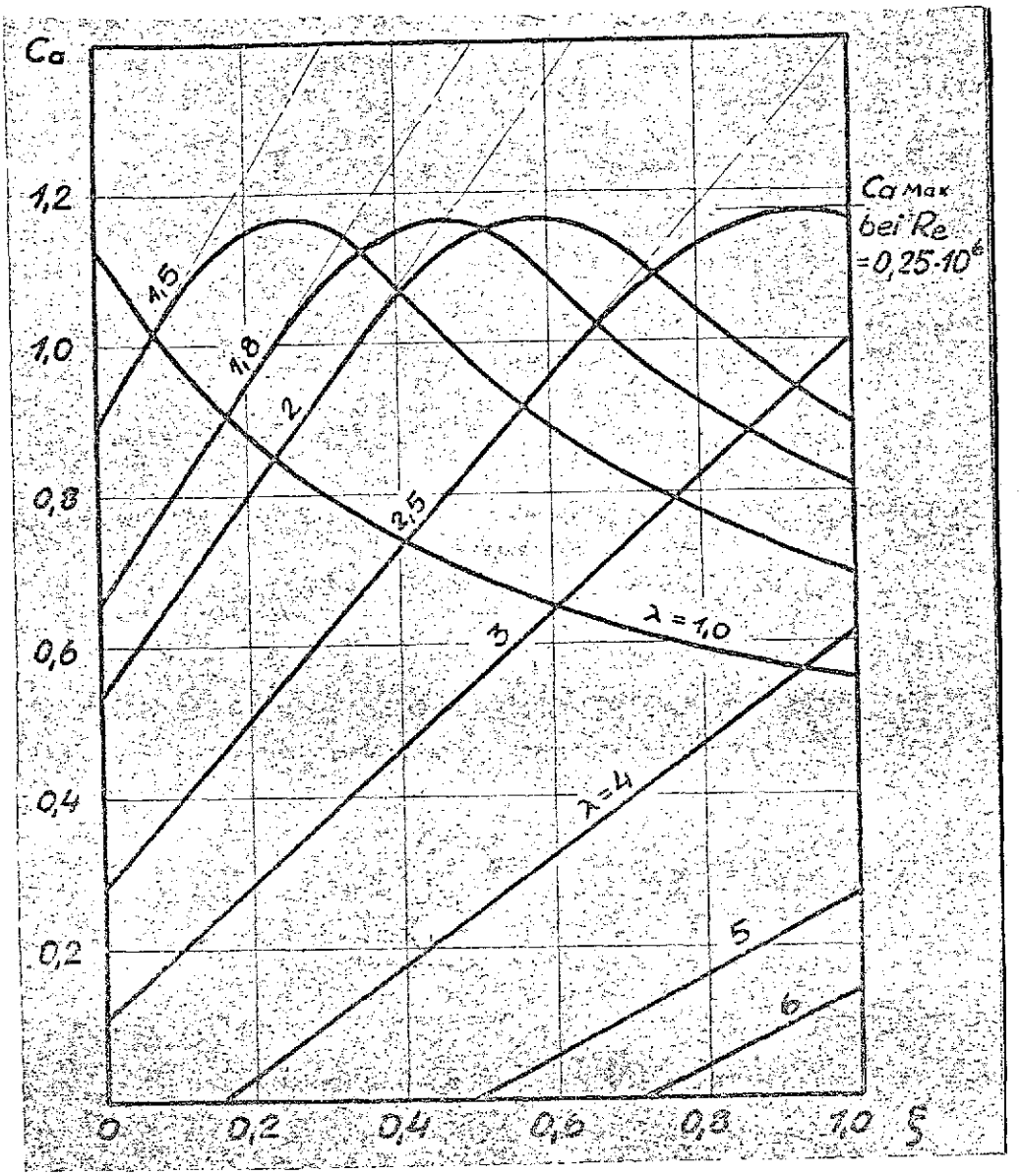

Fig. 35. Lift coefficient c_a from effective profile angle of attack.

Key: bei = at

The relationship between the power coefficient and the specific speed of the rotor element has thus been derived for the case without flow separation.

$$c_{\Sigma} = f(\lambda_o, \xi, E)$$

This case applies to wind rotors of small λ_o and large β_o.

B. Consideration of Separation of Flow /61

In the case of rotor elements designed for a high specific speed, i.e. where β_o is a small angle, flow separates on the blade at low speeds (small λ_o). This circumstance is not covered in (54). This formula can yield lift coefficients which are even higher than $c_{a\,max}$. In order to determine the actual lift coefficients, the linear behavior of c_a is continued beyond $c_{a\,max}$ in measured c_a/α curves, and the ratio of the resultant ideal value of c_a to the actual value of c_a is determined (Fig. 39).

$$p_{c_a} = \frac{c_{a\,effective}}{c_{a\,ideal}} \qquad (55)$$

This ratio is a function of $c_{a\,ideal}$ (Fig. 39). The c_a values resulting from (54), multiplied by the corresponding p_{c_a} values, yield the actual relationship between c_a and ξ for a given λ_o (Figs. 35-37). It should also be considered that the magnitude of $c_{a\,max}$ is a function of Reynolds number (Figs. 38, 39).

C. Application to the Entire Rotor

The λ_o/c_L diagram found for a given element of a rotor can be considered to apply to the entire rotor under the following conditions:

1. The distance of the "effective" element from the axis of rotation must be equal to the distance of the center of gravity of a sector of the rotor's circular area from the latter, if the jet of oncoming air is uniform, i.e.

$$r_{eff} \sim 0.75\, r_a$$

From the measured velocity distribution within this jet or from a consideration of the effect of twist and the effect of continuous vortex separation, we obtain

$$r_{eff} \sim 0.72\, r_a. \qquad (56)$$

2. The specific speed of the effective element must be converted to the λ_o for $r = r_a$: /62

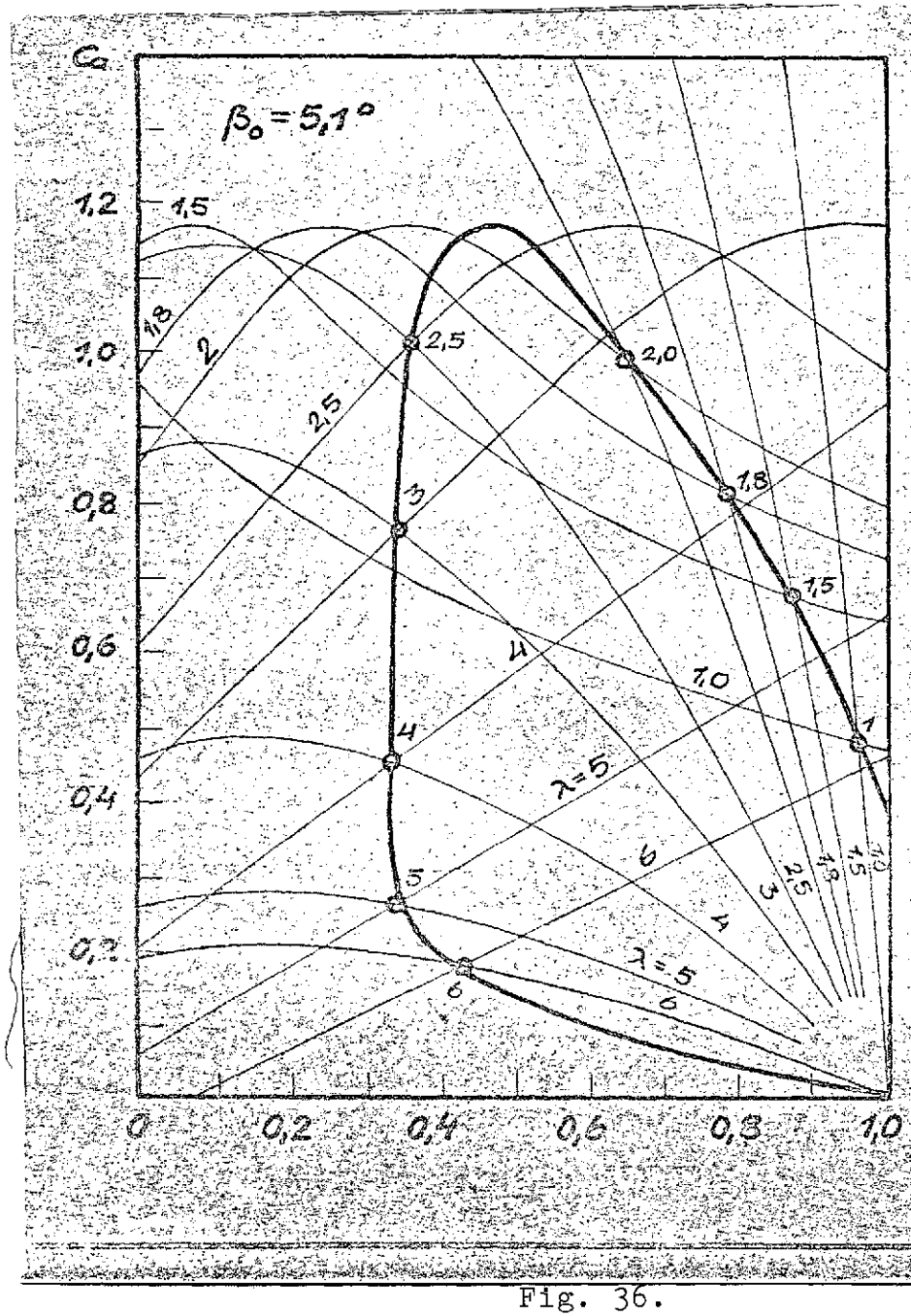

Fig. 36.

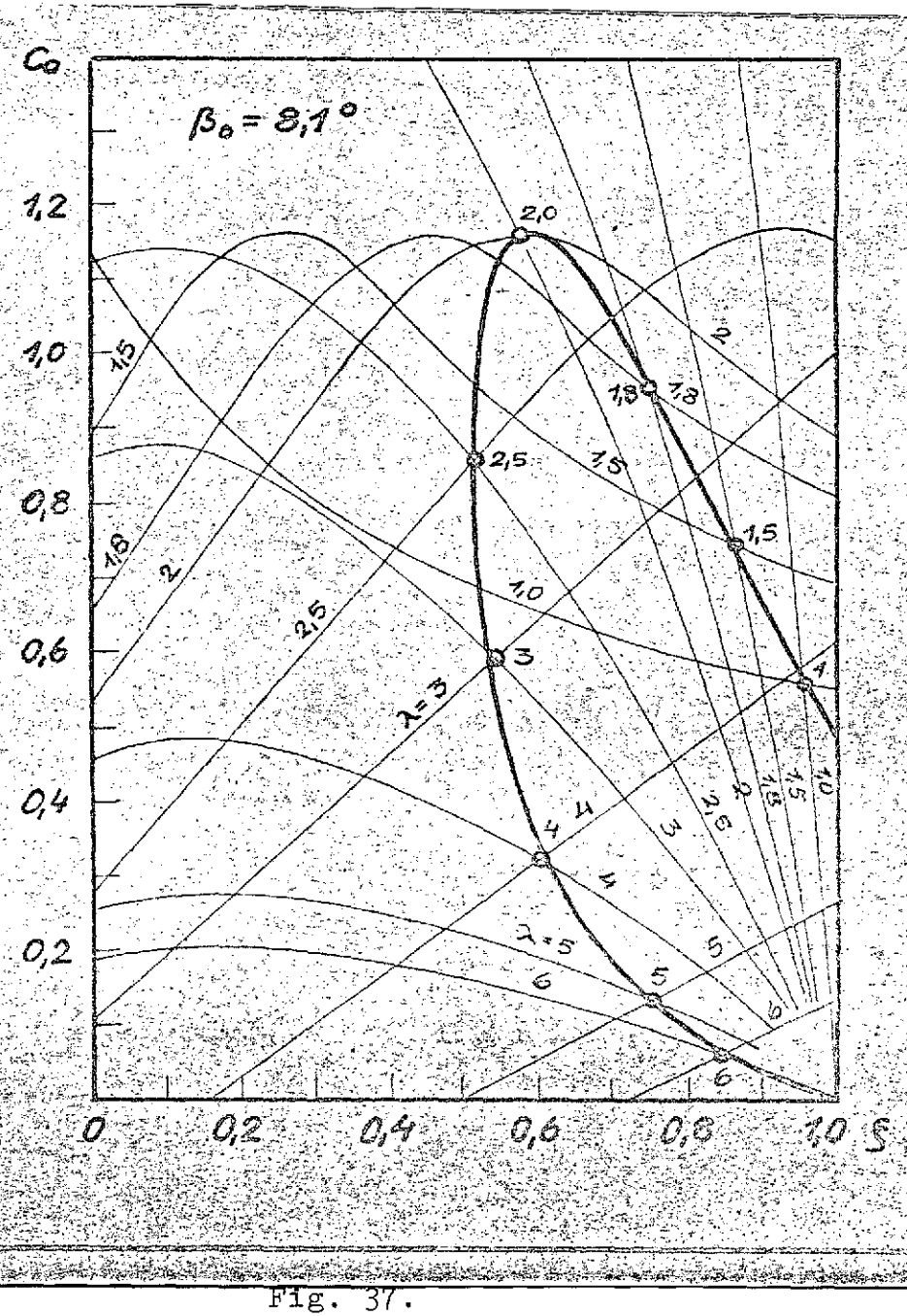

Fig. 37.

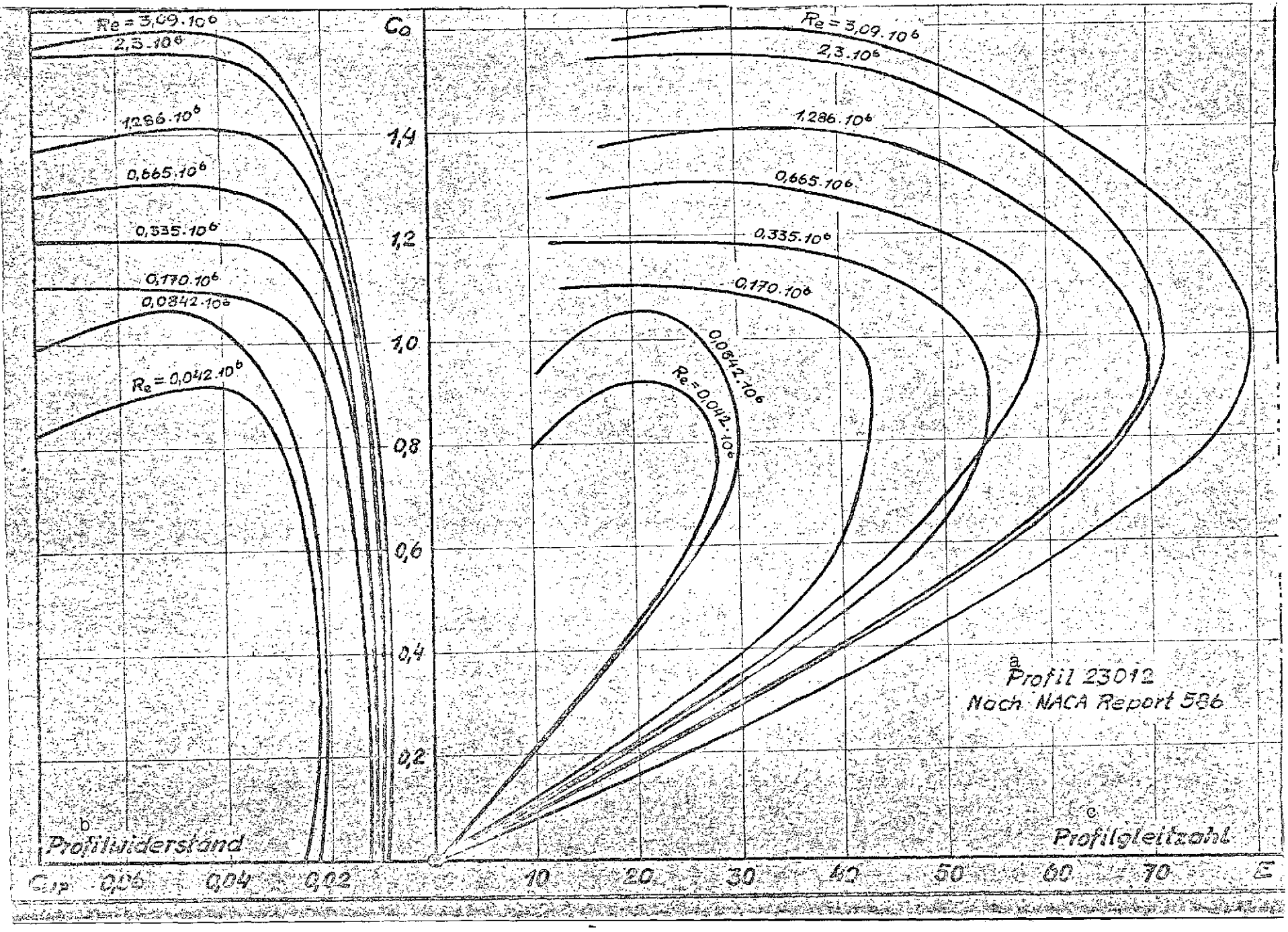

Fig. 38 [key on following page]

Key to Fig. 38

a. Profile 23012 from NACA Report 586
b. Profile drag
c. Profile fineness ratio

$$\lambda_{o\,r=r_a} = \lambda_r \cdot \frac{r_a}{r} \tag{57}$$

3. An additional correction for λ_o must be used to cover the fact that β_o, k_G and η_b are variable over blade radius. All λ_o values are multiplied by the correction factor

$$p_\lambda = \frac{2}{r_a^2 \lambda_{r\,eff\,max.}} \int_0^{r_a} \lambda_{r_{max}} \cdot r\, dr \tag{58}$$

Specific speed for $c_L = 0$, λ_{max} is reached at $\xi = 1$ and

$$\lambda_{o\,max} = -\frac{\beta_o}{2n} + \sqrt{\frac{1}{n} + \frac{\beta_o^2}{4n^2}} \qquad n = \frac{c_{wp}}{2\pi \eta_d k_G} \tag{59}$$

We obtain this result from the condition that $dT = 0$. Then

$$\frac{c_{wp}}{2\pi k_G \eta_d} = \operatorname{arctg} \frac{1}{\lambda_{o\,max}} \left(\operatorname{arctg} \frac{1}{\lambda_{o\,max}} - \beta_o \right) \tag{60}^3$$

The results from calculating a λ_o/c_L diagram for a rotor of given form by the method described here are compared with measurements performed on such a rotor in the wind tunnel and on Tower I of the Ventimotor test system in Fig. 40. The measured λ_{max} values are compared with those calculated with formula (59) in Fig. 60.

[3] In formula (59), we set arc tan $1/\lambda_{max} \sim 1/\lambda_{max}$, valid for large λ_o.

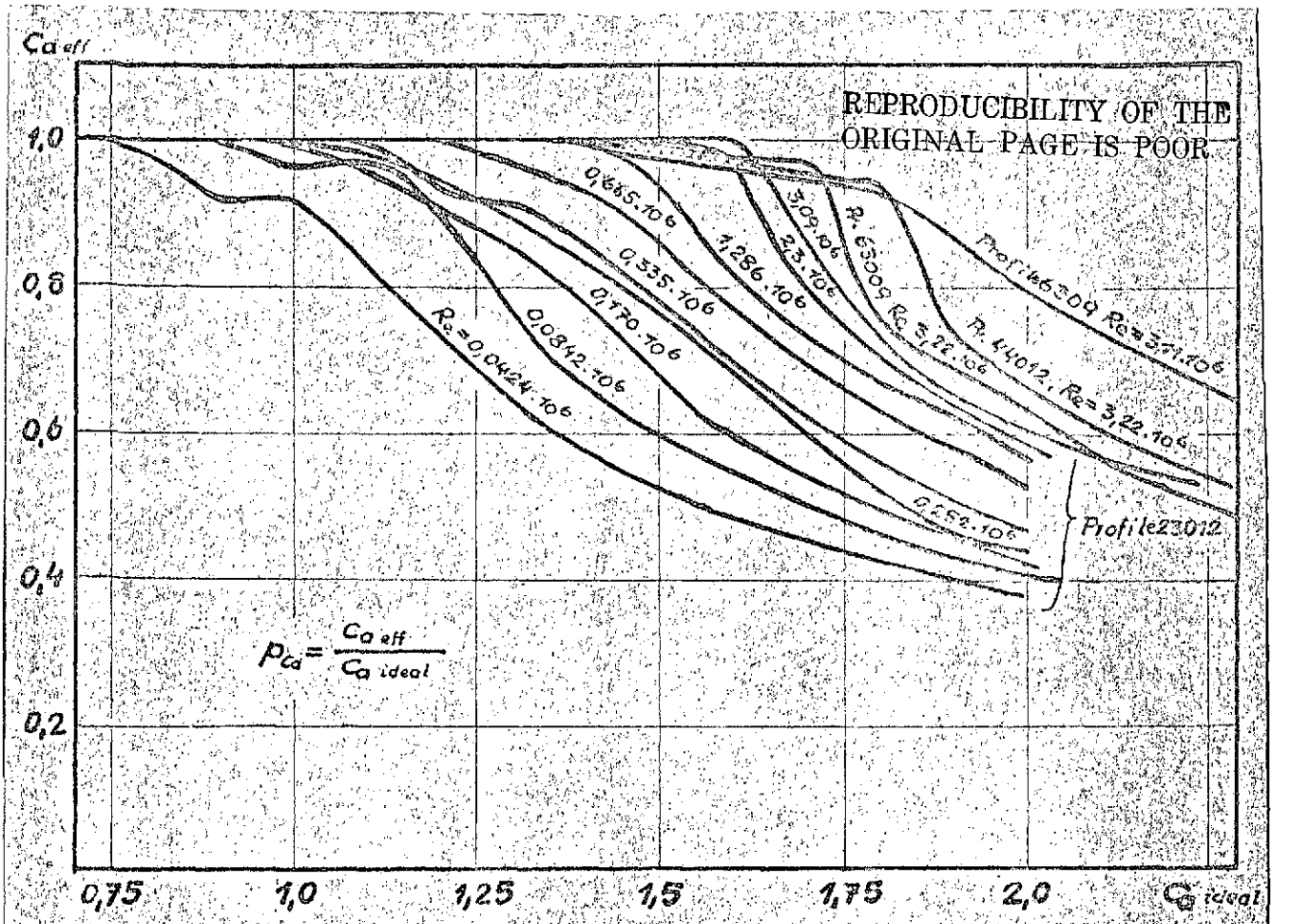

From *NACA Report 586*.

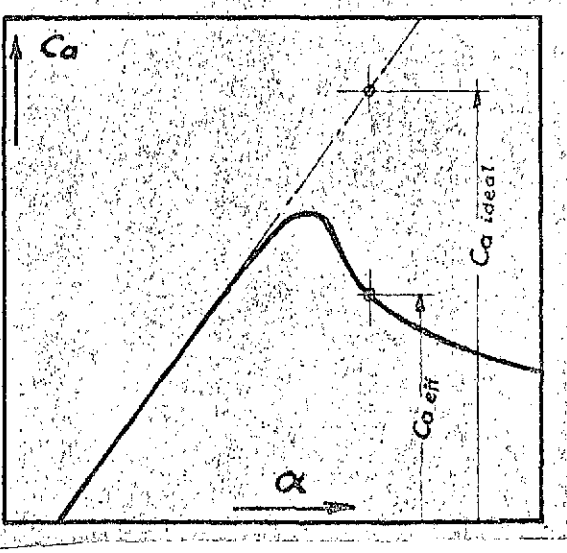

Fig. 39.

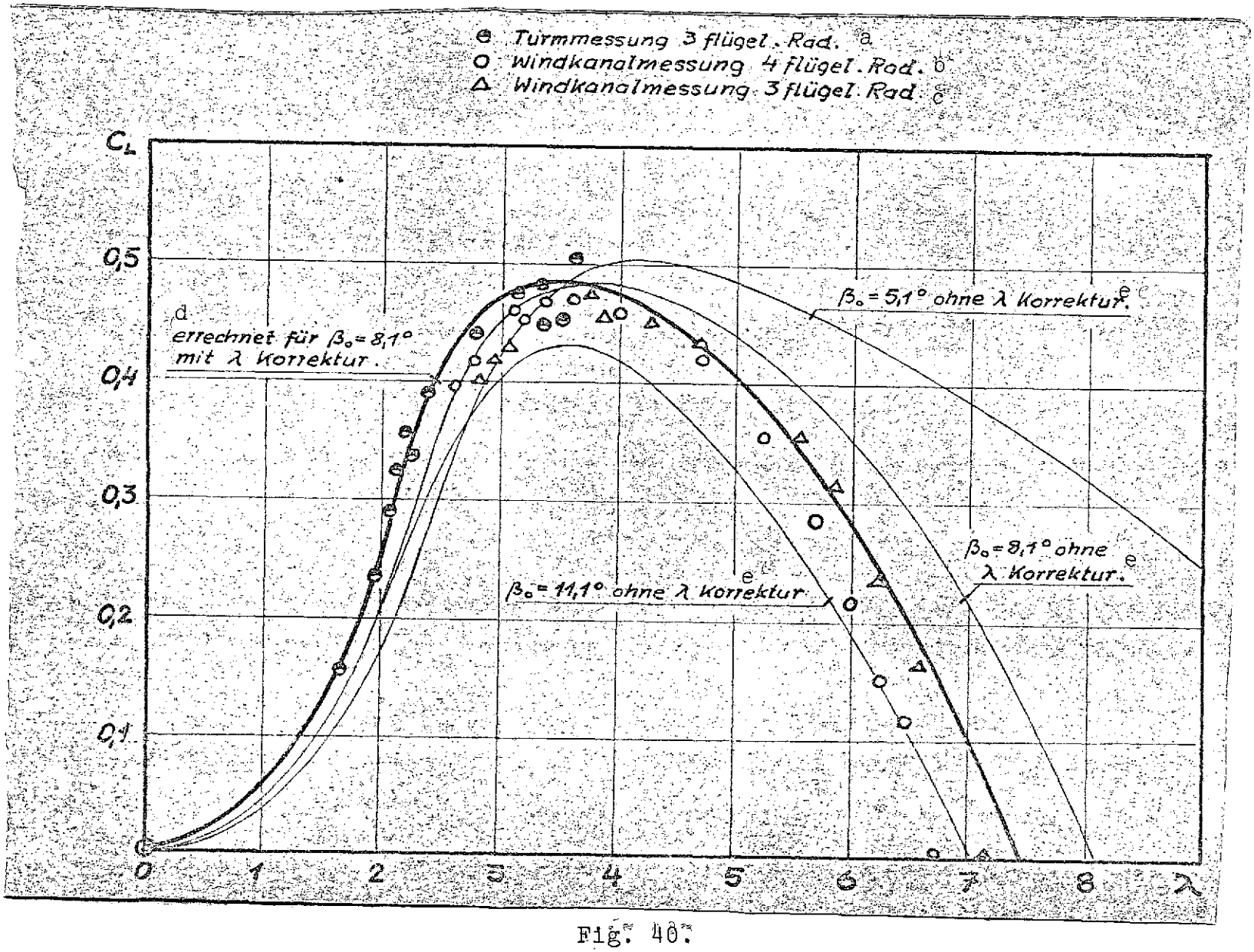

Fig. 40.

Key: a. Tower measurements, three-blade rotor; b. Wind tunnel measurements, four-blade rotor; c. Wind tunnel measurements, three-blade rotor; d. Calculated for β_o = 8.1° with λ correction; e. Without λ correction

6. The Overall Rotor

/64

The discussion has so far referred to the rotor element, which has been represented by a deflection mechanism which, while assumed to have the characteristics of blade sections, has still been assumed to produce a uniform effect on flow over the entire circumference.

Actually, however, only a finite number of profiles of equal depth are arranged about the circumference, the size of which varies in the radial direction, however, i.e. in the direction of the axes of the individual blades.

Circulation also varies in the radial direction; thus a vortex sheet propagates from each blade, stemming from the infinite number of adjacent vortical streamlines of the circulation element proceeding in the direction of flow. This vortex sheet affects the element's directions of oncoming and departing flow. For a given depth distribution over radius, a quite definite circulation distribution is set up; a characteristic of all distributions which can be realized is the continuous decrease in circulation toward the two ends of the blade, at $r = 0$ and $r = r_a$. On a wing, such continuous vortex separation produces an additional, induced drag. The effect on the wind rotor, on the other hand, is primarily that the ideal velocity-reduction ratio cannot be achieved over the entire range from $r = 0$ to $r = r_a$, i.e. less energy can be extracted from the wind than could be with an infinite number of blades. In addition, only small profile fineness ratios are feasible with small local lift coefficients which are obtained with a large local depth but low local circulation

$$c_a = \frac{2\Gamma}{t \cdot w} \qquad (61)$$

A favorable velocity ratio thus cannot be produced at the blade tip, for example, by means of a large profile depth. The poor local profile efficiency η_p would eliminate the gain in axial power coefficient c_{La}. If local blade depth were too small at one /65
point, on the other hand, a separation of flow could then occur there, with all of its disadvantages, in a state of operation in which aerodynamic force is still not sufficient at other points on the blade to produce the necessary axial velocity reduction.

A. Planform

In order to establish conditions for the following considerations, the depth distribution is first determined which (without consideration given to the possibility of actualization) would

yield the same velocity ratio ξ or the optimal velocity ratio for each radius if the mutual influence of individual blade elements were eliminated; this would correspond to a wing of infinite span in airfoil theory:

The energy of the air mass passing through a sector of an annulus subtending angle $\gamma = 2\pi/z$[4] with a given velocity ratio is equated with the power associated with the aerodynamic force acting on the blade element of depth t. It is assumed here for the time being that the blade operates without loss.

$$L_{IDEAL} = -dT_{id} \cdot r \cdot \omega_0 = dR_{id} \cdot \sin\varphi_\infty \cdot r \cdot \omega_0 \qquad (62)$$

$$L_\gamma = \frac{\rho}{2} v_\infty \cdot \gamma \cdot r \cdot dr \left(v_0^2 - v_3^{*2}\right) \qquad (63)$$

$$L_\gamma = L_{IDEAL}$$

$$\sin\varphi_\infty = \frac{v_\infty}{w_\infty}$$

$$dR_{id} = t_0 \cdot dr \cdot c_R \cdot w_\infty^2 \frac{\rho}{2} \qquad c_R \sim c_a$$

After transformation:

$$c_R \cdot t = \gamma \frac{v_0^2 - v_3^{*2}}{\omega_0 \cdot w_\infty} \qquad (64)$$

This formula permits a very simple interpretation: If we multiply /66 both sides of the equation by $w_\infty/2$, we obtain circulation

where

$$\Gamma = \frac{\gamma}{2\omega_0}\left(v_0^2 - v_3^{*2}\right) = c_a \cdot t \cdot \frac{w_\infty}{2}$$

$$\omega_0 = \frac{u_0}{r}$$

$$v_0^2 - v_3^{*2} = 2u_0\left(\sqrt{v_0^2\kappa + u_0} - u_0\right) \qquad (22)$$

[4] Fig. 24.

Thus

$$\Gamma = r \cdot y \cdot v_0 (\sigma - \lambda_0) \tag{65}$$

If we make $\xi = \xi_{opt}$ at all points, we obtain that circulation distribution which corresponds to minimum outflow loss.

For flow without twist $v_3^* = v_3$ and $v_0^2 - v_3^{*2} = v_0^2 \cdot k$, i.e.

$$\Gamma = \frac{y \cdot v_0^2 \kappa}{2 \omega_0} = \text{constant} \tag{66}$$

if ξ = constant likewise; this corresponds to the rectangular wing of infinite span.

From (65) we obtain

$$c_a \cdot t \cdot \frac{w_\infty}{2} = r \cdot y \cdot v_0 (\sigma - \lambda_0)$$

However,

$$w_\infty = \frac{v_0}{\sqrt{2}} \sqrt{\mu + \lambda_0 (\sigma + \lambda_0)} \tag{50a}$$

i.e.

$$t_0 = 2^{1,5} \cdot \frac{r \cdot y}{c_a} \cdot \frac{\sigma - \lambda_0}{\sqrt{\mu + \lambda_0 (\sigma + \lambda_0)}}$$

$$t_0 = \frac{r \cdot y}{c_a} \cdot \Theta$$

$$\Theta = 2{,}8284 \frac{\sigma - \lambda_0}{\sqrt{\mu + \lambda_0 (\sigma + \lambda_0)}} \tag{67}$$

The distribution function Θ is a function only of velocity ratio and specific speed.

We achieve significant simplification of the expression for [sic] with the following transformation of σ:

$$\left(\frac{2\kappa}{\varkappa} z + 1\right)^{\varkappa} \sim \left[\frac{2\kappa}{\varkappa} + 1\right]^{\varkappa} = \vartheta \tag{28a}$$

Thus

$$\Theta = \frac{k}{\lambda_0^2 + \frac{2\mu + \kappa}{8}} \tag{68}$$

/68

As a first approximation for $\lambda_0 >> k$,

$$\Theta \sim k/\lambda_0^2 \tag{69}$$

(Fig. 41).

B. Coefficients for Overall Rotor with Infinite Number of Blades

The depth of individual blades decreases with increasing blade number. According to (67),

$$t_0 = \frac{2r\pi\Theta}{2c_a}$$

0

However, circulation $\Gamma = 0.5t \cdot c_a \cdot w$ and thus circulation dropoff $d\Gamma/dr$ toward the ends of the blade decrease with blade depth.

For an infinite number of blades, the overall rotor behaves like the sum of the rotor elements forming it.

The magnitudes of coefficients c_L, c_d and c_W can be determined from the local coefficients for the elements simply by integration over blade radius.

The power coefficient is

$$c_L = \frac{2}{r_a^2}\int_0^{r_a} c_{L_r}\, r\, dr \tag{70}$$

(71)

where $c_{Lr} = f(r)$, since $\lambda_r = r\lambda_a/r_a$ is directly proportional to radius. Determination of the moment coefficient from the power coefficient is simple: $c_d = c_L/\lambda_a$. The drag coefficient for the overall rotor is likewise determined by integrating over blade radius.

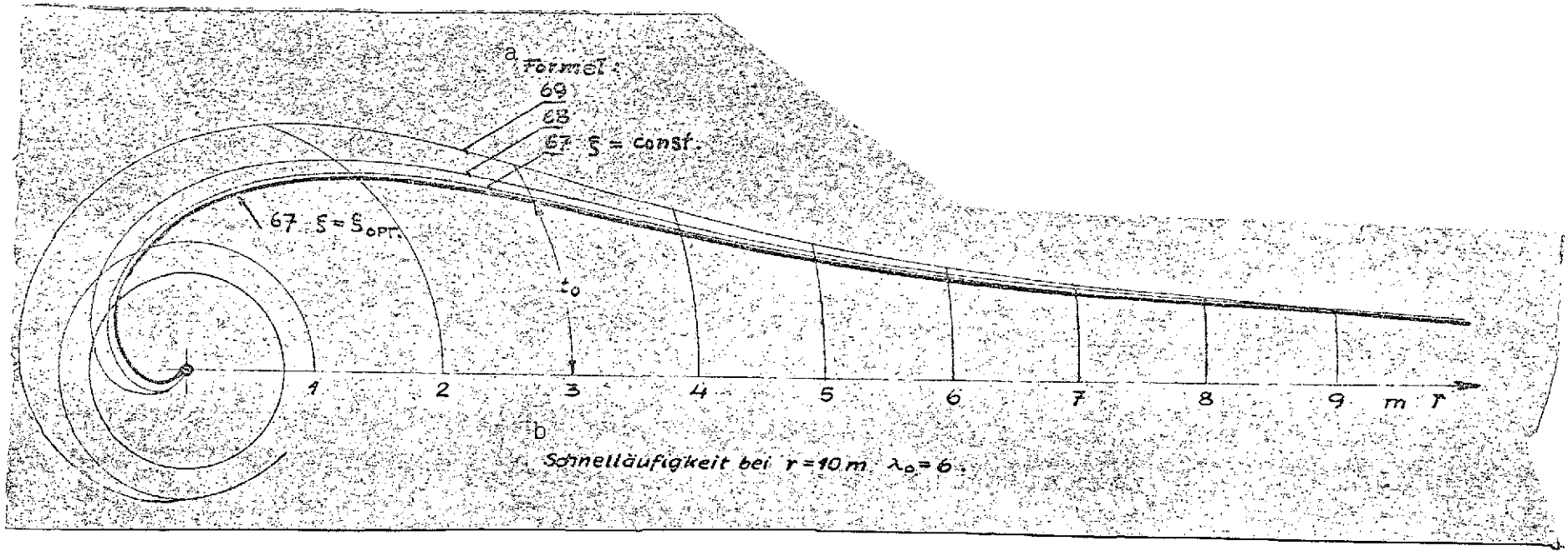

Fig. 41. Planform of blades.

Key: a. Formula; b. Specific speed for r = 10 m, λ_o = 6

$$c_W = \frac{2}{r_a^2}\int_0^{r_a} c_{W_r}\, r\, dr \qquad (71)$$

In both cases, integration is best performed graphically, since computation would become intolerably complex if consideration were given to friction for variable blade thickness and the resultant variability of fineness ratio. /69

C. Effect of Continuous Vortex Separation

The effect of continuous vortex separation must be taken into consideration in the case of an infinite number of blades. According to Betz [3], this is done by making calculations with a reduced diameter:

$$D_{red} = D - 0.44t_o. \qquad (72)$$

Prandtl [14][5] replaces the vortex sheets moving off to the rear with a system of planes perpendicular to the direction of flow and likewise calculates the reduced diameter from this idealized assumption:

$$D_{red} = D(1 - 1.39 \sin \phi_\infty / z). \qquad (73)$$

The dropoff in circulation toward the blade tips is given by the relationship

$$\Gamma = \frac{8 r_a}{z} \cdot \frac{v_\infty}{\lambda_o} \cdot \arccos e^{-\frac{1-\frac{r}{r_a}}{2\pi} \cdot \frac{z}{\sin \varphi_\infty}} \qquad (74)$$

These formulas are completely adequate for predicting the power coefficient and estimating the effect of blade number.

For a comparison of various blade planforms, the distribution of circulation over blade radius can be calculated for a given blade shape starting with Prandtl's familiar integral equation, taking into consideration the variation in freestream velocity

---

[5] The computation was carried out for propellers of low modulus.

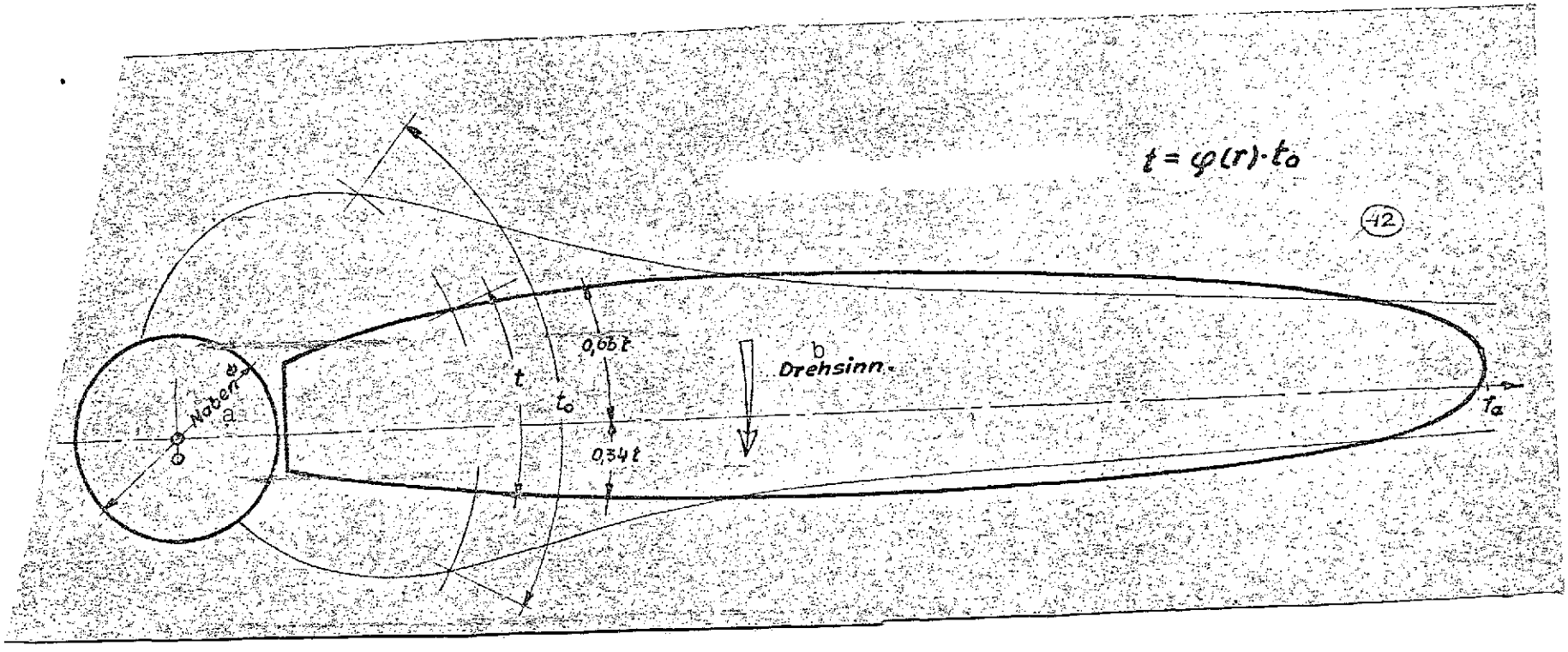

Fig. 42. Ultimate blade planform.

Key: a. Hub
b. Direction of rotation

w_∞ over blade radius and the effect of the vortex surfaces moving off helically in the direction of flow.

The local lift coefficient is determined from the local magnitude of circulation and the given blade depth. We thereby obtain both E and velocity ratio ξ. The latter is calculated (graphically) from c_a and specific speed, known from the assumptions made, from formula (51). /70

From formula (41), we obtain the local power coefficient c_{Lr} with the values so found.

By integrating over r in accordance with (70), we obtain the power coefficient for the overall rotor.

D. Most Desirable Number of Blades

The ratio of power coefficients for a rotor of z blades and for a rotor with an infinite number of blades can be calculated from (73):

(Fig. 43)

$$c_{L\,z\,\text{blades}} = c_{L\,z=\infty}\left(1 - 1{,}39\,\frac{\sin\varphi_\infty}{z}\right)^2 \qquad (75)$$

The effect of the number of blades on the power coefficient is considerably smaller for high specific speed than for small λ_o.

An increase in blade number is accompanied by an increase in rotor cost, which is almost proportional to blade number. This is explained by the fact that the number of individual rotor parts increases in proportion to the number of blades, whereas there is only a slight decrease in the weights of individual blades due to the reduction in design height. We can thus determine the costs of systems with rotors having different numbers of blades as in Section 3/B. We thereby obtain the economic efficiency of a system with a rotor of z blades (comparison with the values obtained in 3/B):

$$w_z = w_{z=3}\,\frac{c_{Lz}}{c_{L\,z=3}}\cdot\frac{K_{A\,z=3}}{K_{Az}} \qquad (76)$$

(The economic efficiencies of the systems covered in Section 3 were calculated for blade numbers z = 3.) /72

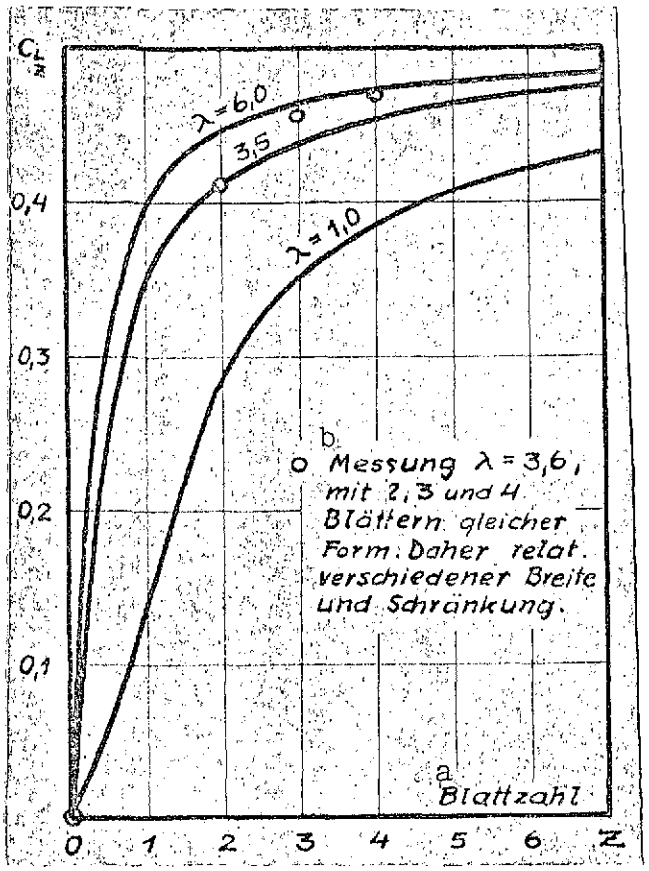

Fig. 43.

Key: a. Number of blades; b. Measured for $\lambda = 3.6$ with two, three and four blades of this same shape. Thus different relative width and pitch.

The results of calculation show that for high specific speed, the most desirable number of blades is smaller than for small λ_o (Figs. 44 and 45).

In the range of λ_o values for which the optimum power coefficient is achieved with feasible profile fineness ratios ($\lambda_o \sim 4$ to 7), the best number of blades is $z_{optimum} = 3$.

The best value for the power coefficients of windmills is $\lambda_o \sim 1.8$ to 2.2. In calculating their most desirable number of blades, it is necessary to consider that tower costs do not have to be covered.

Thus the effect of an increase in blade costs is greater than for electrical systems.

This justifies the age-old use of windmills with four as the most desirable number of blades.

The fact that slow-moving rotors must have large numbers of blades also becomes understandable.

E. Distribution of Angles over the Radius

The setting angle of individual profiles of a wind rotor blade will refer to the angle β_o enclosed by the profile's zero-freestream direction and the rotor's plane of rotation. The distribution of these angles over the radius is determined by the following quantities:

1. by the effective specific speed λ_∞ of the particular section,

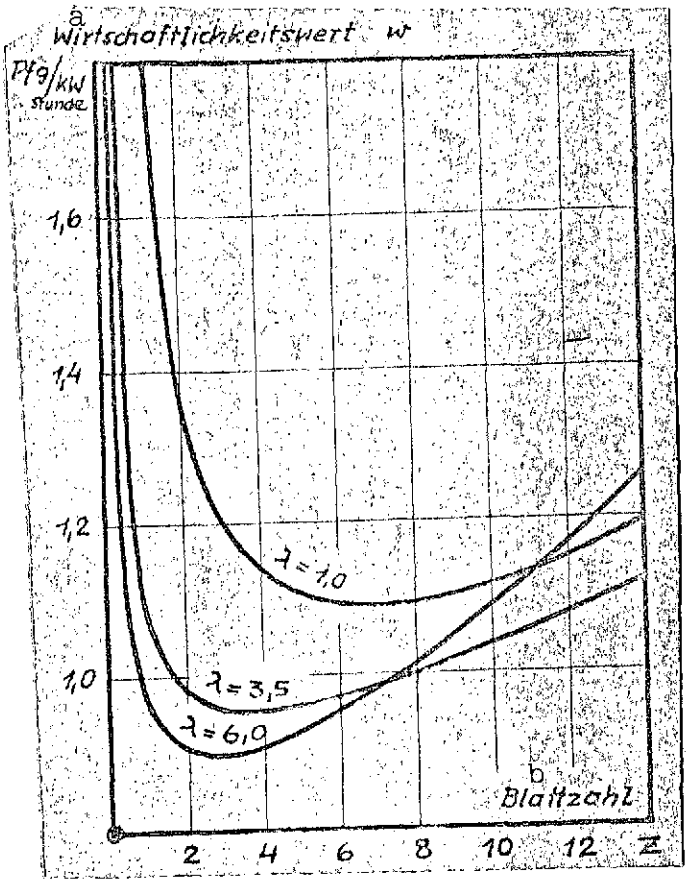

Fig. 44.

Key: a. Economic efficiency w in pfennigs/kWh; b. Number of blades

2. by the local lift coefficient c_{ar} which is assumed to be achieved (not the one which is actually achieved, taking continuous vortex separation into consideration),

3. by the lattice constant k_G, /73

4. by the profile constant η_d.

We have

$$c_a = 2\pi \eta_d k_G \left(\operatorname{arctg} \frac{1}{\lambda_\infty} - \beta_0 \right)$$

i.e.

$$\beta_0 = \operatorname{arctg} \frac{1}{\lambda_\infty} - \frac{c_a}{2\pi \eta_d k_G} \qquad (77)$$

The most desirable blade planform is calculated for a given lift coefficient (for which $E \sim E_{opt}$).

Since the decisive quantity is not the lift coefficient, however, but circulation and thus the product $c_a \cdot t$, blade planforms which are particularly simple to produce can be constructed if we accept local deviations from the best value of c_a.

A correction for the pattern of twist can be used to bring $c_a \cdot t$ to the required value.

E. Profiles for Wind Rotor Blades

Profiles for wind rotors are selected exclusively from the point of view of obtaining the best possible fineness ratios. Their dependence upon the individual profile characteristics of thickness, thickness distribution, contour, camber height, camber

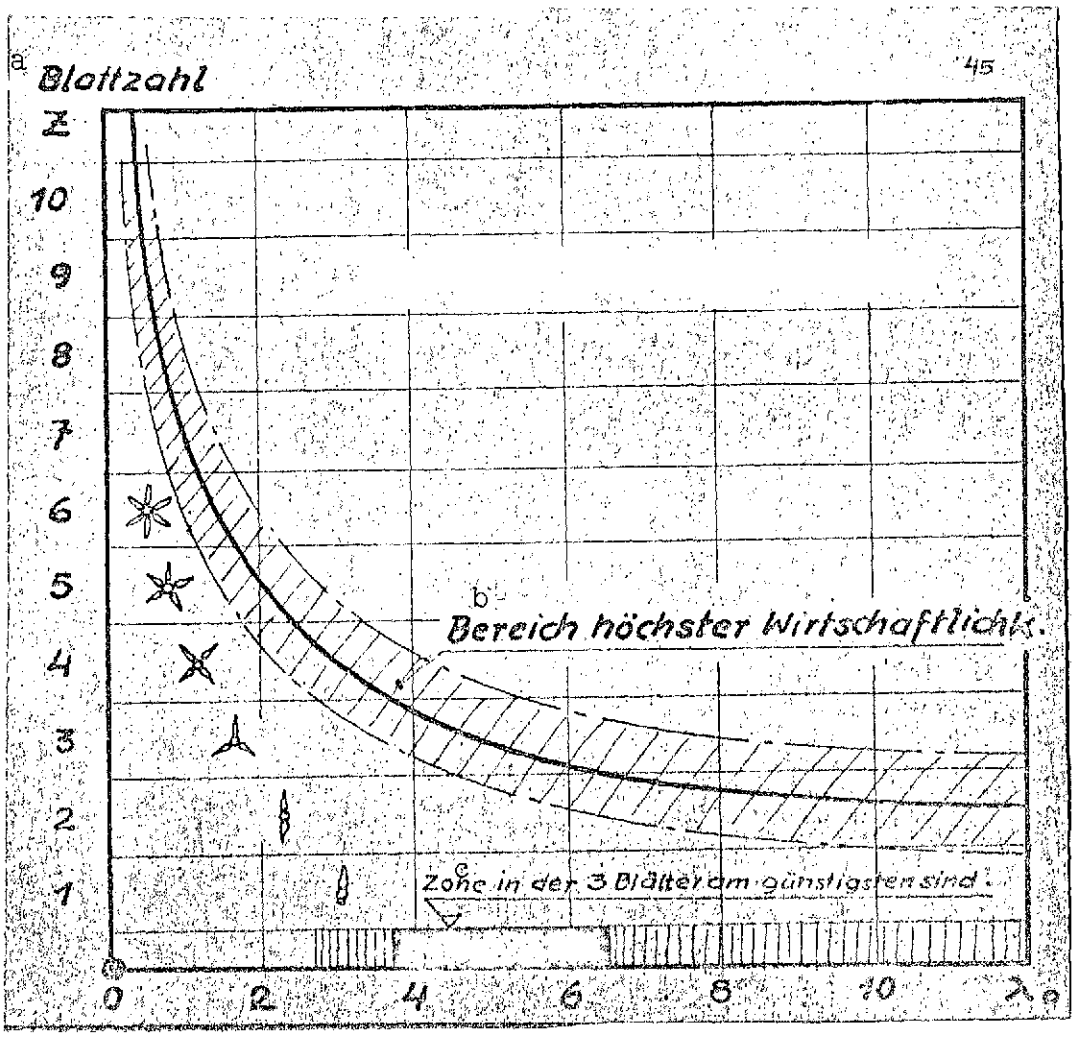

Fig. 45. Most economically efficient number of blades.

Key: a. Number of blades
b. Region of maximum economy
c. Zone in which three blades are most desirable

location[6] and upon Reynolds number can be obtained from the innumerable works published on airfoil profiles [21-28].

Aside from the highest possible optimum for fineness ratio E, we must also attempt to employ a profile with the flattest possible optimum and fineness ratio, since the peak of the λ/c_L diagram is thereby widened, and losses on the part of the rotor

[6] All of these values are specified in % of profile depth.

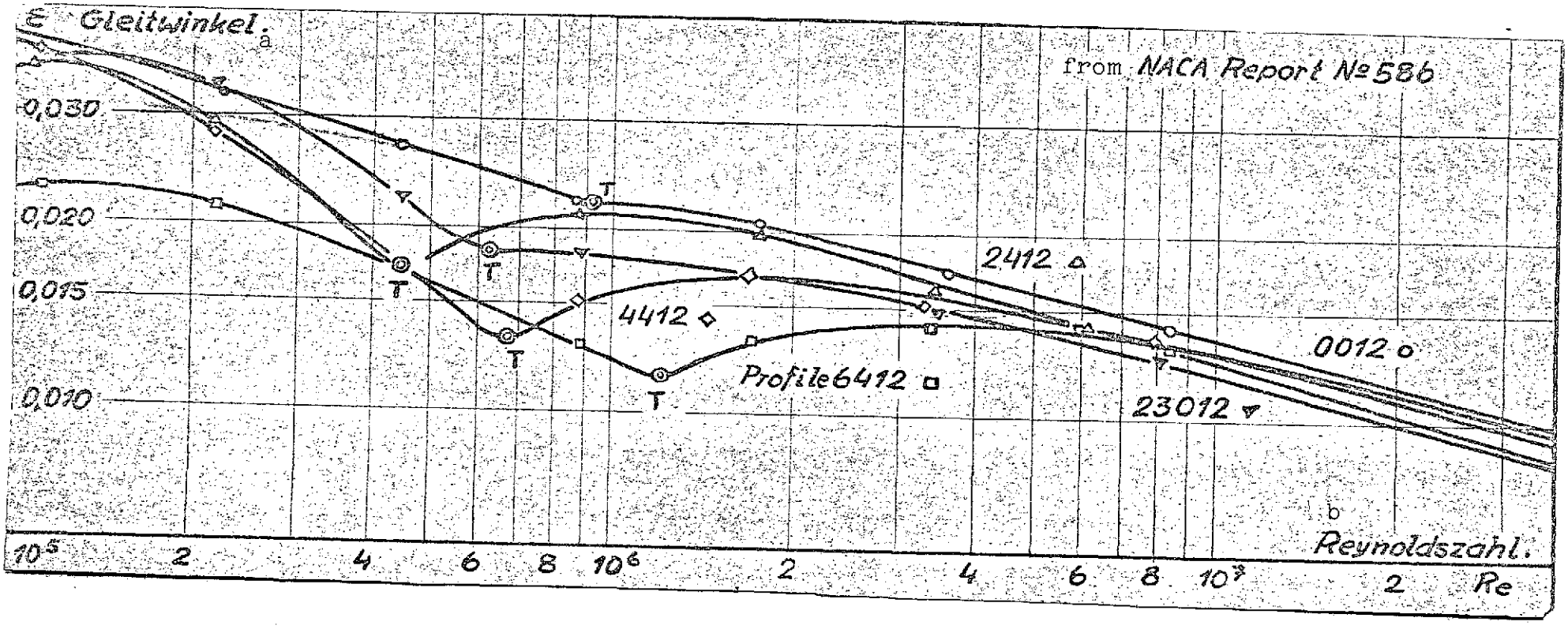

Fig. 46.

Key: a. Glide angle
b. Reynolds number

accompanying continuous fluctuations in operation conditions remain small.

The position of the optimum in fineness ratio on the polar curve is a function of profile thickness and camber height and is obtained at approximately $c_a \sim 0.7$ to 0.9 for almost all profiles coming under consideration (Fig. 48). /74

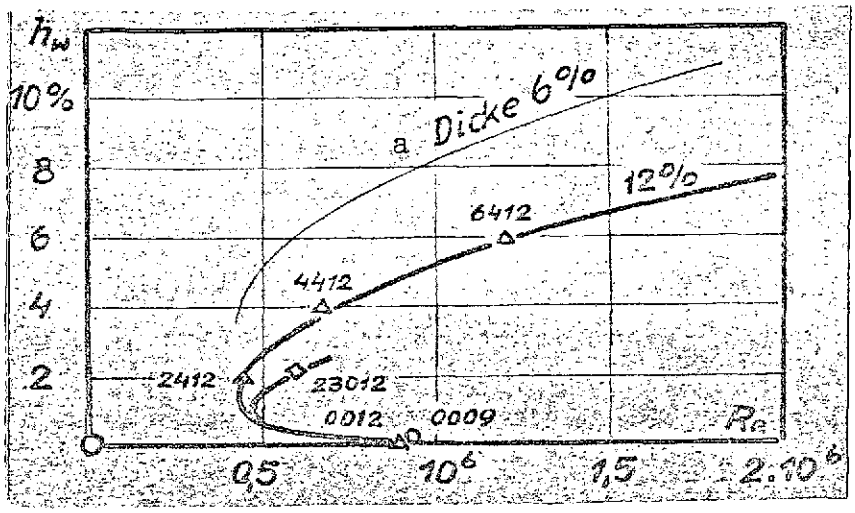

Fig. 47. Optimum camber heights h_w in % of depth versus Reynolds number at depth position T.

Key: a. Thickness

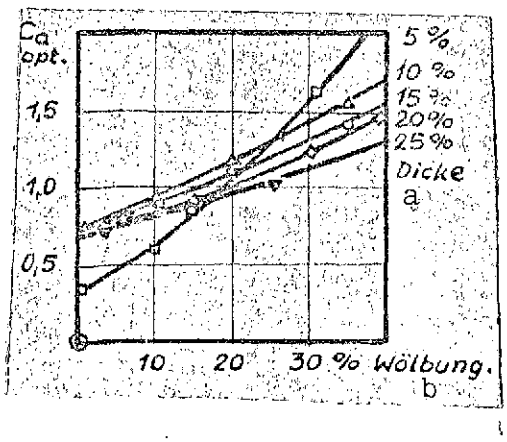

Fig. 48.

Key: a. Thickness;
b. Camber

As the thickness and camber of a profile are varied, it is found that the optimum in fineness ratio for relatively thick profiles occurs at a smaller camber height than in the case of thinner profiles. The most desirable camber height is thus determined not primarily by the camber on the camber line, but by the camber on the suction side of the profile. This fact is manifested quite clearly if we plot the best values of E obtained from the systematic variation of camber and thickness in a field containing lines of constant suction-side camber (Fig. 50).

The length of initial laminar flow along a profile is a function of Reynolds number and profile shape. Large initial distances result in low profile drags, i.e. good fineness ratios. The Re number at which the fineness ratio of a profile reaches a maximum is a function, among other things, of camber height. For a given Re number, a fineness ratio that could only be achieved with Re numbers several times greater can be obtained just through the selection of a quite

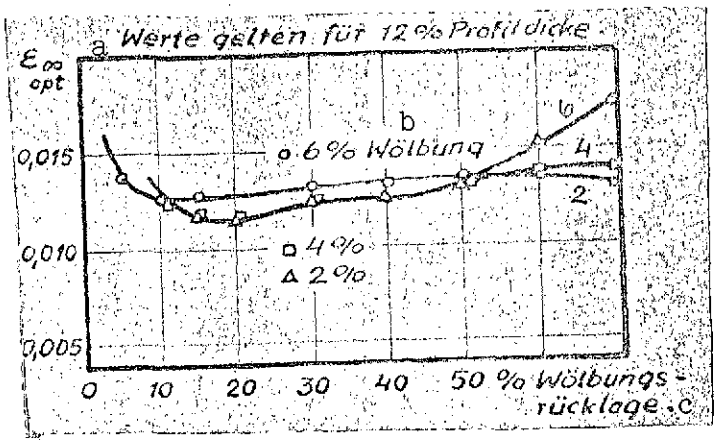

Fig. 49.

Key: a. Values apply to 12% profile thickness; b. Camber; c. Camber location, from front

specific camber. The above-mentioned intimate relationship between profile thickness and most desirable camber height also retains its validity here (Figs. 46 and 47).

The dependence of fineness ratio upon camber location is considerably less than the above-mentioned dependencies. A rather flat optimum occurs with a camber location of about 20% from the leading edge (Fig. 49).

The root of an individual rotor blade must almost always be designed with a relatively large design height, due to strength considerations. Here, as in aircraft construction, we now encounter the question of whether it is more desirable to achieve this large design height with profiles of greater thickness, in terms of percent, or with profiles of lesser thickness but greater depth. Up to very large profile thicknesses, thickening the profile while maintaining the depth to be expected from the optimum planform is more advantageous, as a comparison between the changes in glide angle accompanying an

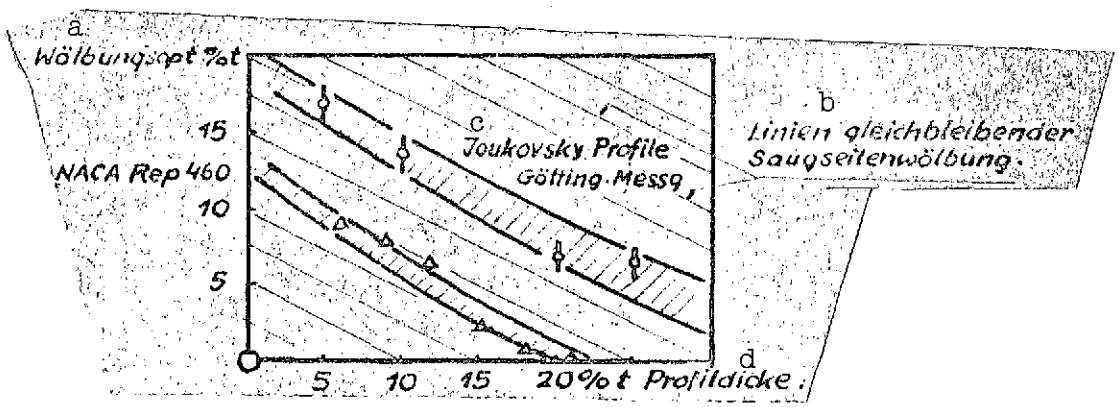

Fig. 50.

Key: a. Optimum in camber
b. Lines of constant suction-side camber
c. Joukovsky profiles, Göttingen measurements
d. Profile thickness

increase in thickness with constant profile depth and the change in glide angle accompanying an increase in depth with constant profile thickness shows (Fig. 51). /75

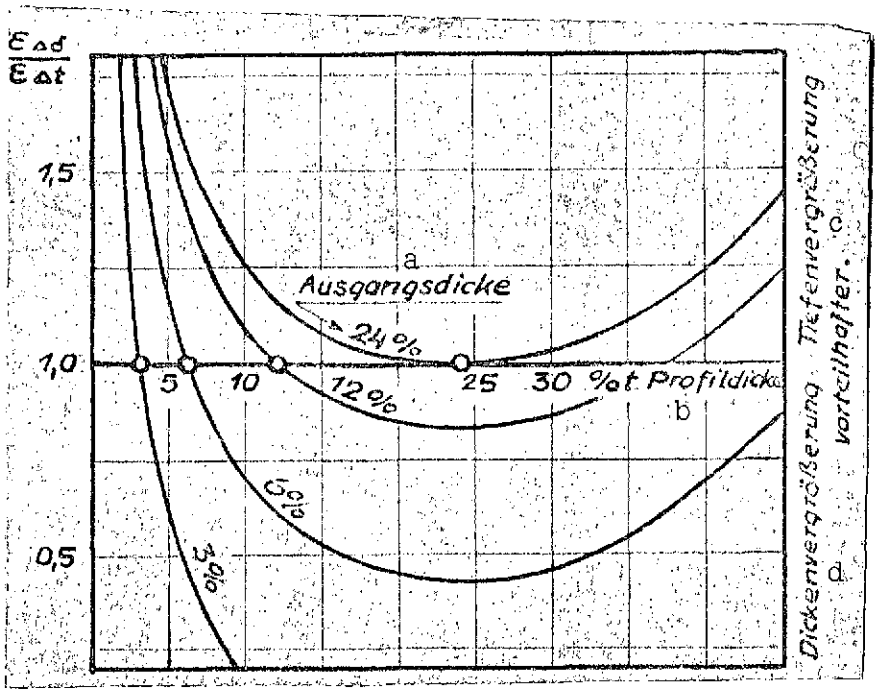

Fig. 51.

Key: a. Initial thickness
b. Profile thickness
c. Increase in depth more desirable
d. Increase in thickness more desirable

7. Execution of Measurements /79

A. Wind Measurements

Wind measurements carried out by the author cover only the region between 0.01 and 1 m above ground. The measurements were carried out for the purpose of establishing the curve of velocity increase versus height in this lowermost range in purely qualitative terms. Thus averages were not taken over periods of years; rather, only the ratio of velocity in the region described to velocity at an altitude of about 2 m above ground was measured.

Velocity 2 m above the ground was measured with a cup anemometer and a Bruhn double nozzle with attached liquid manometer.

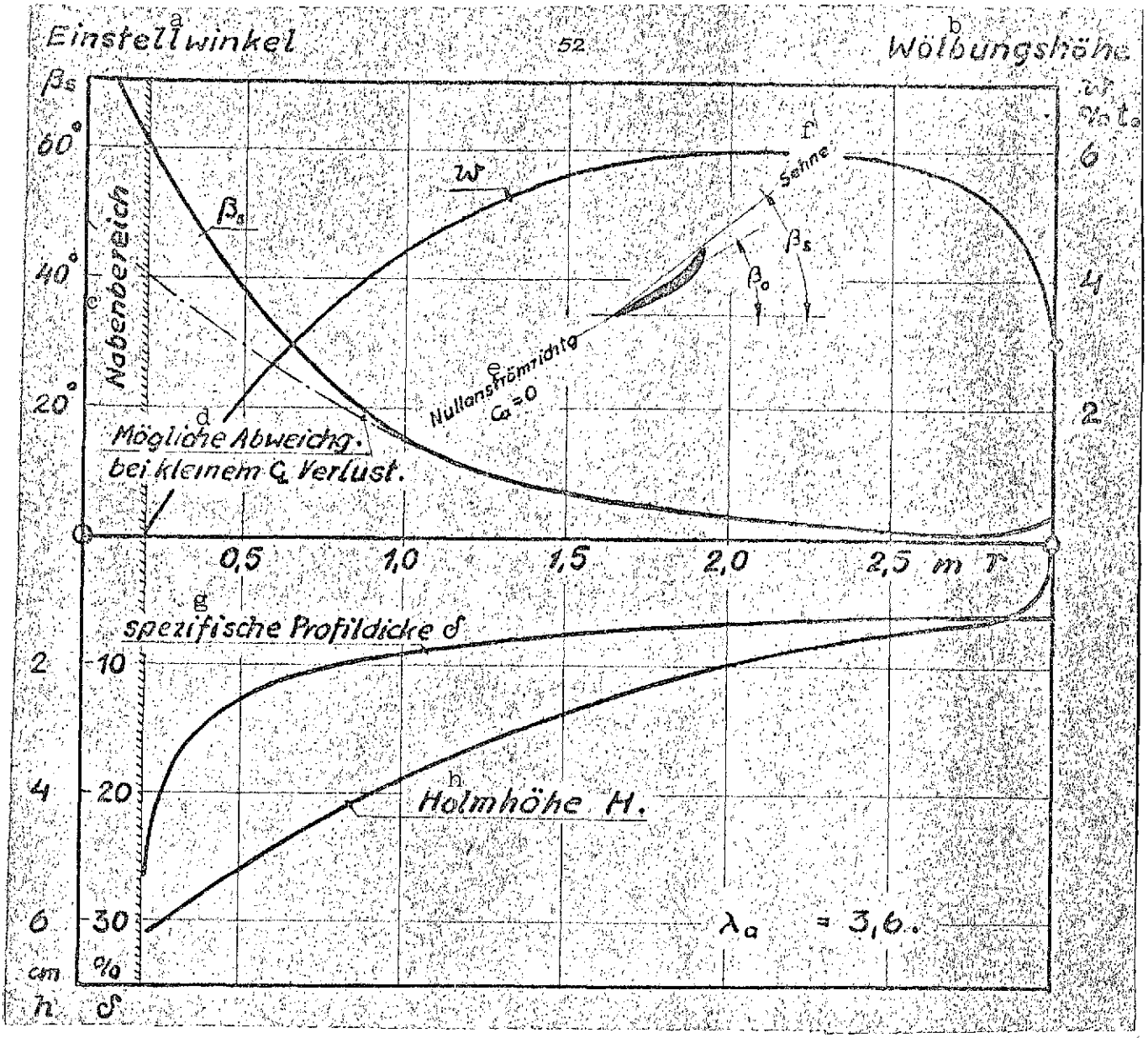

Fig. 52.

Key:
a. Setting angle
b. Camber height
c. Hub area
d. Possible deviation with small c_L loss
e. Zero-freestream direction
f. Chord
g. Specific profile thickness
h. Spar height

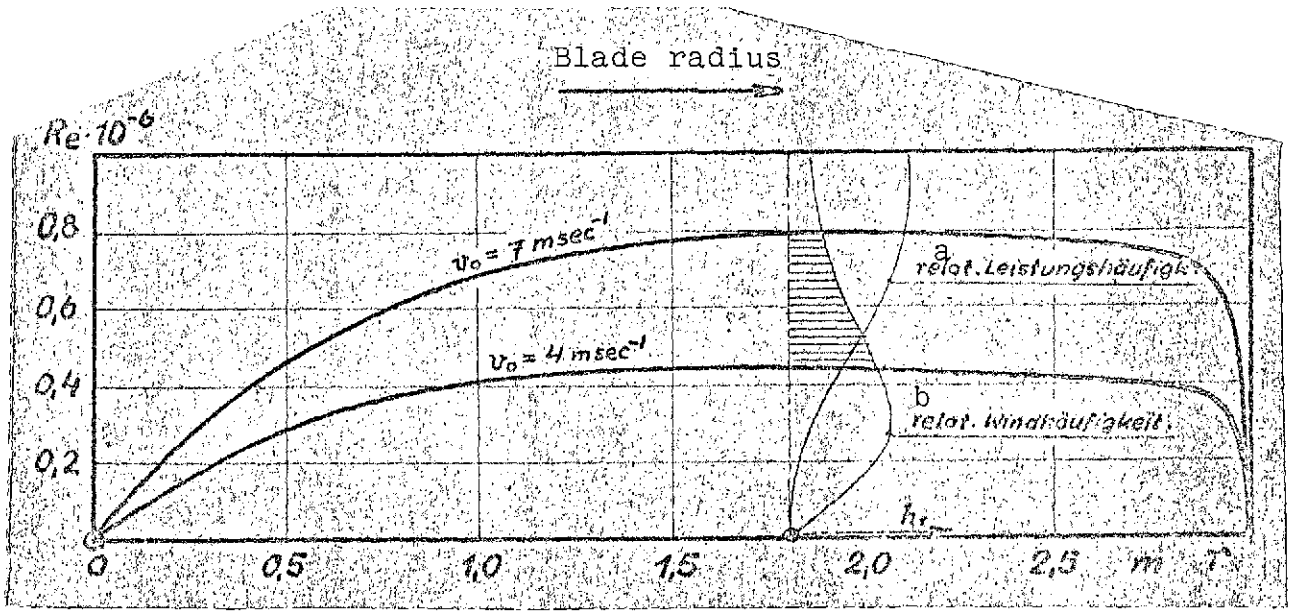

Fig. 53.

Key: a. Relative power frequency
b. Relative wind frequency

Velocity at various elevations was measured with a Prandtl nozzle and a micromanometer (Fig. 64).

B. Power Measurements Performed on a Wind Rotor Model in the FKFS 2-m-diameter Wind Tunnel, Stuttgart-Untertürkheim

The following had to be measured simultaneously during these measurements:

jet velocity
rotor axial thrust
rotor torque
rotor rpm.

Jet velocity was measured with a Betz micromanometer corresponding to the design published in "Ergebnissen der Aerodynamischen Versuchsanstalt zu Göttingen [Results from the Göttingen Aerodynamic Laboratory]," No. 4, p. 12.

Axial thrust was determined by weighing in the normal manner. Torque was generated with an eddy-current brake and likewise determined by weighing (see Enclosure 2 and 3). Torque could be varied from the balance area by varying the current sent through the armature of the eddy-current brake. The rotor's speed of rotation was measured stroboscopically with a Zeiss instrument (Figs. 54-62 and 65, 66). /80

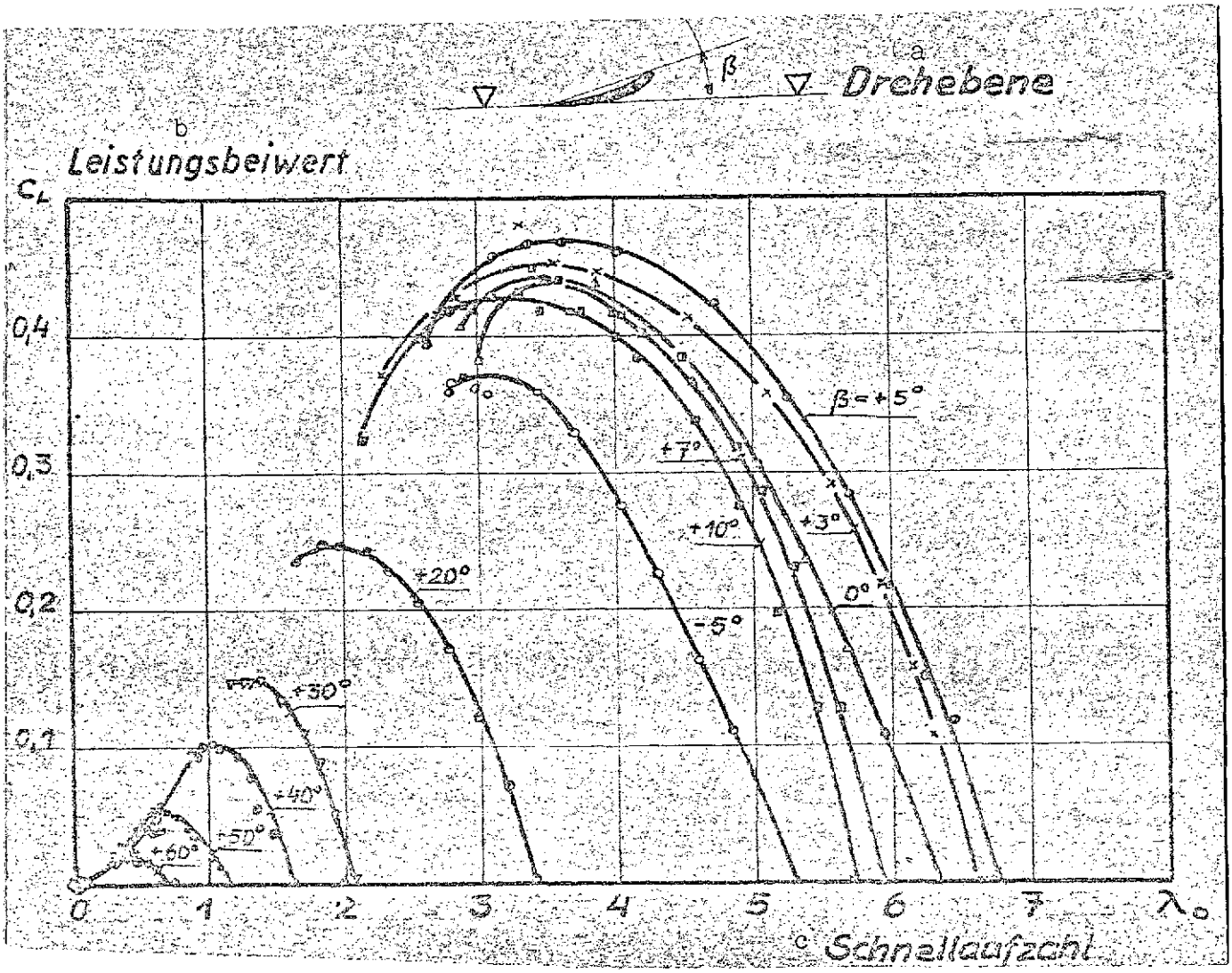

Fig. 54.

Key: a. Plane of rotation
b. Power coefficient
c. Specific speed

C. Measurement of Velocity Distribution in the Wake of the Model Rotor in the Engineer's School Wind Tunnel at Weimar

In order to obtain points of reference concerning the distribution of aerodynamic forces over blade radius and concerning velocity equalization downstream from a wind rotor, a scale model of the 5.7-meter-diameter rotor (see Enclosure 4) was tested in the 0.6-meter-diameter wind tunnel at the Weimar Engineers' School.

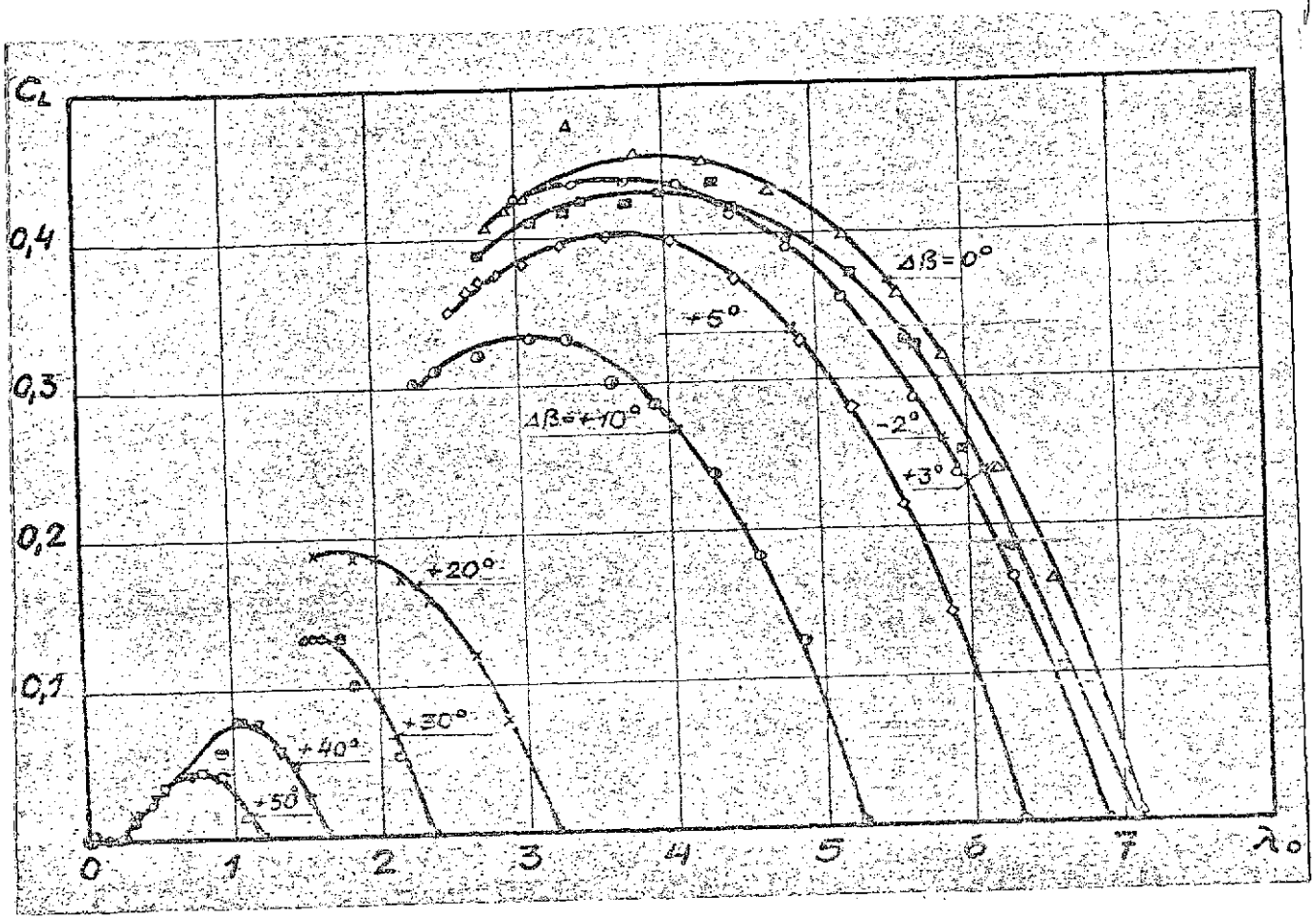

Fig. 55. Three-blade rotor.

The latter is an Eiffel wind tunnel, and thus it is very difficult to keep velocity constant in the airstream. Axial velocity in the wake of the model was measured with a Prandtl nozzle and a micromanometer, as was velocity at the reference point outside the plane of the circular area swept by the rotor (Figs. 4, 67, 68). The magnitude of velocity fluctuation at the two manometers was determined by observation over a relatively long time. After conversion to velocity at the reference point, velocity fluctuation at the measurement point was then indicated by the maximum and minimum in observed velocity. These maxima and minima are plotted in the graph of the results in Fig. 4. The region between these two values is finely hatched.

A series of measurements were performed on tower I of the test system in a free flow of air for comparison with the results obtained with the model in the wind tunnel. Good agreement was obtained between the two sets of measurements (Fig. 4).

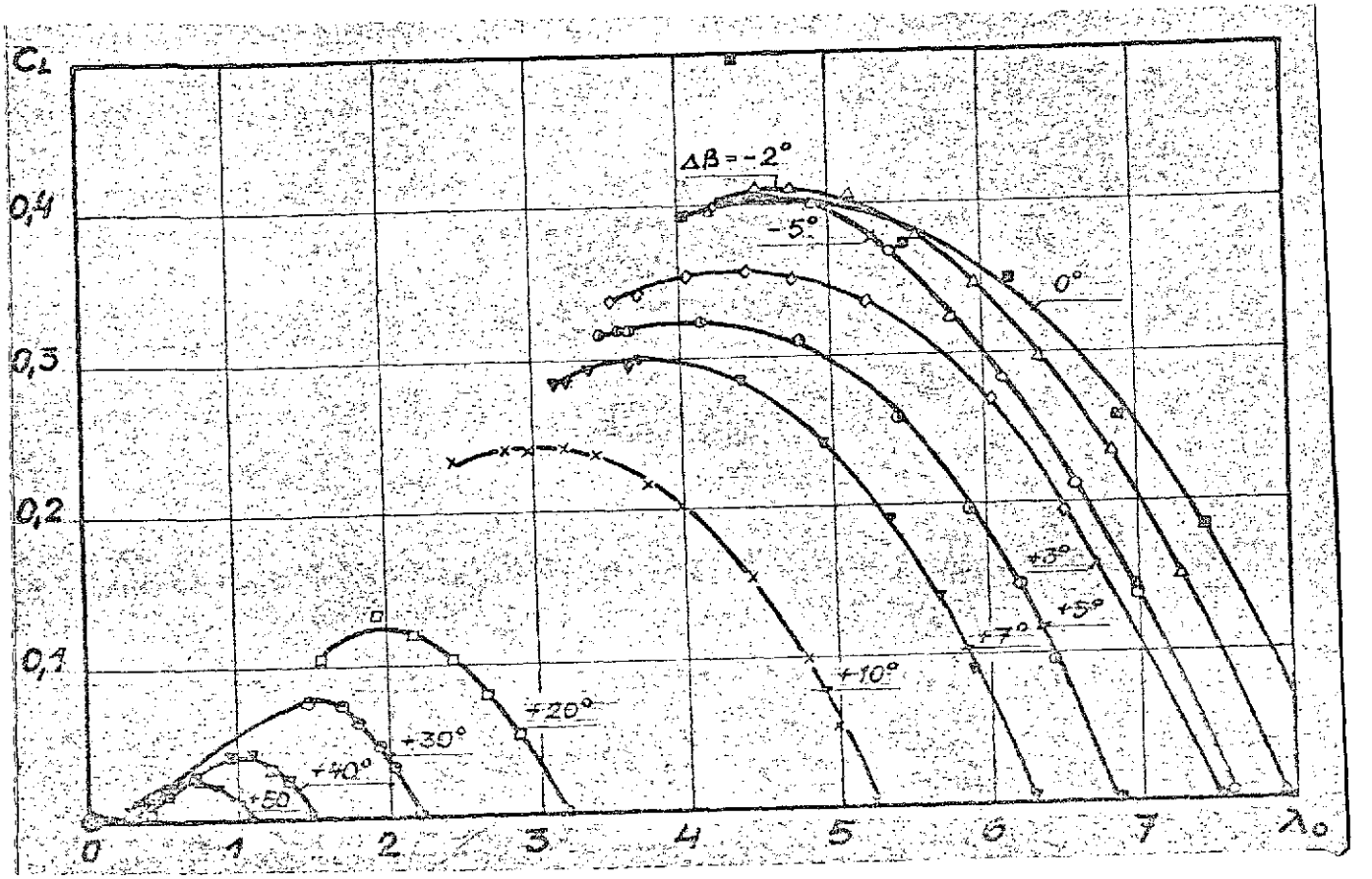

Fig. 56. Two-blade rotor.

8. Summary

The magnitude of the power available in the atmosphere is determined from the radiation balance and the distribution of velocity as a function of altitude. It is found that a multiple of the estimated power from all water resources exists in the form of wind power throughout the world. The magnitude of this power is shown as a function of the altitude up to which energy is removed with wind power plants and as a function of the size of the area covered by these power plants. /91

In addition, the most economically efficient principal dimensions for the tower height and rotor diameter of a wind power plant of given basic design are determined by comparing their actual output with the cost of their production. It is found that the most desirable dimensions are a tower height of about 35 m and a rotor diameter of 40 m --location makes little difference. The reasons why precisely this point on the very flat optimum is selected are explained.

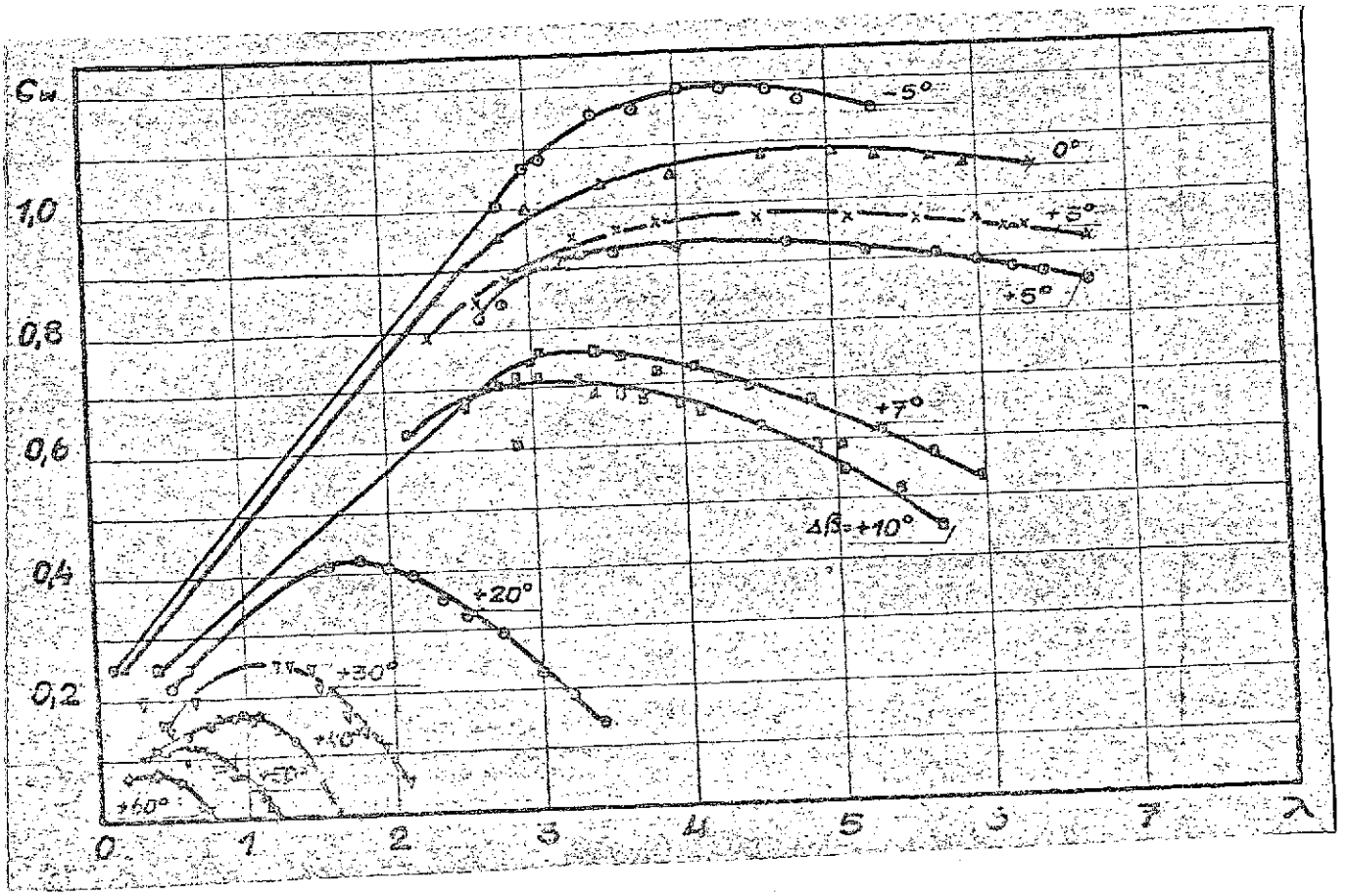

Fig. 57. Four-blade rotor.

Relative and absolute axial and peripheral velocities are determined for a blade element of a rotor from momentum and energy considerations.

The power coefficient of a rotor element is expressed by means of the pure axial power coefficient

$$c_{La} = \lambda_0 \mu (\sigma - \lambda_0)$$

$$\mu = 1 + \xi$$

$$\xi = \frac{U_3}{U_0}$$

$$\sigma = \sqrt{1 - \xi^2 + \lambda_0^2}$$

$$\lambda_\infty = \frac{\lambda_0 + \sigma}{\mu}$$

and profile efficiency

$$\eta_p = \frac{2\lambda_0 (E - \lambda_\infty)}{\mu (E\lambda_\infty + 1)}$$

by means of which friction at the blade element is taken into consideration.

$$c_{L\ element} = c_{La} \cdot \eta_p .$$

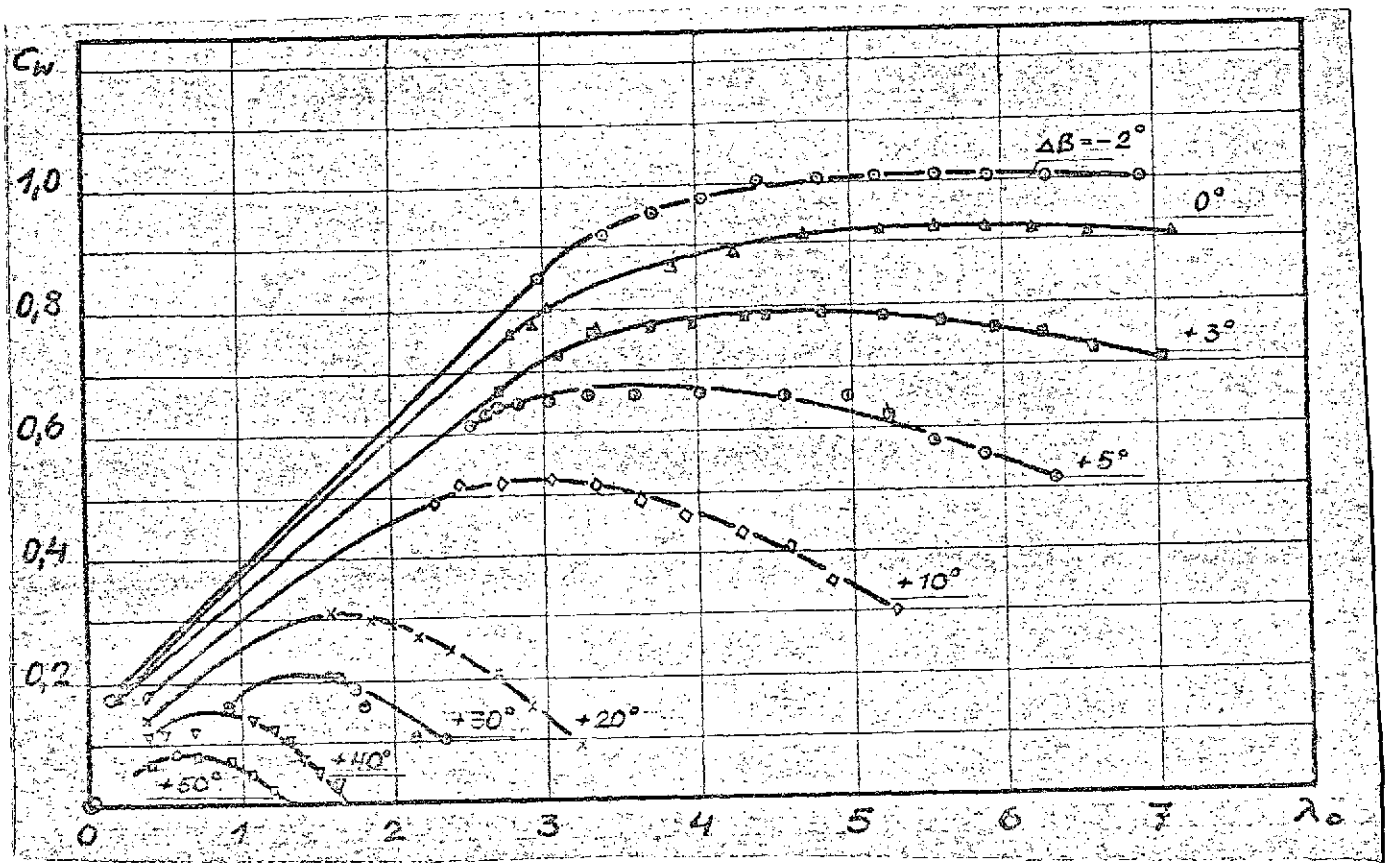

Fig. 58. Three-blade rotor.

Likewise, the drag coefficient

$$c_w = (1-\xi^2)\left(1+\frac{\lambda_\infty}{E}\right) \qquad X$$

and the moment coefficient

$$c_d = c_L''/\lambda_o$$

are determined for the rotor element.

The power coefficient / specific speed diagram is obtained by the graphic solution of two equations in the variables λ_o, ξ and c_a. The lift coefficient c_a is determined here from a consideration of momentum and energy, on the one hand, and, on the other, from the increase in the coefficient with effective angle of oncoming flow. /92

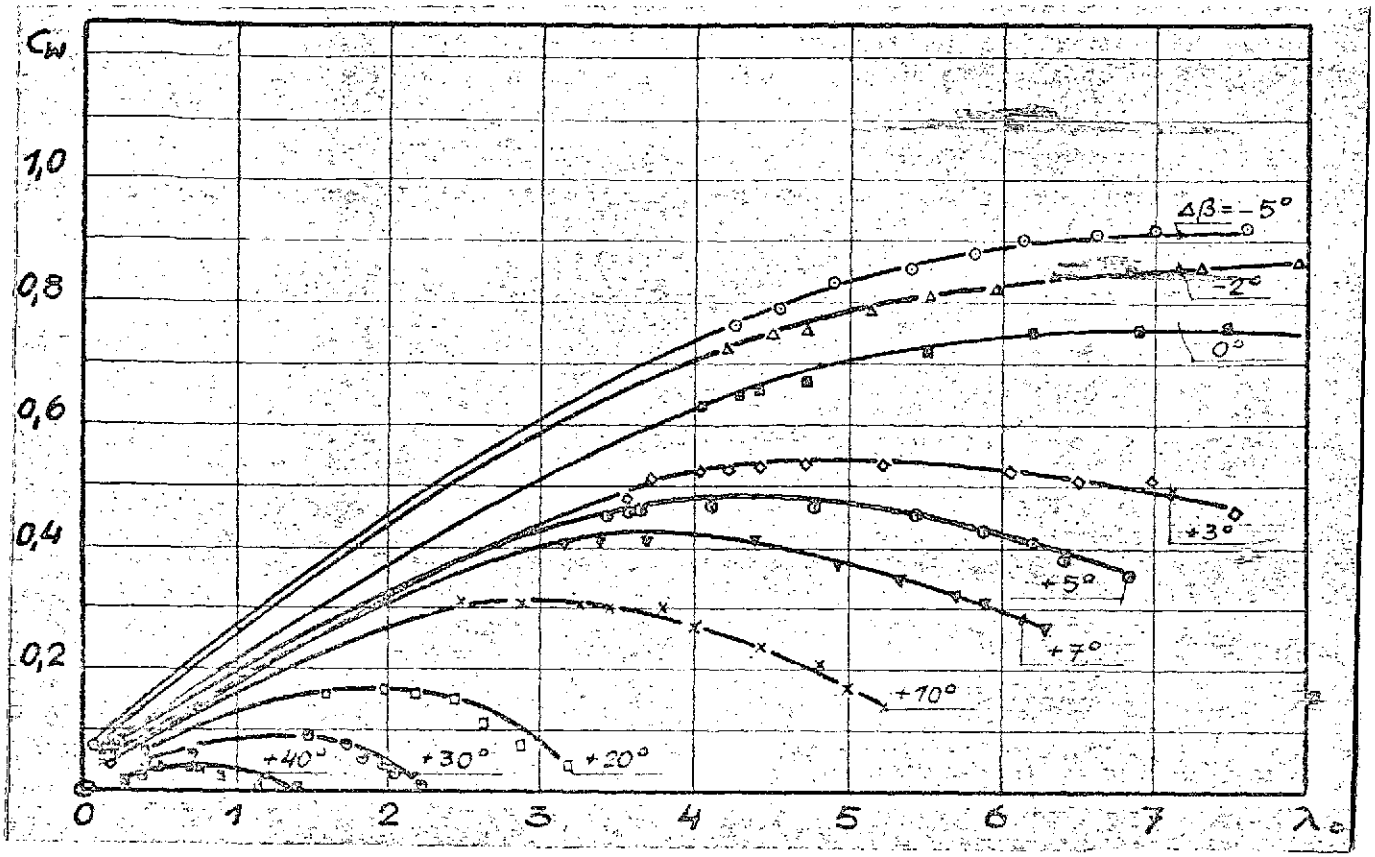

Fig. 59. Two-blade rotor

$$c_a = 4r\mu \frac{\sqrt{(1-\xi)^2 + (\sigma-\lambda_0)^2}}{\mu^2 + (\sigma+\lambda_0)^2}$$

$$c_a = \frac{2\pi k_a \eta_a}{\sqrt{\mu^2 + (\sigma+\lambda_0)^2}} \cdot [\mu \cos\beta_0 - (\sigma+\lambda_0)\sin\beta_0]$$

The power coefficient is then calculated from the formulas derived for the element's power coefficient, using λ and ξ and the E obtained from c_a.

Effective radius, i.e. the radius of the element, whose λ/c_L diagram is valid for the entire rotor, is determined from axial velocity in the wake. The effect of the actual distribution of

Fig. 60. Four-blade rotor [key on following page].

Key to Fig. 60

a. Specific speed
b. Setting angle
c. Calculated (element)
d. Measured (overall rotor)

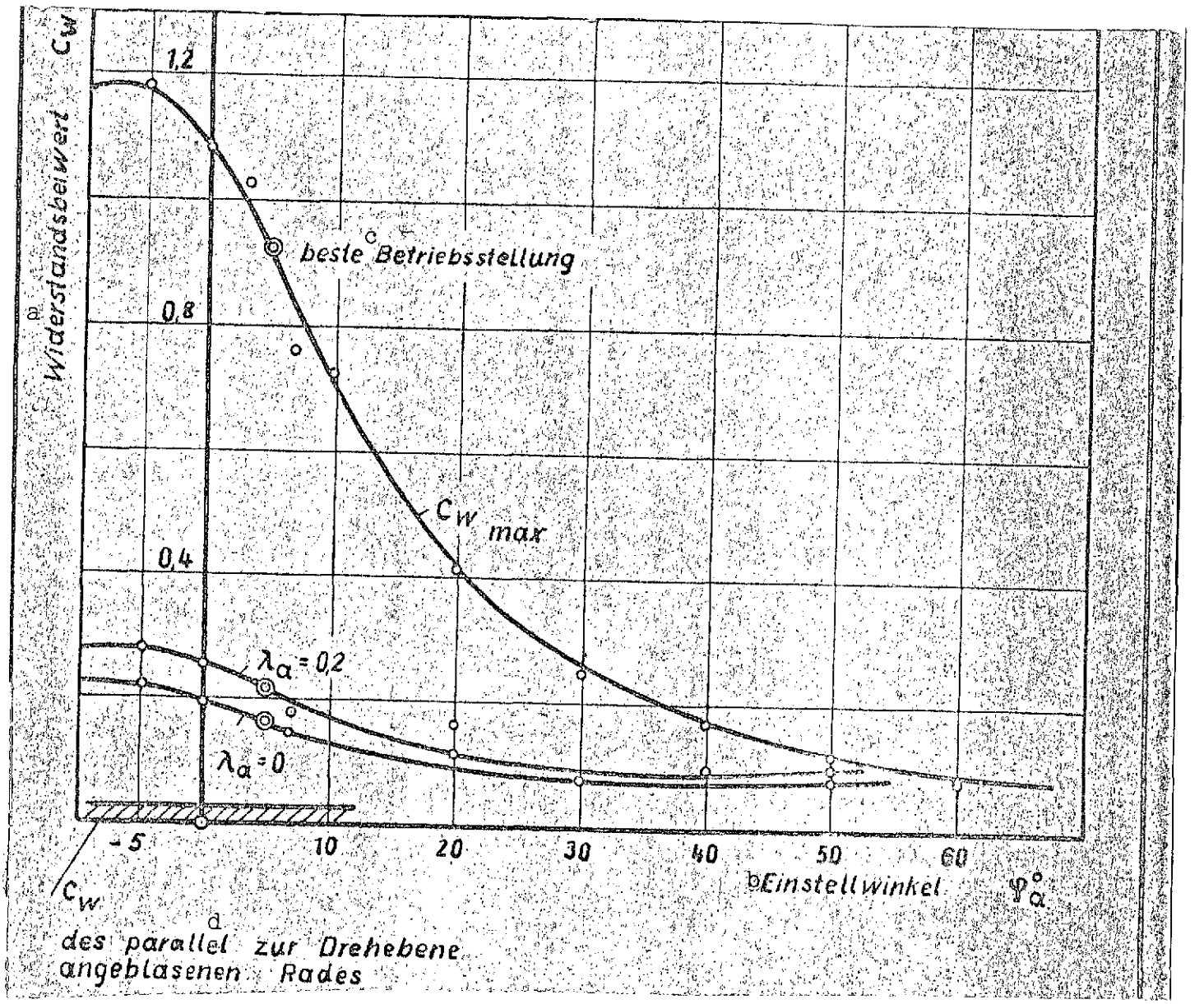

Fig. 61.

Key: a. Drag coefficient; b. Setting angle; c. Best operating setting; d. Drag coefficient for rotor in freestream parallel to plane of rotation

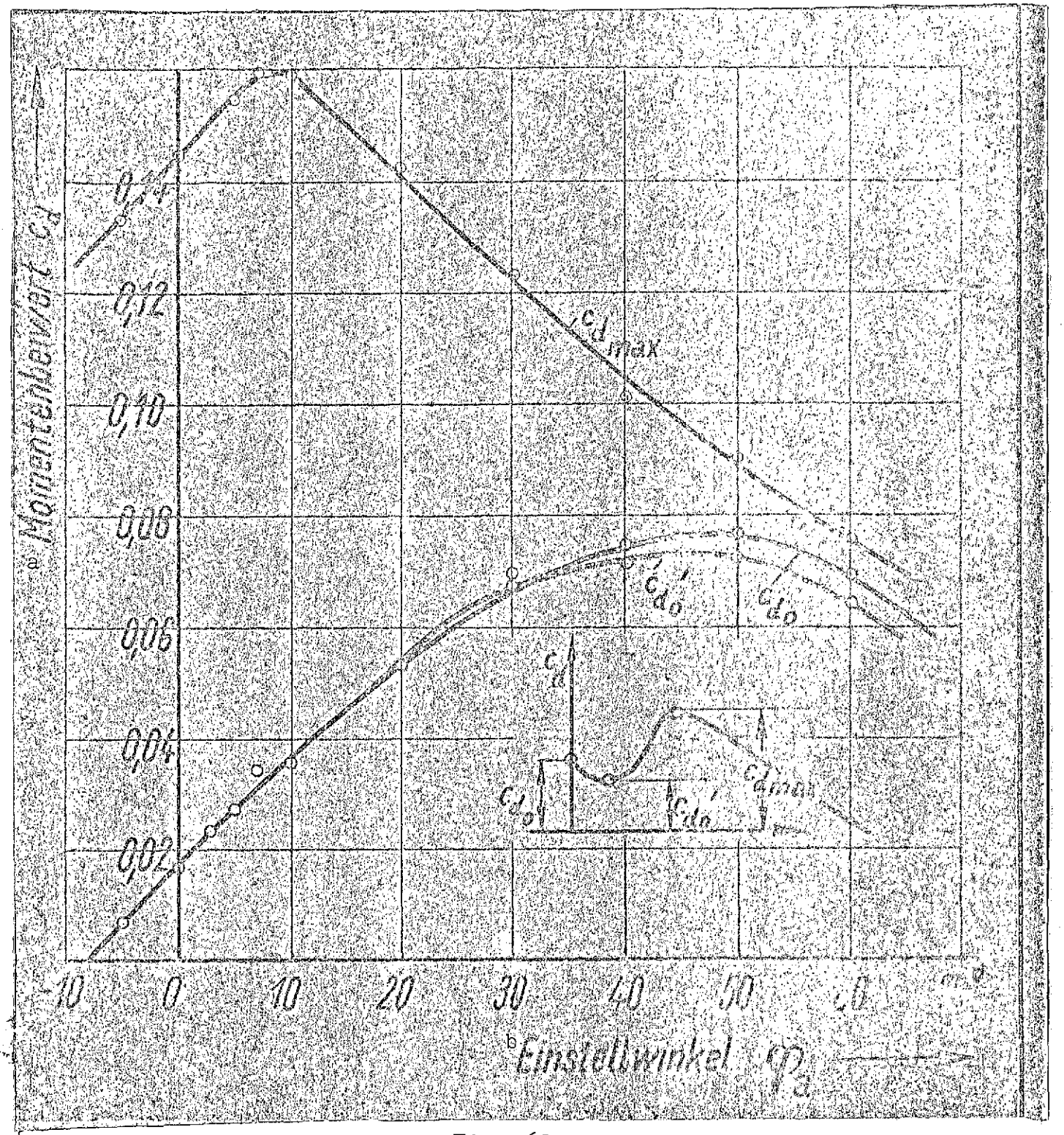

Fig. 62.

Key: a. Moment coefficient
b. Setting angle

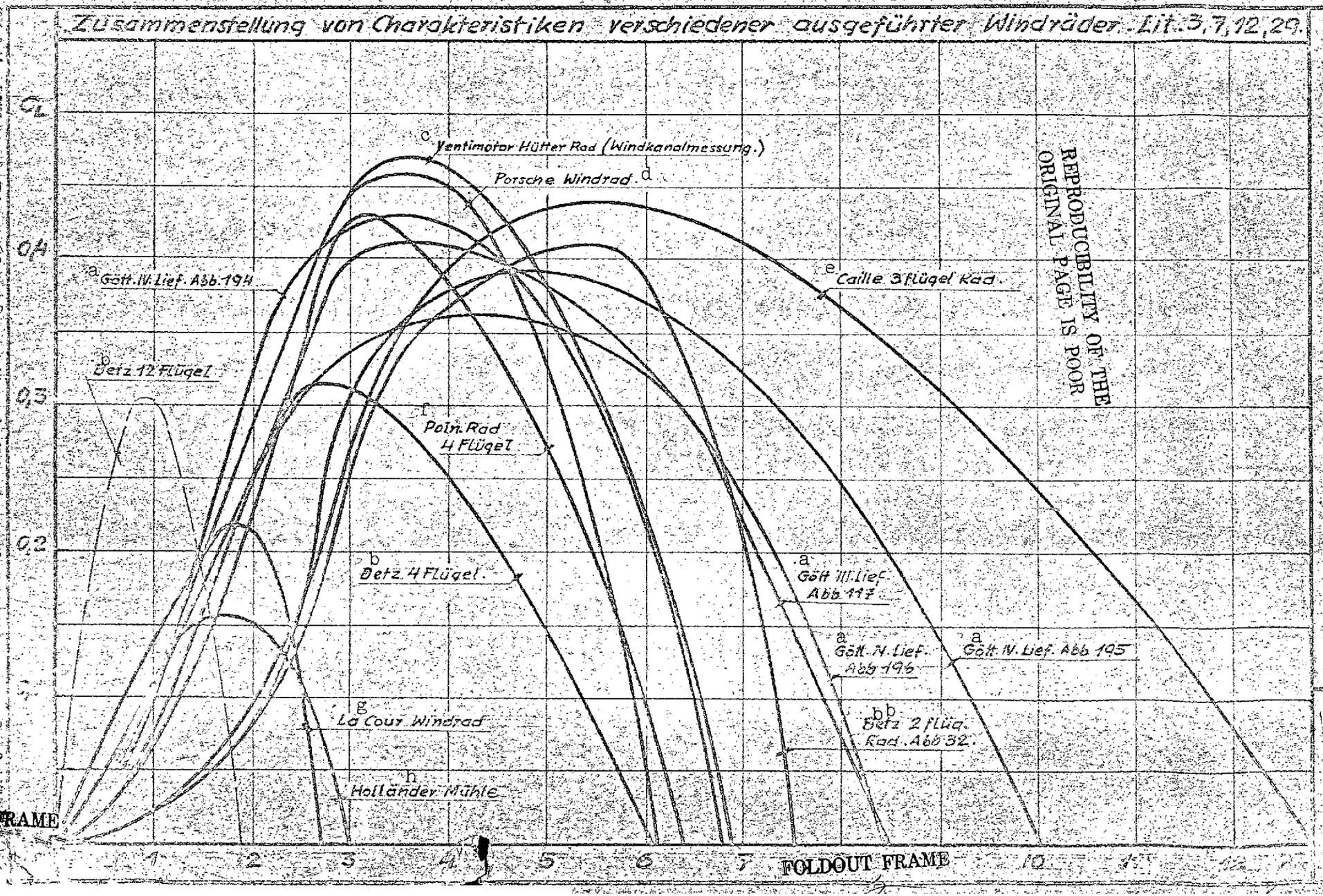

Fig. 63. [Caption and key on following page.]

Fig. 63. Summary of characteristics of various rotor designs, [3, 7, 12, 29].

Key: a. Göttingen, No. ... , Fig. ...
b. Betz, ... blades
bb. Betz, two-blade rotor, Fig. 32
c. Ventimotor Hütter rotor (wind tunnel measurements)
d. Porsche wind rotor
e. Gaille three-blade rotor
f. Polish rotor, four blades
g. LaCour wind rotor
h. Dutch mill

---

angles over blade radius is covered by a factor with which specific speed is corrected. The good agreement between the predicted diagram and measurements is demonstrated by comparison with the results of measurements performed in the wind tunnel and on a test system.

The transition from the blade element to the entire blade is outlined. In particular, an indication is given as to how the planform of a blade is obtained from the requirement of equality between the energy taken up by the blade element and the energy passing through an annular sector:

$$t_0 = \frac{r \cdot \gamma}{c_a} \cdot 2{,}8284 \cdot \frac{\sigma - \lambda_0}{\sqrt{\mu + \lambda_0 (\sigma + \lambda_0)}}$$

The effect of continuous vortex separation is pointed out. /93
In particular, reference is made to its effect on the power coefficient for various numbers of blades, and it is shown that for the specific speeds coming under consideration, z = 3 blades proves to be an optimum in terms of economy.

Finally, those considerations are described which resulted in the selection of blade profiles especially suitable for wind rotors. In particular, the dependence of the most desirable blade camber upon Reynolds number and upon profile thickness is shown, and it is demonstrated that in order to obtain the greatest possible design height, it is of greater advantage to employ thickened profiles than greater blade depths.